Space Manipulator Vibrations

by

Michael Ray

A Thesis Submitted to the
Faculty of Engineering
in Partial Fulfillment of the Requirements
for the Degree of

MASTER OF APPLIED SCIENCE

Major Subject: Mechanical Engineering

DALHOUSIE UNIVERSITY – DALTECH

Halifax, Nova Scotia 1999

DEDICATION

This work is dedicated to my wife, Shelley, and my two sons, Spencer and Cameron. Without their support it would have been impossible to have completed this thesis.

TABLE OF CONTENTS

TABLE OF CONTENTS

TABLE OF CONTENTS

List of Figures

List of Figures

Nomenclature

Note that matrices and vectors are in bold print and scalars are in normal print.

δ	logarithmic decrement
γ	angle between link and line to center of gravity of ensuing links
γ	absolute local angular position
$\dot{\gamma}$	absolute local angular velocity
$\ddot{\gamma}$	absolute local angular acceleration
θ	absolute angular position
$\dot{\theta}$	absolute angular velocity
$\ddot{\theta}$	absolute angular acceleration
ξ	damping ratio
Ψ	absolute posture angular position
$\dot{\Psi}$	absolute posture angular velocity
$\ddot{\Psi}$	absolute posture angular acceleration
τ	drive torque
ω_{ni}	natural frequency
$\mathbf{A}$	Coriolis and centrifugal matrix
a_i	length of the link

Nomenclature

$\mathbf{C}$	damping matrix
C_i	cosine of the posture angle
C_{i+j}	cosine of the sum of posture angle $\mathbf{Q}_i$ and $\mathbf{Q}_j$
c_i	damping coefficient of the joint
$\mathbf{d}$	displacement vector
DOF	Degree of Freedom
FFT	Fast Fourier Transform
g	gravitational constant
i	link or joint number
I_i	moment of inertia of the link
$\mathbf{J}_{\omega i}$	Jacobian transfer matrix
$\mathbf{J}_{vGi}$	Jacobian transfer matrix
$\mathbf{K}$	stiffness matrix
k	joint stiffness
l_i	axial coordinate for the centroid of the link
$\mathbf{M}$	inertia matrix
m_l	mass of the link
M_{ii}	component ii of the corresponding matrix
n	number of links

Nomenclature

$\mathbf{p}$	joint coordinate
$\mathbf{Q}$	posture coordinate (angular)
$\dot{\mathbf{Q}}$	posture angular velocity
$\ddot{\mathbf{Q}}$	posture angular acceleration
$\mathbf{q}$	local coordinate (angular)
$\dot{\mathbf{q}}$	local angular velocity
$\ddot{\mathbf{q}}$	local angular acceleration
$\mathbf{R}_{o}^{i}$	Rotation matrix
S_i	sine of the posture angle
S_{i+j}	sine of the sum of posture angle $\mathbf{Q}_i$ and $\mathbf{Q}_j$
$\mathbf{T}_{Gi}$	transformation matrix

ACKNOWLEDGEMENTS

I would sincerely like to thank Dr. Marek Kujath for his guidance, support, motivation and patience. Without his support, both educationally and financially through research grants and teaching positions, it would not have been possible for me to have publish this work.

Dr. Kefu Liu's guidance at the beginning and end of this work was instrumental in helping generate the focus of this thesis.

Dr. Ted Hubbard supported this work both as a member of the guiding committee and the graduate coordinator. His help in placements as a teaching assistant was greatly appreciated.

I also want to acknowledge graduate students in the department. They had a willingness to discuss and help with the completion of this thesis.

All the staff in the engineering department, including Cathy Wood, Felix Roma, Angus MacPhearson, Antonio Beneficia and Peter Jones, need to be acknowledged for their support.

ABSTRACT

The author investigates the dynamics of very flexible manipulator structures and studies modes of vibrations for a wide range of manipulator postures. The study includes postures for which vibration modes become decoupled by the manipulator joints, i.e. individual modes involve only motion of a single joint. The research originated from a study of dynamics of large space manipulators that are very flexible and that on earth cannot support their own weight. The reported study is based on a theoretical analysis, but focuses on an experimental verification of the theoretical findings using scaled down physical models of space manipulators. The models exhibit similar dynamic properties similar to the space manipulators including very low natural frequencies. The physical models were designed, fabricated and tested. A low frequency harmonic exciter was also designed and fabricated. The non-contact lab measurements were based on video image processing. A photo-geometric method was adapted from Scion Image and ATI Capture. The experimental data were compared with computer simulated results.

CHAPTER 1

INTRODUCTION

1.1 **Background**

Space manipulators are designed to have a large range of reach and they are used to execute similar tasks that construction cranes, on earth, perform. Because in space there are essentially no gravity forces, the manipulators are designed as very long flexible objects. Due to the flexibility and length of these manipulators, they exhibit long lasting free oscillations at very low frequencies especially while handling payloads. The manipulators are mounted on space structures or space vehicles that experience constant vibrations due to attitude and orbit adjustments, crew movements, electric motor motion, etc. Effective control of the manipulators is necessary, but challenging to obtain due to the flexibility. Therefore, a detailed knowledge of the dynamics of the space manipulator structure that is attached to a vibrating base is very important. Understanding the dynamics will allow for more effective control.

This reported study uses physical and numerical models to simulate flexible manipulators for practical and economical reasons.

1.2 **Physical Methods of Simulating Space Manipulators**

Numerous methods have been used to physically model structures that behave as if they are free of the effects of gravity. The following table includes some of these

methods and their advantages and disadvantages.

Method	Advantages	Disadvantages
Test model placed in liquid (ex. water) [1]	The liquid helps support the weight of the model and allows for low frequency vibration. 3-D testing is possible.	The damping is very high. All equipment must be submerged.
Long cables that hang from above and support the weight of the test model [2]	Easy and inexpensive.	The cables need to be very long to limit their effects. Only 2-D testing possible. High bay needed.
Test model floating on bed of air (similar to an air hockey table) [3]	Easy access Small safety hazards	Expensive. Added masses of the air floaters. Only 2-D testing possible.
Passive Constant Force Mechanism [4]	With long enough cables 3-D motion is possible. If large enough a full-scale model could be tested.	Expensive. Added inertia, stiffness and damping.

1.3 **Flexible Space Manipulators**

Most of the work that has been done flexible space structures has centered on the dynamics of motion of these structures and control issues [5]. Time varying studies [6] have also been done based on dynamic forces of the manipulator. How adding a payload to the end of a space manipulator effects attitude controlled satellites [7] and 'free

floating' satellites [8] has also received attention [9]. This thesis studies the effects of base vibrations on space manipulators in a constant posture. Mobile manipulators affected by base vibrations have been studied [10], but not expanded to outer space.

1.4 **Scope of the Project**

The scope of the project involves the following:

- Design, fabrication and testing of a scale model of a space manipulator structure that would have the 'free space' quality of motion in 2-D i.e. gravity not affecting the dynamics of the structure. The manipulator is based in the horizontal plane.
- Design of a low frequency harmonic exciter for frequencies below 3 Hz.
- Design and integration of an economically feasible optometric system for non-contact measurements.
- Development of mathematical model for vibrating manipulators in a plane.
- Numerical simulation of the dynamic behavior of manipulators for wide ranges of postures.

1.5 **Objectives of the Thesis**

The objectives of the thesis are as follows:

1. To study the modes of vibrations of a flexible manipulator that varies their geometric

posture over a very large range.

2. To investigate the possibility of mode separation by the manipulator joints (individual modes involving only a single joint).
3. To design and fabricate a physical model that represents a space manipulator in planar motion with minimal damping.
4. To design a low frequency harmonic exciter with a high harmonic fidelity.
5. To develop and fabricate a non-contact method of measuring motion of a very delicate model
6. To integrate a laboratory setup that would include sensors, manipulator and software.
7. To develop mathematical models for the study of physical model motion.
8. To investigate experimentally, numerically, and analytically properties of flexible structures that vary their geometric postures.

1.6 **Layout of the Thesis**

The main body of the thesis is essentially divided into three parts. The first part is contained in Chapter 2, which deals with development of the theory. The second part is contained in Chapters 3 and 4, which deal with design and experimentation of the physical model. The third part, which is in Chapter 5, deals with numerical simulation.

The thesis ends with Chapter 6, conclusions and recommendations for extending the research. Figures are found at the end of each chapter. The Appendices contain long derivations, simulation files, calculations and parameters.

CHAPTER 2

THEORETICAL ANALYSIS

2.1 Introduction

This chapter deals with the derivation of equations of vibratory motion for a slender manipulator. The derivation is based on separation of coordinates: posture coordinates for changing the posture and local coordinates for the elastic oscillations. It is assumed that the elastic motion takes part only in the joints.

2.2 Equations of Motion

The derivation of the inertia and inertia terms in the equations of the motion is based on a procedure outlined by Spong and Vidyasager [11]. In this study, the motion coordinates are separated into two parts. The two separated motion coordinates components are: (1) geometrically large posture motion coordinates **Q** and (2) small oscillatory motion coordinates **q**. A total coordinates is a sum of **Q** and **q**. The assignment of coordinates is illustrated in Figure 2.1. The derivation of the equation of motion was part of this project and details of it are collected in Appendix I. In this study the oscillation of the arm **q** is studied when the posture is not changing. The equation of motion is of the following form:

$$\mathbf{M}\ddot{\mathbf{q}} + \mathbf{A}\dot{\mathbf{q}} + \mathbf{C}\dot{\mathbf{q}} + \mathbf{K}\mathbf{q} = 0 \qquad (2.1)$$

M is the inertia matrix, **A** is the Coriolis and centrifugal effect matrix, **C** is the damping matrix and **K** is the stiffness matrix. The angular accelerations, velocities and displacements are represented by the vectors $\ddot{\mathbf{q}}$, $\dot{\mathbf{q}}$ and **q** respectively.

The following list of terms represents the matrix components:

$$M_{11}= m_1 l_1^2 + m_2(a_1^2 + l_2^2 + 2a_1 l_2 C_2) + m_3(l_3(l_3 + a_2 C_3 + a_1 C_{2+3}) + a_2(l_3 C_3 + a_2 + a_1 C_2) + a_1(l_3 C_{23} + a_2 C_2 + a_1)) + I_1 + I_2 + I_3 \quad (2.2)$$

$$M_{12} = M_{21} = m_2(l_2^2 + a_1 l_2 C_2) + m_3(l_3(l_3 + a_2 C_3 + a_1 C_{2+3}) + a_2(l_3 C_3 + a_2 + a_1 C_2)) + I_2 + I_3 \quad (2.3)$$

$$M_{13} = M_{31} = m_3(l_3(l_3 + a_2 C_3 + a_1 C_{2+3})) + I_3 \quad (2.4)$$

$$M_{22} = m_2 l_2^2 + m_3 a_2^2 + m_3 l_3^2 + 2m_3 a_2 l_3 C_3 + I_2 + I_3 \quad (2.5)$$

$$M_{23} = M_{32} = m_3 l_3^2 + m_3 a_2 l_3 C_3 + I_3 \quad (2.6)$$

$$M_{33} = m_3 l_3^2 + I_3 \quad (2.7)$$

$$A_{11} = (-m_2 a_1 l_2 S_2 - m_3 a_1 l_3 S_{23} - m_3 a_1 a_2 S_2)\dot{q}_2 + (-m_3 a_2 l_3 S_3 - m_3 a_1 l_3 S_{23})\dot{q}_3 \quad (2.8)$$

$$A_{12} = (-m_2 a_1 l_2 S_2 - m_3 a_1 a_2 S_2 - m_3 a_1 l_3 S_{23})\dot{q}_1 + (-m_2 a_1 l_2 S_2 - m_3 a_1 a_2 S_2 - m_3 a_1 l_3 S_{23})\dot{q}_2 + (-m_3 a_2 l_3 S_3 - m_3 a_1 l_3 S_{23})\dot{q}_3 \quad (2.9)$$

$$A_{13} = (-m_3 a_2 l_3 S_3 - m_3 a_1 l_3 S_{23})\dot{q}_1 + (-m_3 a_2 l_3 S_3)\dot{q}_3 \quad (2.10)$$

$$A_{21} = (-m_2 a_1 l_2 S_2 - m_3 a_1 a_2 S_2 - m_3 a_1 l_3 S_{23})\dot{q}_1 + \tfrac{1}{2}(-m_3 a_1 l_3 S_2 - m_3 a_1 a_2 S_2)\dot{q}_2 + (-m_3 a_2 l_3 S_3)\dot{q}_3 \quad (2.11)$$

$$A_{22} = (-m_3 a_2 l_3 S_3)\dot{q}_3 \tag{2.12}$$

$$A_{23} = (-m_3 a_2 l_3 S_3)\dot{q}_1 + (-m_3 a_2 l_3 S_3)\dot{q}_2 + (-m_3 a_2 l_3 S_3)\dot{q}_3 \tag{2.13}$$

$$A_{31} = (-m_3 a_2 l_3 S_3 - m_3 a_1 l_3 S_{23})\dot{q}_1 + (-m_3 a_2 l_3 S_3)\dot{q}_2 \tag{2.14}$$

$$A_{32} = (-m_3 a_2 l_3 S_3)\dot{q}_1 + (-m_3 a_2 l_3 S_3)\dot{q}_2 \tag{2.15}$$

$$A_{33} = 0 \tag{2.16}$$

$$C_{11} = 2\xi\sqrt{M_{11}K_{11}} \tag{2.17}$$

$$C_{22} = 2\xi\sqrt{M_{22}K_{22}} \tag{2.18}$$

$$C_{33} = 2\xi\sqrt{M_{33}K_{33}} \tag{2.19}$$

$$C_{12} = C_{21} = C_{13} = C_{31} = C_{23} = C_{32} = 0 \tag{2.20}$$

$$K_{11} = K_{22} = K_{33} = k \tag{2.21}$$

$$K_{12} = K_{21} = K_{13} = K_{31} = K_{23} = K_{32} = 0 \tag{2.22}$$

$$C_2 = \cos(Q_2) \tag{2.23}$$

$$C_3 = \cos(Q_3) \tag{2.24}$$

$$S_2 = \sin(Q_2) \tag{2.25}$$

$$S_3 = \sin(Q_3) \tag{2.26}$$

$$C_{2+3} = \cos(Q_2 + Q_3) \tag{2.27}$$

$$S_{2+3} = \sin(Q_2 + Q_3) \tag{2.28}$$

where a_i is the length of the link, l_i is the axial coordinate for the centroid of the link, I_i is

the central mass moment of inertia, m_i is the link's mass, ξ is the joint damping ratio, and k is the joint stiffness. A complete derivation can be found in Appendix I.

The force from the motion of the base link is known as the kinematic excitation. The kinematic excitation is the force of the products of the first link's (1) inertia parameters and acceleration, (2) Coriolis and centrifugal forces and of (3) the product of the stiffness parameters and displacement. Moving the kinematic excitation to the driving force side of the equation leaves a series of 2 x 2 matrices that contain the system parameters for a two-degree of freedom system. By expanding the Coriolis and Centrifugal forces and reorganizing back to the original form it is possible to write

$$A_{22} = -2m_3a_2l_3S_3(\dot{q}_3) \tag{2.29}$$

$$A_{23} = -m_3a_2l_3S_3(\dot{q}_3) \tag{2.30}$$

$$A_{32} = 2m_3a_2l_3S_3(\dot{q}_2) \tag{2.31}$$

$$A_{33} = 0 \tag{2.32}$$

where A_{22} from Eq. (2.29) now becomes A_{11} in the newly formed 2x2 Coriolis and Centrifugal matrix. The terms A_{23}, A_{32} and A_{33} similarly become A_{12}, A_{21} and A_{22} respectively in the newly formed 2x2 Coriolis and Centrifugal matrix.

The Coriolis force is now represented by $A_{22}\,\dot{q}_2$. The terms $A_{23}\,\dot{q}_3$ and $A_{32}\,\dot{q}_2$ represent the centrifugal forces. In 2-DOF terms the Coriolis force is represented by $A_{11}\,\dot{q}_1$. The terms $A_{12}\,\dot{q}_2$ and $A_{21}\,\dot{q}_1$ represent the centrifugal forces.

$$A = \begin{bmatrix} A_{11}\dot{q}_1 & A_{12}\dot{q}_2 \\ A_{21}\dot{q}_1 & 0 \end{bmatrix} \tag{2.33}$$

Note that the equations of motion are dynamically coupled by the inertia matrix **M** and the Coriolis and centrifugal matrix **A**. To decouple the matrix the off-diagonal terms have to vanish [12]. The matrices **C** and **K** are diagonal for the chosen set of coordinates and therefore they do not couple the equations of motion.

2.3 **Decoupled Modal Vibration**

Selection of a proper posture of the arm diagonalizes the inertia matrix **M** in Equation (2.1). For the system parameters listed in Appendix I this occurs when Q_2 = 131.38 degrees (see Appendix III for calculations). For most of the range of the manipulator postures all joints take part in modal motion (resonance). The diagonalization of the inertia matrix is the major factor in limiting the vibration to only a single joint for each mode of vibration. The equations of motion are almost decoupled when diagonalizing the inertia matrix. There is still some coupling caused by the centrifugal and Coriolis terms. The decoupling posture angle Q_2 was located using a spreadsheet and varying Q_2 until the diagonal terms of the inertia matrix were relatively negligible. Eigen vectors and mode shapes gave the same results in locating the decoupling posture angle Q_2 for the given parameters (see Appendix II).

This suggests that there are two distinct vibration modes in terms of local joint

coordinates $\mathbf{q}$. In the first mode the lower and upper arm oscillate as a single rigid body with the lower arm angle $\mathbf{q}_1$ oscillating and the upper arm angle $\mathbf{q}_2$ remaining unchanged (see Figure 2.2 for illustration.). In the second mode the lower arm angle remains unchanged, therefore the lower arm does not move and the upper arm moves with the angle $\mathbf{q}_2$ oscillating (see Figure 2.3 for illustration).

Inserting values for the system parameters, and assuming negligible damping, the decoupled equations have the following form for free vibration:

$$\begin{bmatrix} 9.93 & 0 \\ 0 & 3.28 \end{bmatrix} (10^{-3})\,\ddot{\mathbf{q}} + \begin{bmatrix} -7.46\,\dot{q}_2 & -3.73\,\dot{q}_2 \\ 3.73\,\dot{q}_1 & 0 \end{bmatrix} (10^{-4})\,\dot{\mathbf{q}} + 0.326 \begin{bmatrix} 1 & 0 \\ 0 & 1 \end{bmatrix} \mathbf{q} = 0. \qquad (2.34)$$

The equation formed by the top line of Equation 2.31 is a function of $\mathbf{q}_1$ and its first two time derivatives and $\dot{\mathbf{q}}_2$. The equation formed by the bottom line of Equation (2.34) is a function of $\mathbf{q}_2$ and its first two time derivatives and $\dot{\mathbf{q}}_1$. Only the joint velocities couple these two equations. The main coordinate (acceleration, velocity and displacement) of an equation is the coordinate associated with the diagonal term of the inertia and stiffness matrices, i.e., for the top line of the equation $\mathbf{q}_1$ is the main coordinate. The coriolis matrix **A** is not constant, but it is a function of velocity products. The coupling velocity-terms involve other velocities than the main coordinate velocity. The off diagonal terms of the matrix **A** still couple the two equations, but have very little effect on the motion because:

1. They are proportional to velocities which for very flexible manipulators are small.
2. The velocities of the coupling coordinates become smaller when the inertia and stiffness matrices are diagonal because the main coordinates significantly dominate the vibration modes. The inertial forces and Coriolis and centrifugal forces were plotted to demonstrate the domination of the inertial forces on the system (see Figure 2.4)
3. When the entries of the matrix **A** are multiplied by the velocity vector $\dot{\mathbf{q}}$ they produce squares of the coupling velocities making the results even smaller. The diagonal terms represent the Coriolis terms and the off-diagonal represent the centrifugal forces.

Hence an assumption can be made that the terms of matrix **A** approach zero and the equation of motion can be linearized. Experimental and simulated results verified this assumption.

Assuming the matrix **A** approaches to zero the two equations of motion become

$$.00993\ \ddot{\mathbf{q}}_1 + 0.326\ \mathbf{q}_1 = 0 \tag{2.35}$$

and

$$.00328\ \ddot{\mathbf{q}}_2 + 0.326\ \mathbf{q}_2 = 0 \tag{2.36}$$

From these equations the two natural frequencies are calculated to be 0.911 Hz and 1.59 Hz (see Appendix IV for calculations).

All the natural frequencies of the joint angle Q_2 varying from 0 degrees to 180 degrees were calculated at 1 degree steps (see Figure 2.4 for plot and Appendix II for the M-File).

2.4 Variations of Derivations

Using energy methods and the same coordinate system **Q** and **q** produces the same equations of motion as Equation (2.1) and its subsequent parameters (Eq. (2.2) – Eq. (2.28)). The equations can be found in the Ph.D. thesis "Vibrations of Time-Varying Mechanical Systems" presented in 1993 [6].

Another derivation was done using absolute coordinates. These coordinates were transferred into the same coordinates used in the body of this thesis by means of a Jacobian transfer giving the same results. This derivation is found in Appendix IV.

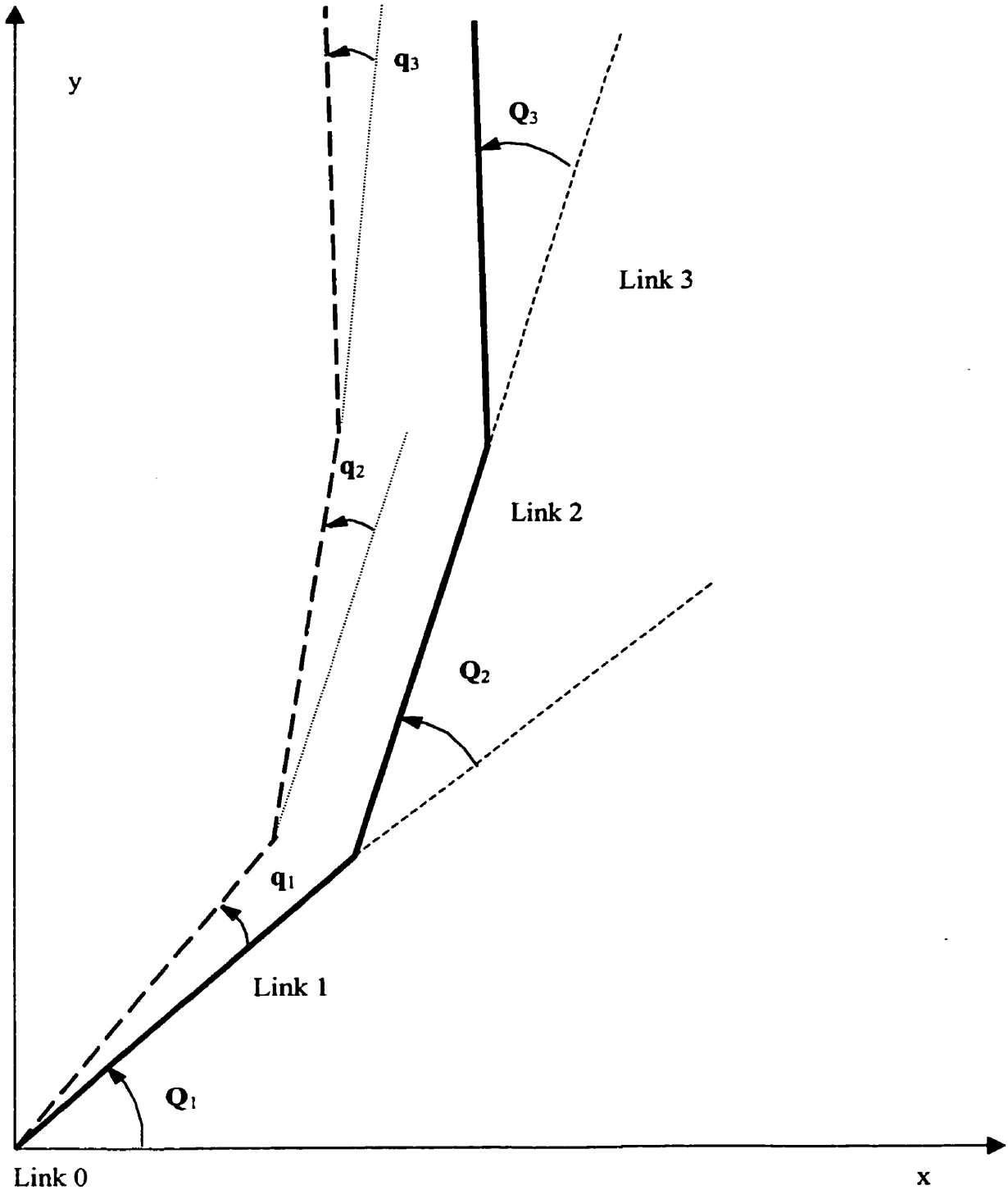

Figure 2.1: The assignment of coordinates. Motion coordinates **q** and posture coordinates **Q**.

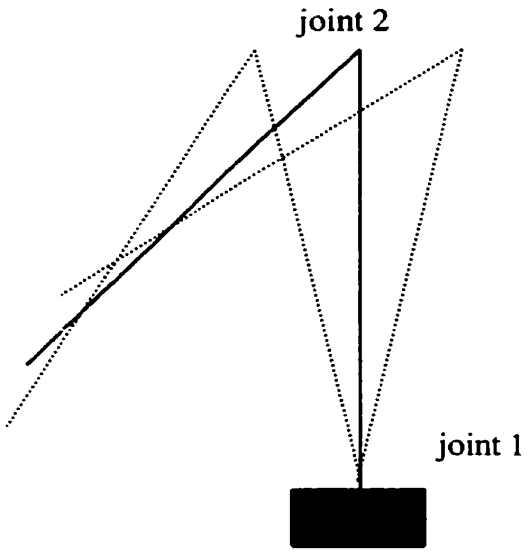

Figure 2.2: The first decoupled mode: only joint 1 flexes.

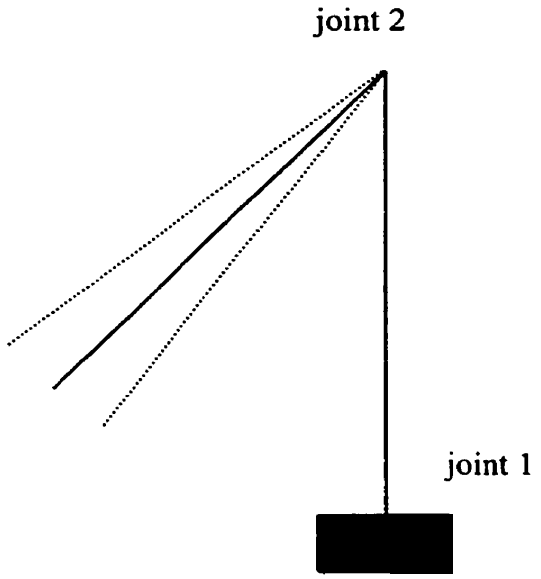

Figure 2.3: The second decoupled mode: only joint 2 flexes.

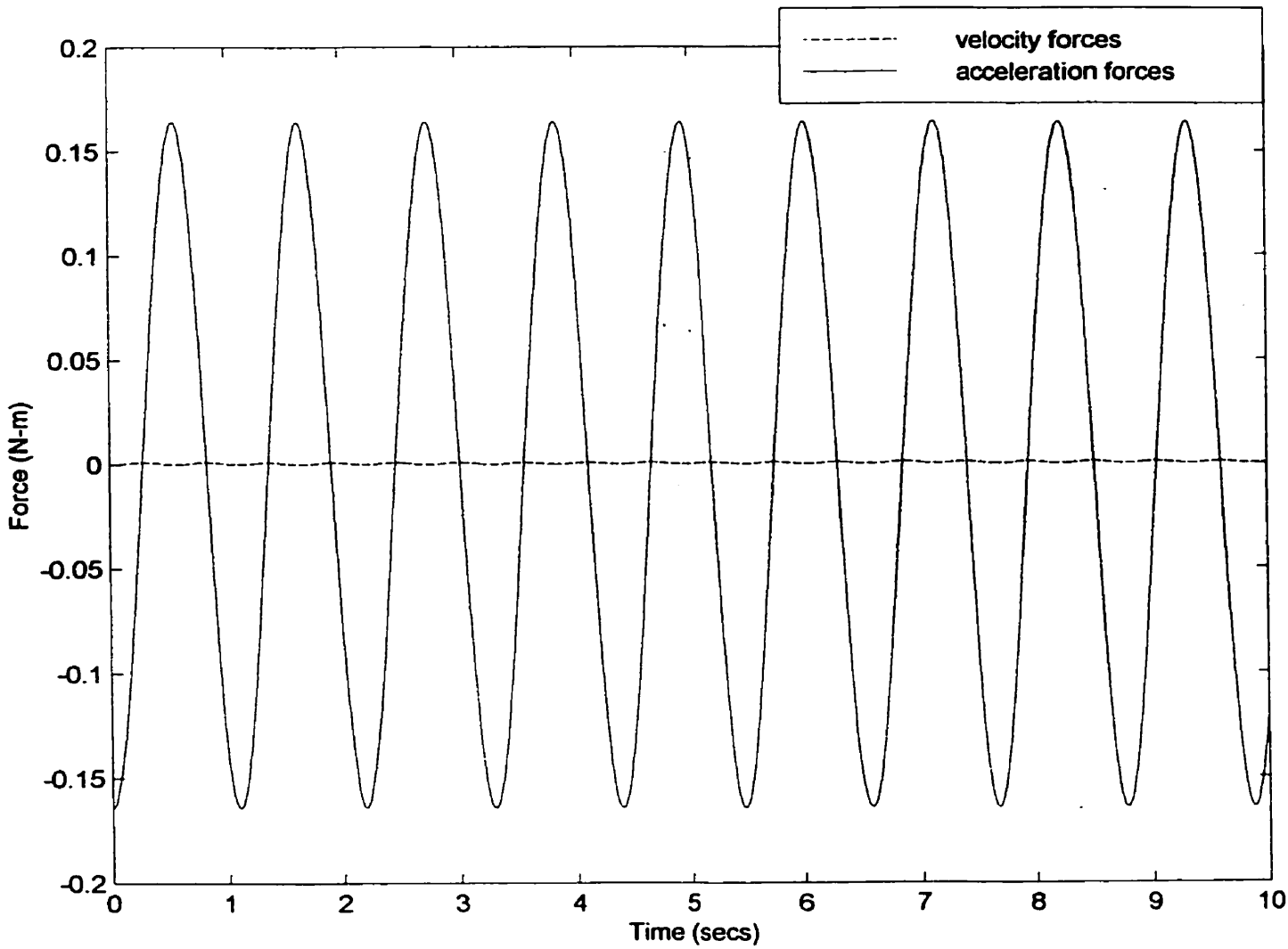

Figure 2.4: Comparison of acceleration forces and velocity forces.

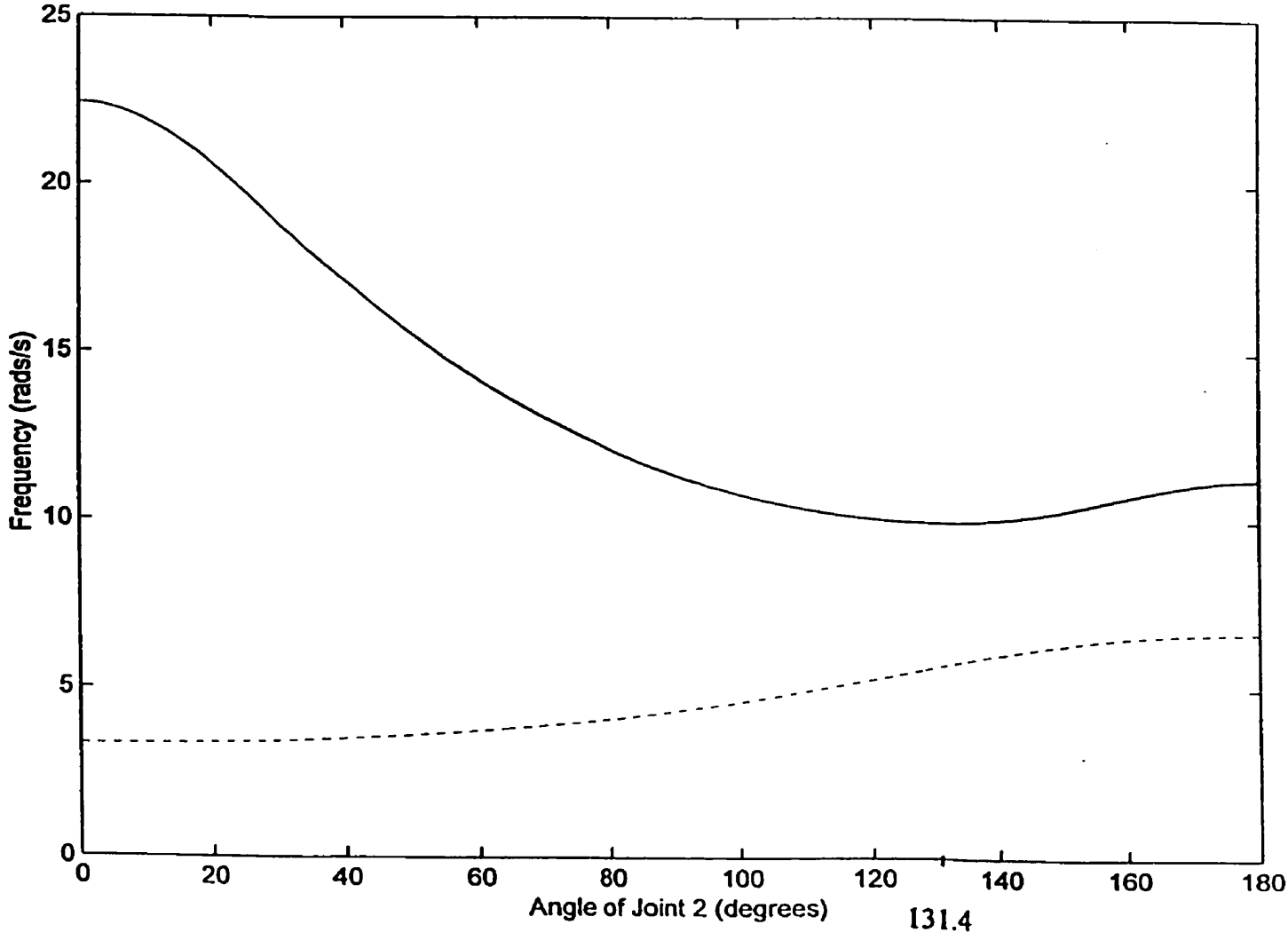

Figure 2.5: Variation of natural frequecies for varying posture angle Q_2. Where 131.4^0 is the angle of posture which decouples the inertia matrix.

CHAPTER 3

DESIGN OF THE PHYSICAL MODEL

3.1 Design Criteria

To verify the theoretical studies a laboratory experiment was conducted. To facilitate the experiments a physical model of a space manipulator was developed. The objective was to build a physical model that is flexible, lightly damped, has adjustable posture and produces vibratory motion that is not affected by gravitational forces.

The concept of the design was to build a self-supporting structure. The links were to support the weight of the system. They were to be measurably stiffer than the joints. The joints were to support the weight as well, but they were to be flexible in the horizontal plane only. The damping of the joints was to be very light. To meet the criteria of very low damping the joints were designed with flat springs.

3.2 Joint Design

In order to model the flexibility of a manipulator joint a flat spring joint was used. The spring was mounted vertically with the edges pointing in the z-direction, i.e. the axis of rotation (See Figure 3.1). The spring was sufficiently rigid in the edge-on plane (x-z plane) so that its flexibility could be ignored in this direction. The flexibility of the joint was only in the x-y plane that was perpendicular to the spring's surface. This rigidity

provided the support of the weight of the arms in the vertical planes while allowing lightly damped motion, in the horizontal planes, free of gravitational forces. In this fashion, the weightlessness was simulated for motion in the x-y plane.

The flat springs were mounted in specially designed hinges (see Figures 3.2 and 3.3). The main functions of the hinges were the following: (1) to contain the springs, (2) to join the adjacent arms and (3) to allow alignment of the flat spring surfaces with the centroids of the arm. The flat springs needed to be aligned with the manipulator centroids to avoid their twisting. Hence, the first spring, supporting the lower arm was aligned with the combined centroid of the lower and upper arm. The second spring, supporting the upper arm, was aligned only with this arm's centroid. The static gravitational loads create only bending moments in the on-edge planes of the springs, i.e. the direction of their high rigidity.

The hinges were clamped to the ends of the flat springs using screws. The hinges were symmetrical along the vertical axis so as to not alter the moments of inertia when their alignment was changed.

The joint was designed with adjustable stops that would ensure that the displacements would not become so large that the bending in the springs would cause permanent deformation or damage. The hinges were made from aluminum. The flat springs were from rolled steel with a thickness of 0.2286 mm (9/1000 of an inch).

The spring constant for the flat spring showed little variation as experimental tests demonstrated for the ranges of +/- 0.17 radians encountered in this application. The spring constant was established experimentally, by applying known forces and measuring the spring displacement (see Figure 3.4). The results gave a spring constant of 0.326 N-m/rad (see Figure 3.5).

3.3 **Design of Links**

The links were designed to support the weight of the system and to be more than 800 times stiffer than the joints in the x-y plane. The dimensions of the links are shown in Figure 3.6. The connection of the links is shown in Figure 3.7.

3.4 **Design of Harmonic Exciter**

In order to excite the system low frequencies a yoke mechanism was designed. It was designed to have an adjustable stroke from 20 mm to 80 mm. The yoke mechanism involved a translational follower attached to a tension spring with a stiffness of 100 N/m this in turn was attached to the manipulator model's base, the first link (see Figure 3.8).

The yoke frame was made of aluminum. It included a round shaft supported by ball bearings. The round shaft had a flexible coupling on one end to attach it to a gearbox and motor. The opposite end of the radial shaft had a radial slot for attachment of a rectangular arm. The arm had a roller that drove the translational follower (see Figure

3.9). An old photocopier sliding frame was used as the follower. The yoke mechanism was clamped to the copier frame. The spring was sufficiently stiff to avoid separation due to acceleration forces, but flexible enough to ensure that the gearbox and motor provided enough torque in the yoke to maintain a constant angular velocity.

3.5 **Assembly of the Physical Model**

The assembly of the physical model involved three links and two joints. The first link was the base and it was clamped by a vice to a three point leveling board. A point mass was added to the end of the last link, link 2, to ensure the center of gravity is at the center of the link. This is due since the mass of the joints is equally divided among the connecting links. The dimensions of the leveling board are shown in Figure 3.10.

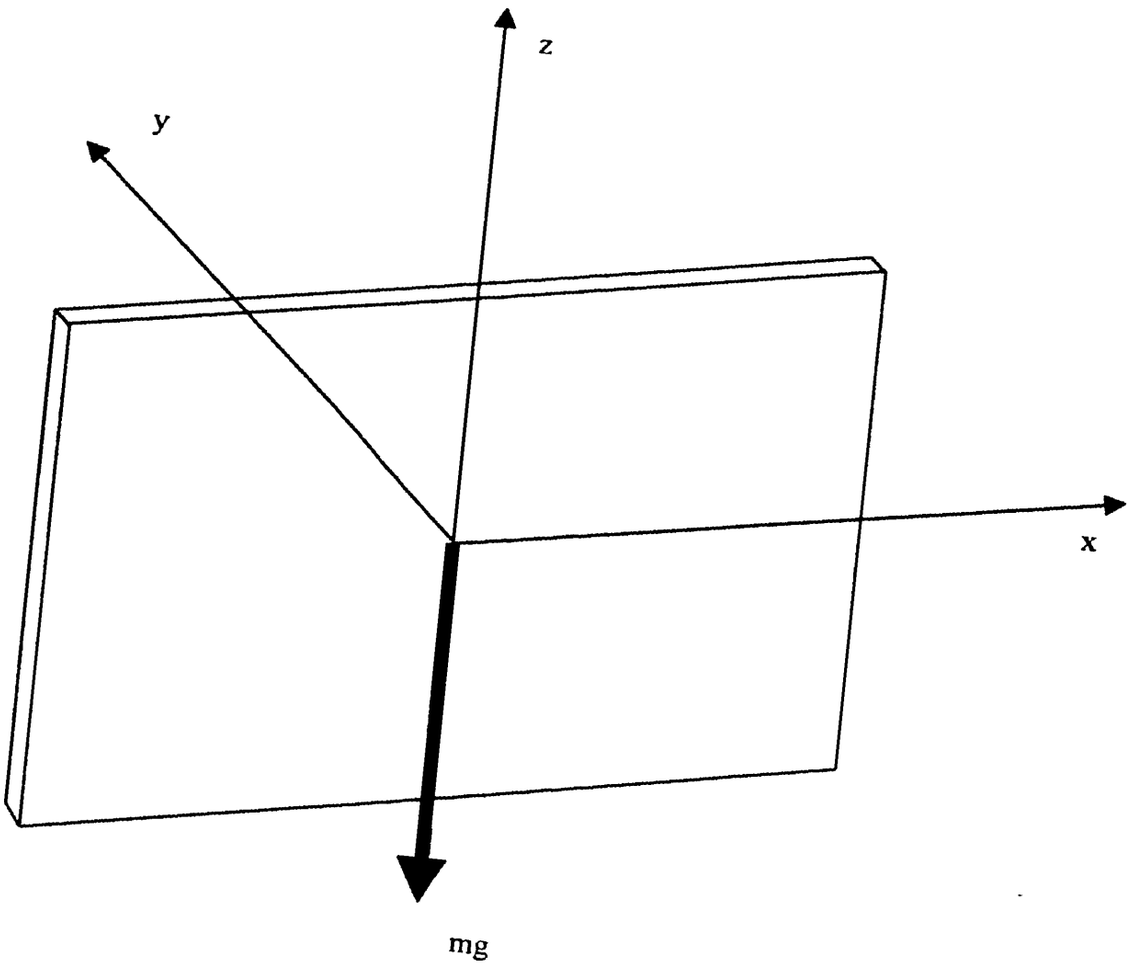

Figure 3.1: Orientation of the flat spring and gravitational forces

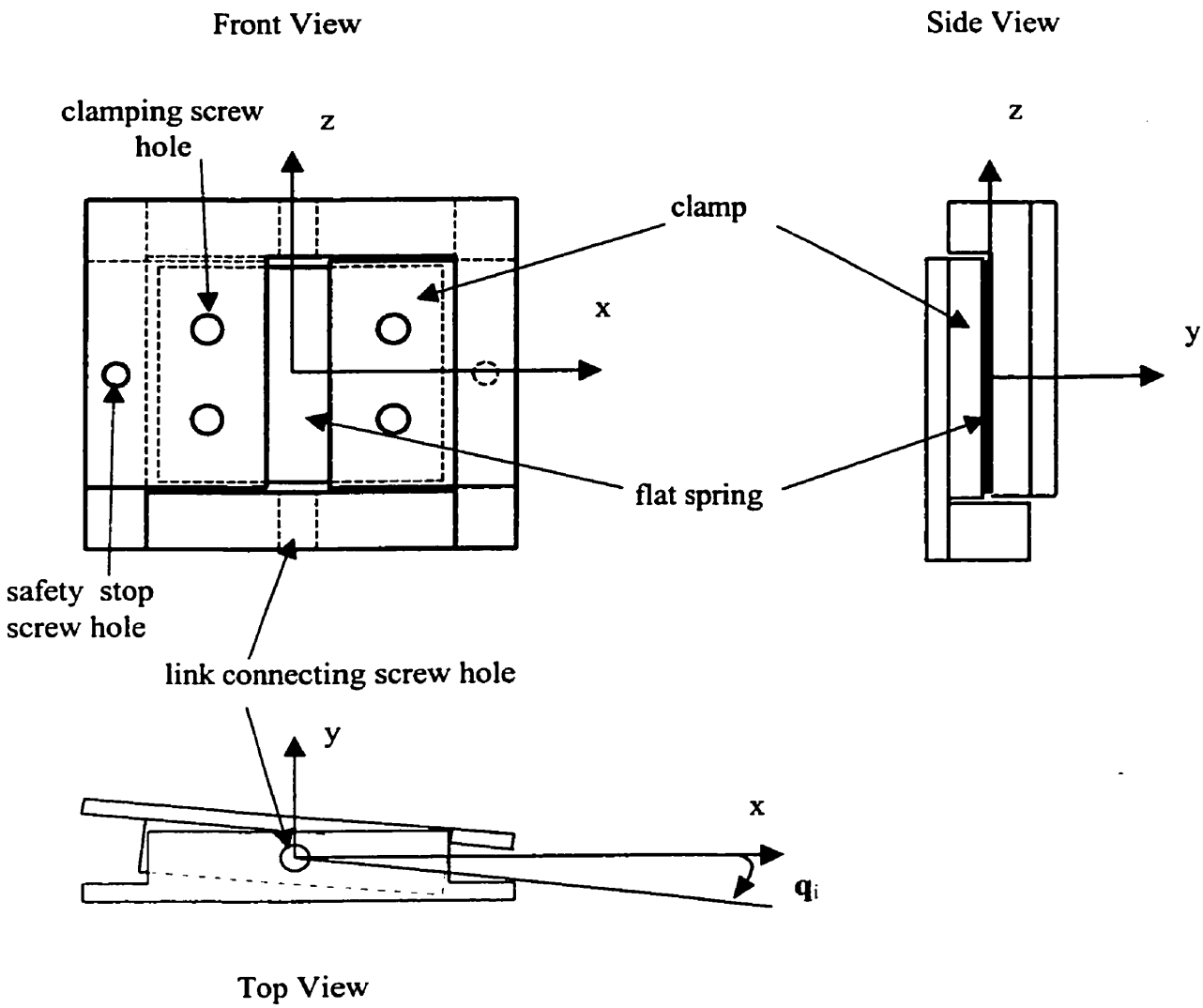

Figure 3.2: The design of the hinge joint.

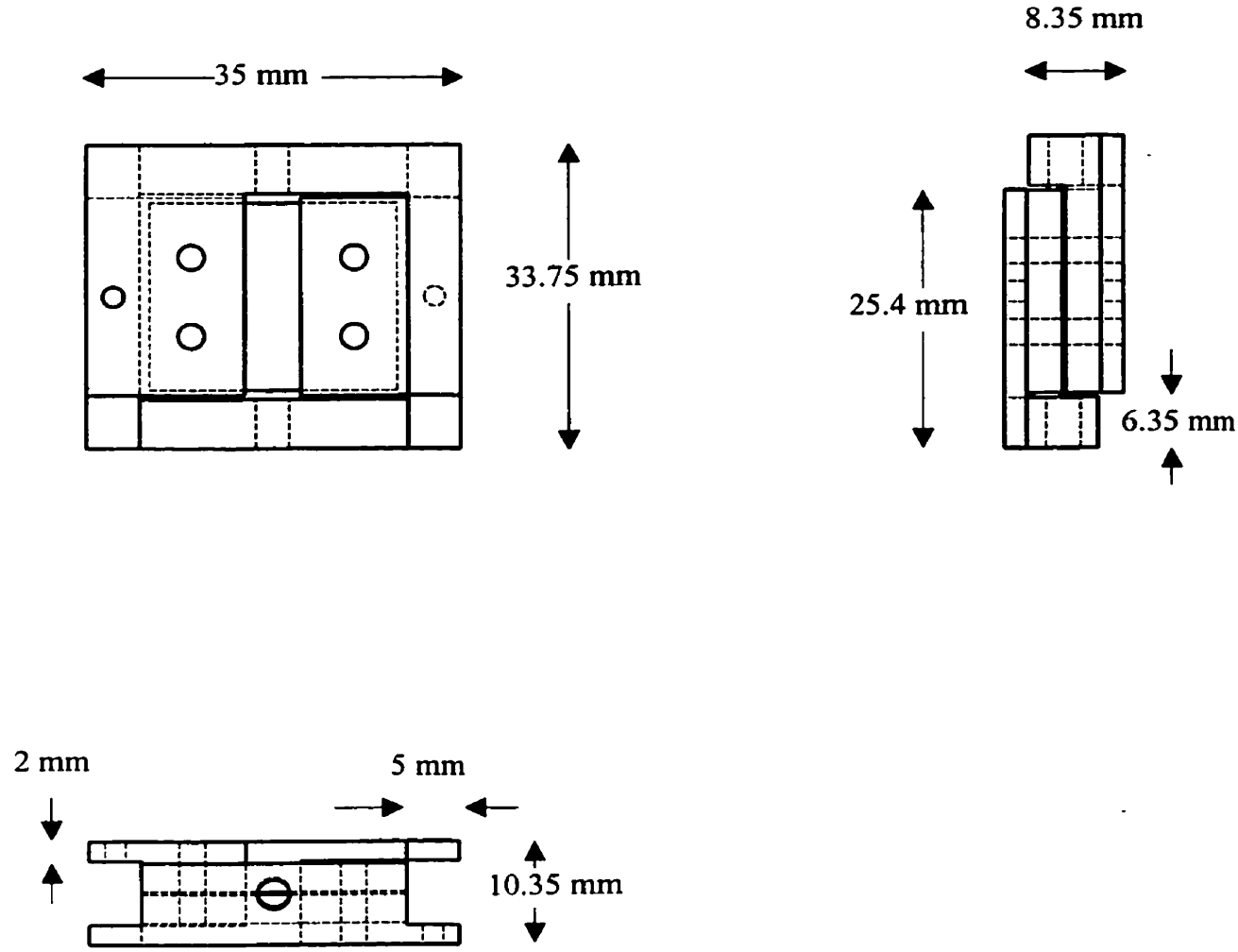

Figure 3.3: The dimensions of the hinge joint.

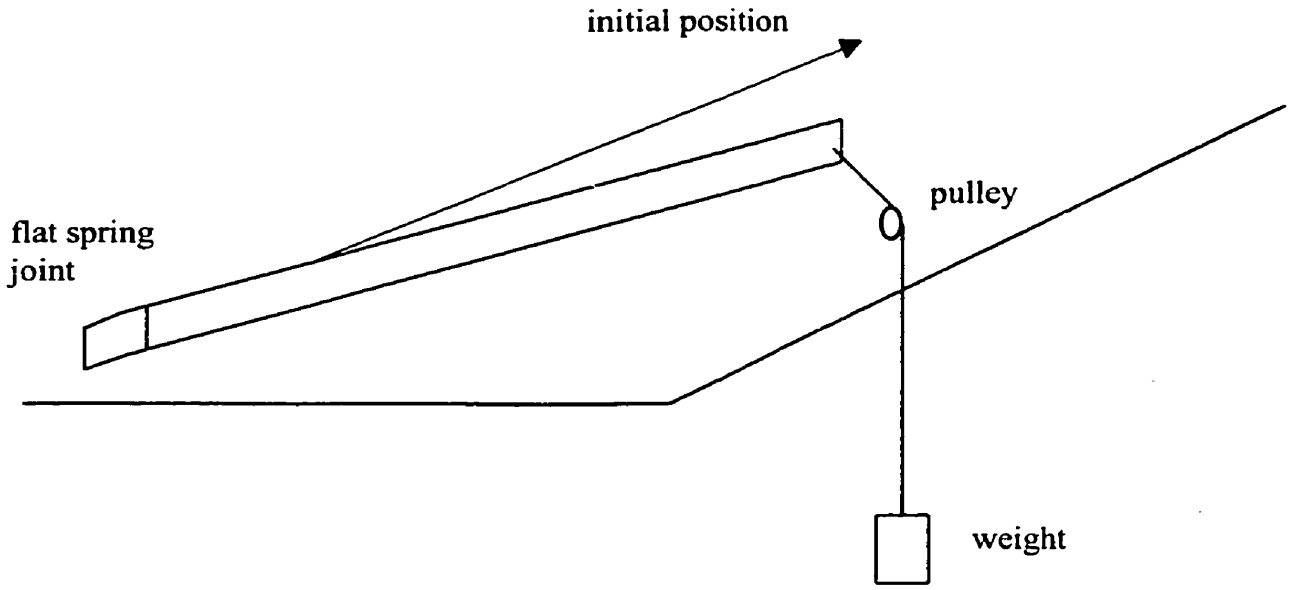

Figure 3.4: The setup for measuring the stiffness of a flat spring.

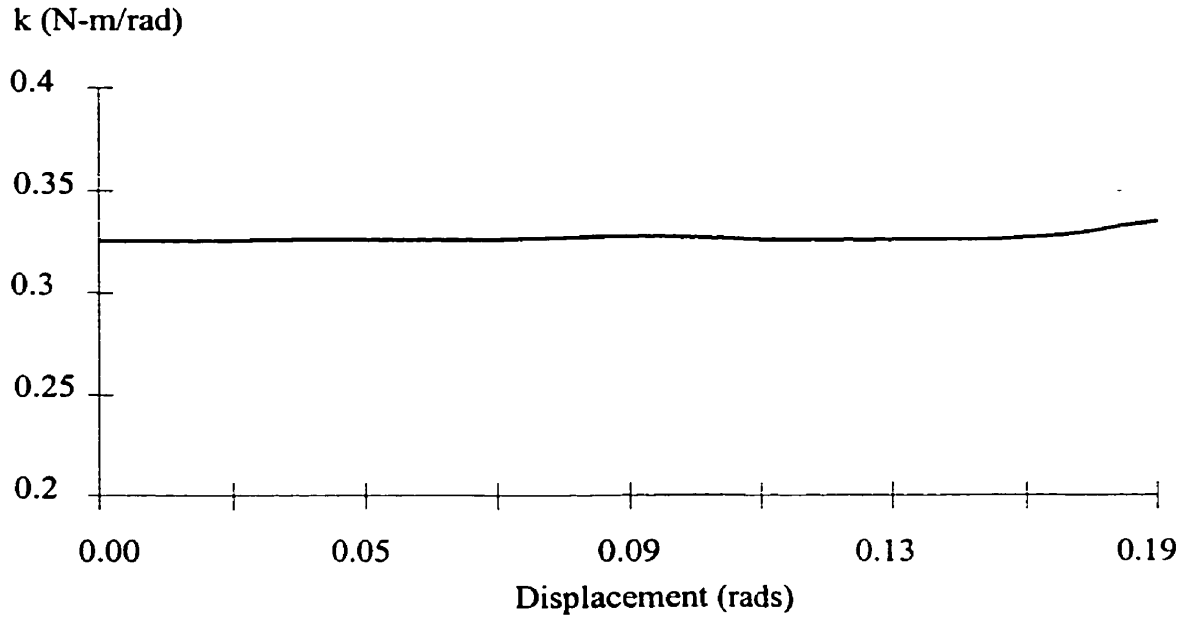

Figure 3.5: The stiffness of a flat spring vs. angle of displacement

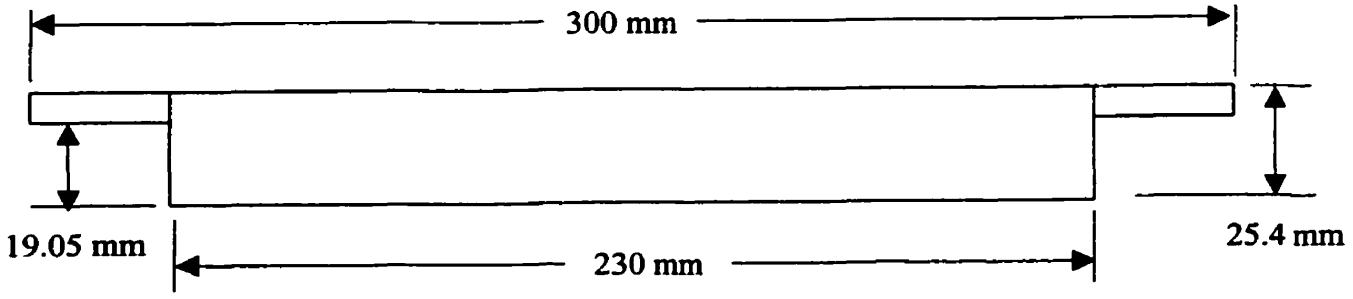

Front View

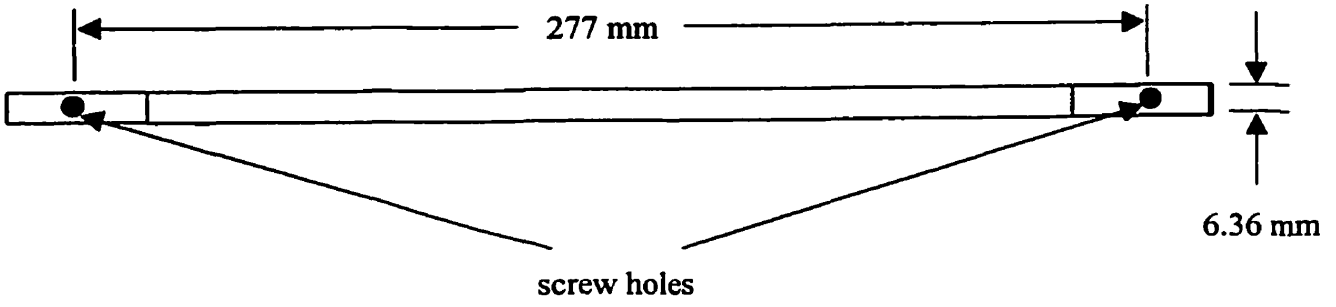

Bottom View

Figure 3.6: The Design of the links.

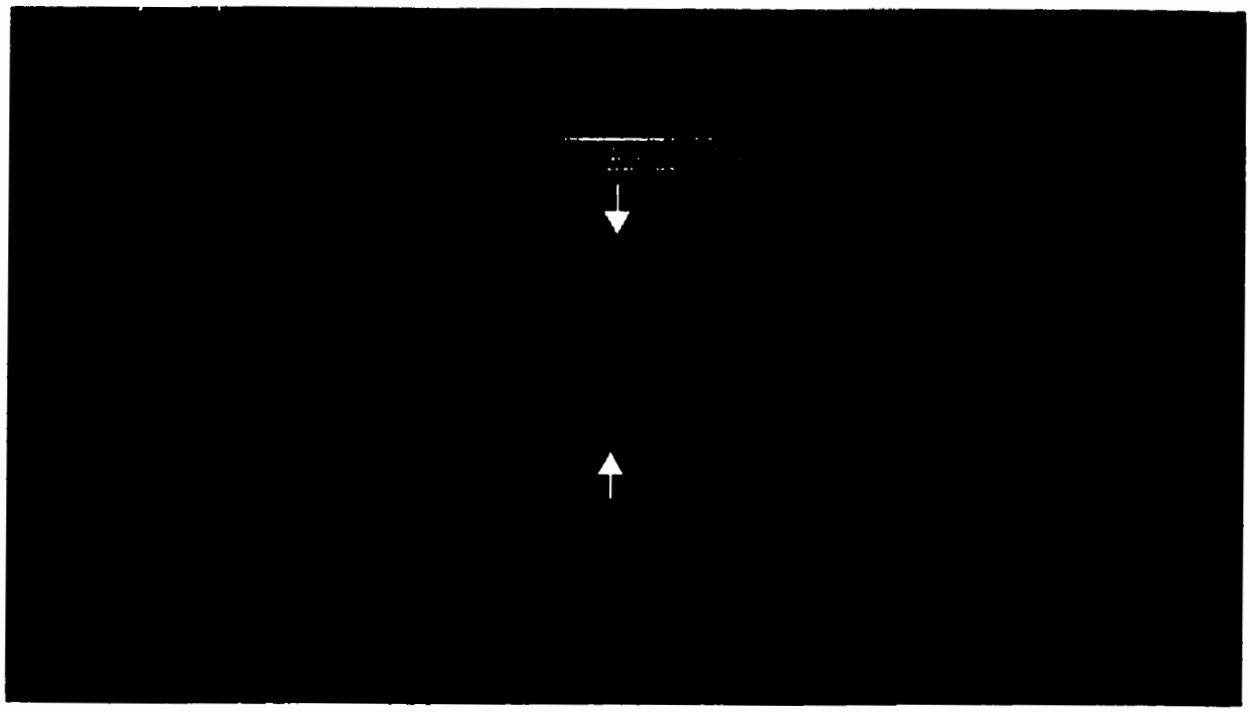

Figure 3.7: The connecting of links and joints

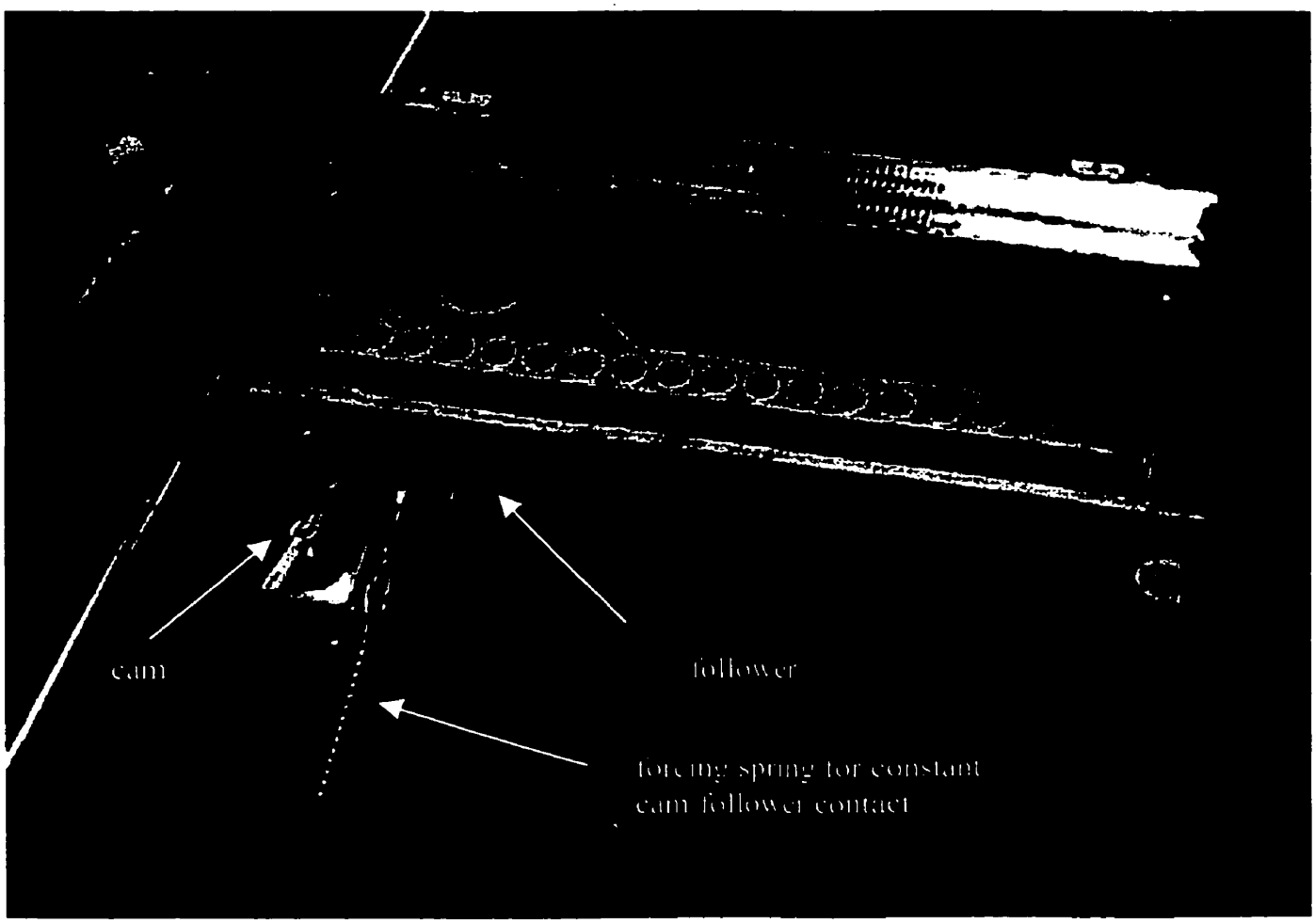

Figure 3.8: Harmonic excitor

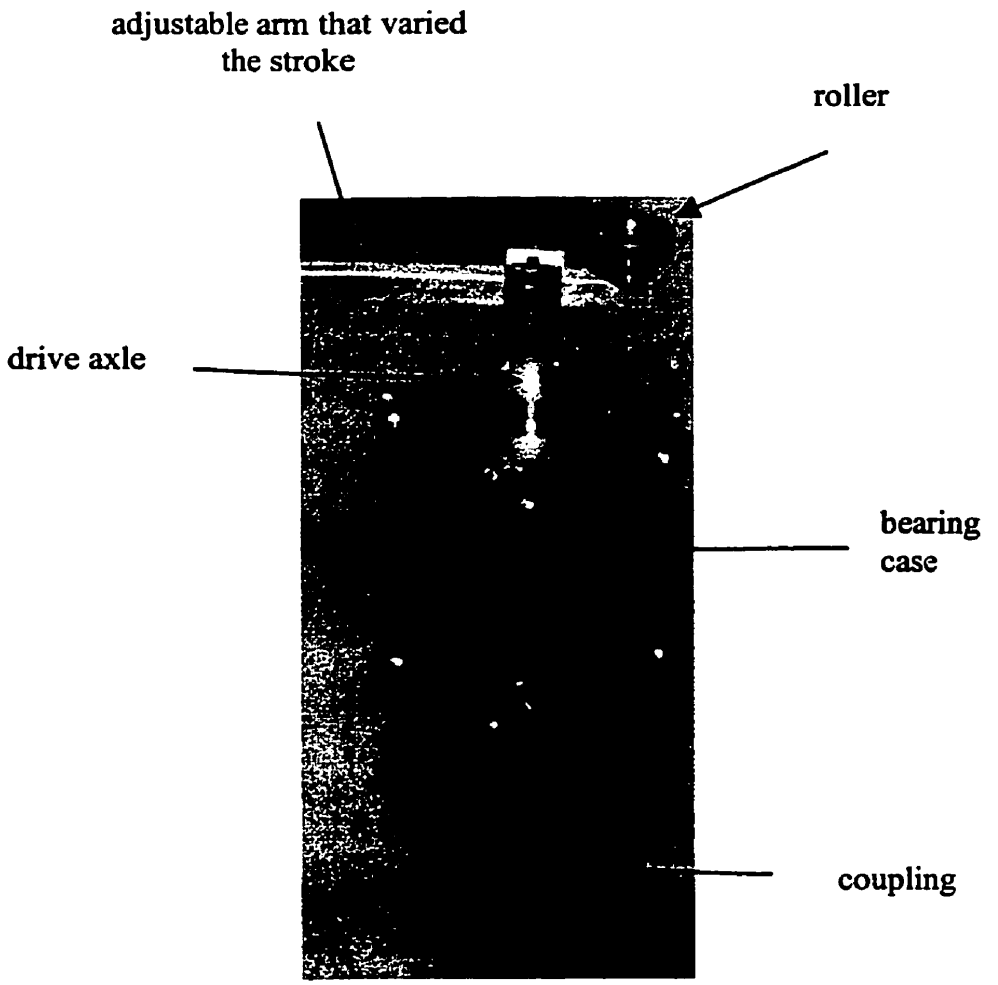

Figure 3.9: Yoke with variable stroke of 20mm to 80mm

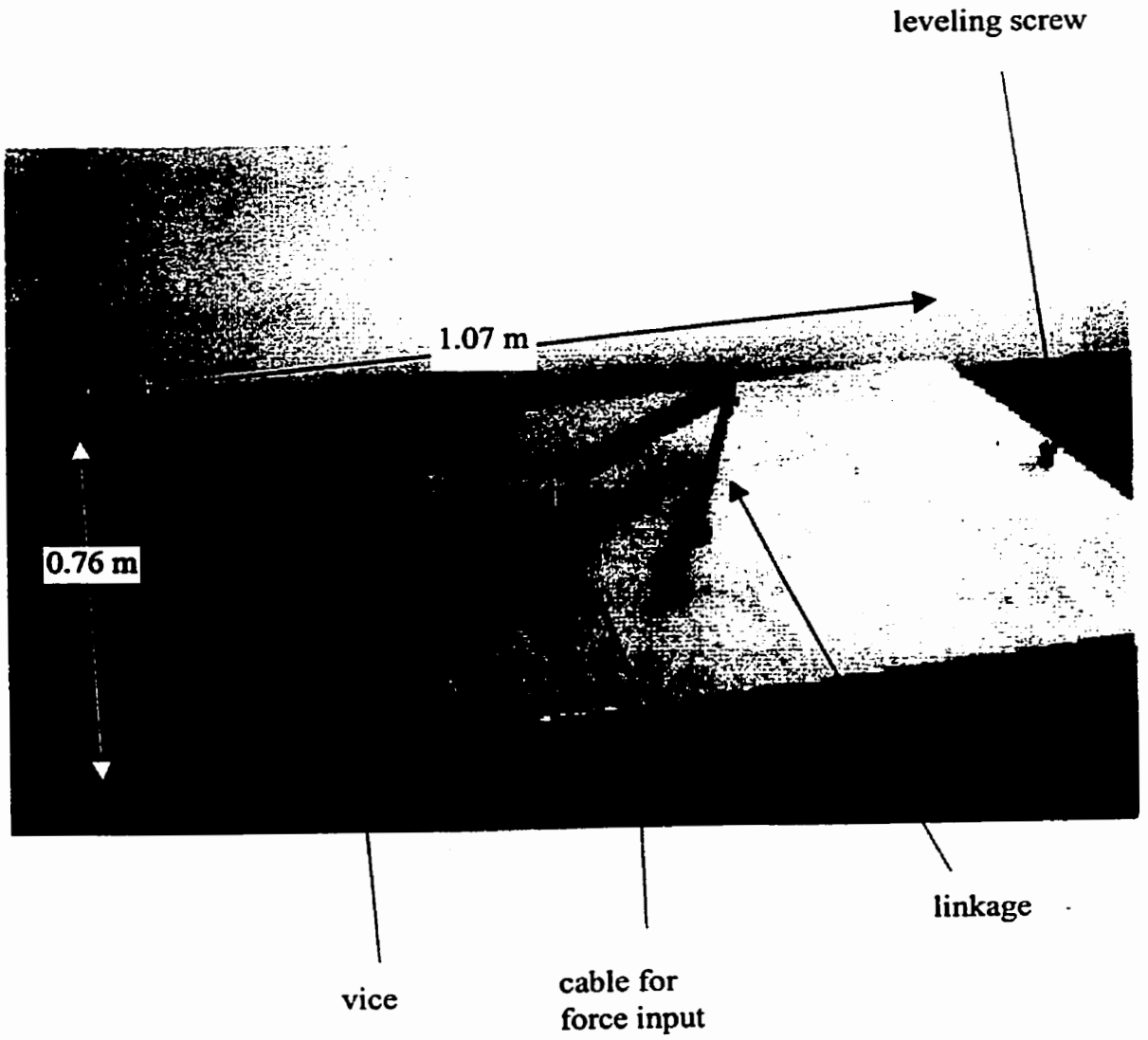

Figure 3.10: Setup of physical model on leveling board

CHAPTER 4

EXPERIMENTATION

4.1 Setup of the Experimentation

To verify the theory that modal motion would be limited to a single joint for the individual modes the physical model of a manipulator was tested. To view the vibration modes of the physical model the system was excited at the base by a harmonic force at one of the natural frequencies. The frequency was tuned such that each of the two mode shapes was clearly observed and separately measured for 5 to 10 seconds.

The test setup involved the arm attached horizontally to a mounting board by a vise (See Figure 3.10). The mounting board had three adjustable points for leveling. Leveling was important to avoid gravity forces in the plane of motion and torsion of the spring joints.

The arm was excited by means of the yoke mechanism. This setup provided a harmonic excitation. The force was varied by a variation of the yoke displacement and the frequency was varied by the drive motor speed. The yoke was driven by an A/C motor (Fracmo model # 43109088) with a variable speed control (Techequipment, Type No. E3, Unit No. 126) and a 50 to 1 ratio gearbox. The motor had a speed range from 100 rpm to 5500 rpm.

4.2 Collection of Data

Another encountered technical challenge was the collection of vibratory data that would accurately describe the motion of the links. The addition of conventional accelerometers would change the mass distribution. Connection wires to a central processing unit would also affect the response of the system.

One possibility was to use strain gages placed on the flat springs of the joints, but attaching the strain gages to the flat springs presented a complication. The magnitude of displacements needed to view vibration modes, were too large for the gages.

Laser reflecting was too difficult to implement, as there was a two-dimensional motion and accurate tracking of the link tips was a far too complicated problem.

Commercial options, such as Optitrac, which used sensored targets and a camera with three separate lenses to capture 3-D motion, were not financially viable. The approximate cost would be about $60,000 [13]

Methods used in bio-mechanics involving a special camera and reflectors were not accurate enough for this application, but led to development of the method that was eventually used in the project.

The chosen method of motion measurement involved a high quality 8mm analog

video camera, a PC with a video capture card, photo targets and video processing software. To capture the motion of the linkage without affecting the mass and the inertia of the system, only very light video targets were placed on the linkage. They added 0.23% of mass and 0.03% of inertia to each link. The center of gravity of the end link moved by 0.23% since the target on the tip was twice the mass of the added target mass at the other end of the link. The video camera was placed seven and a half feet directly above the arm. The view window of the camera was zoomed to allow for maximum arm view size while ensuring that all the necessary motion was recorded (see Figure 4.1 for system setup).

An analog video camera (Sony – CCD TVR95) and a PC capture card (ATI – All in Wonder Pro) along with software (ATI Player) were used to record frames at rates of 28 and 29 frames/sec. Due to the limitation of the PC and capture card higher frame rates could not be used. At a high frame rate the majority of the time, while capturing video of the motion, frames were dropped; however, if enough runs are done it is possible to capture a run where no frames are dropped. It was also important to keep the frame size (the number of pixels) as large as possible without affecting the capture frame rate. This is why the data was captured at two different rates. These recordings were extracted by a software package (Microsoft Videdit) and transferred into individual DIB files for each frame.

Black disks of a light weight bulletin card, with a diameter of an inch, were mounted on to the model. The centers of the disks (0.3 grams) were aligned with the

centers of the joints. The disks served as photographic targets (see Figure 4.2).

Using Scion Image software each frame was converted into a black and white image with no shades of gray (see Figure 4.3). This conversion was done by controlling the contrast level. Every pixel that had light intensity above the contrast level was white and every pixel below that level was black. The images of the photographic targets were extracted by varying the contrast of the recorded frames. At the correct contrast level only the photographic targets were present in the image. This procedure assured that only the images of the moving targets were saved to a file. The Scion Image software was used to analyze the images of the targets as large sets of pixels and the centers of black density (center of the disk) were computed. This provided an accurate location of the marked points on the system. Knowing the captured video frame rate and the frame number, the positions of the targets were plotted versus time. The upper left corner of the picture frame was used as a reference point since there was no relative motion between the camera and the mounting platform of the vibrating model.

4.3 **Natural Frequencies**

The first two modes of a two-link manipulator model were investigated in the experiment. The system was separately excited at its two natural frequencies and then it was left free to vibrate. The system was excited and the frequency varied until the first mode was observed. This occurred at a recorded frequency 5.7 rads/s (0.906 Hz). This result agrees to within ± 0.52% with the expected computed frequency of 5.73 rads/s

(0.911 Hz) of the first mode. The second mode was observed at the frequency of 9.95 rads/s (1.58 Hz) that is within ± 0.20% of the expected result that was a computed frequency of 9.97 rads/s (1.59 Hz). The displacement of the joints for each corresponding mode was plotted in angular and tip displacements (see Figures 4.4, 4.5, 4.6 and 4.7).

The input frequencies were measured by counting the number of cycles of the follower of the excitation yoke for three minutes. For the first mode 163 cycles were visually counted over three minutes. For the second mode 285 cycles were counted over three minutes.

The output frequencies in the first mode were ω_{n1} for joint 2 and $2\omega_{n1}$ for joint 3. The presence of $2\omega_{n2}$ suggests there is non-linearity in the system. This is further discussed later on in the thesis (Chapter 5). The output frequencies for the second mode were ω_{n1} for the joint 2 and ω_{n2} for joint 3. The displacement of joint 2 in the second mode does not appear smooth. This is due to the small size of the displacements of joint 2. The displacements of joint 2 were so small that they could not accurately be measured, but the measurements still gave a general idea of the motion.

4.4 **Damping**

For the obtained results it was possible to analyze the decrease of amplitude over time and determine the damping of the system (see Appendix III). The value for the damping ratio ξ was found to be 0.00175 ± 0.00003. The ratio ξ was calculated from

three different numbers of cycles (25, 35 and 50) between measurements and then the average was taken. These measurements lead to the computation of the damping coefficients c_1 and c_2 being 0.000197 and 0.000117 respectively.

4.5 **Force Orientation**

The forcing function was supplied at different orientations. This only affected the rate of increase of the amplitude of the system output. Once enough time had passed for a sufficient displacement in the link was reached, it was left to vibrate freely.

This demonstrated that direction of the forcing function affects the rate at which the amplitude of displacement increased. The angle of orientation of the forcing function affects the horizontal and vertical components of the force. As expected the rate of increase of the amplitude became greater as the orientation of the forcing function approached being perpendicular to the link in motion for the corresponding mode being excited.

It was observed that as the orientation of the input excitation approached being applied in a direction parallel to the link for the corresponding frequency, there was a decrease in the rate of increase in the amplitude of displacement. There was not an angle of orientation found that changed from the expected motion of links, namely modal motion being limited to a single joint. This result was expected and agrees with accepted vibrational theory [14].

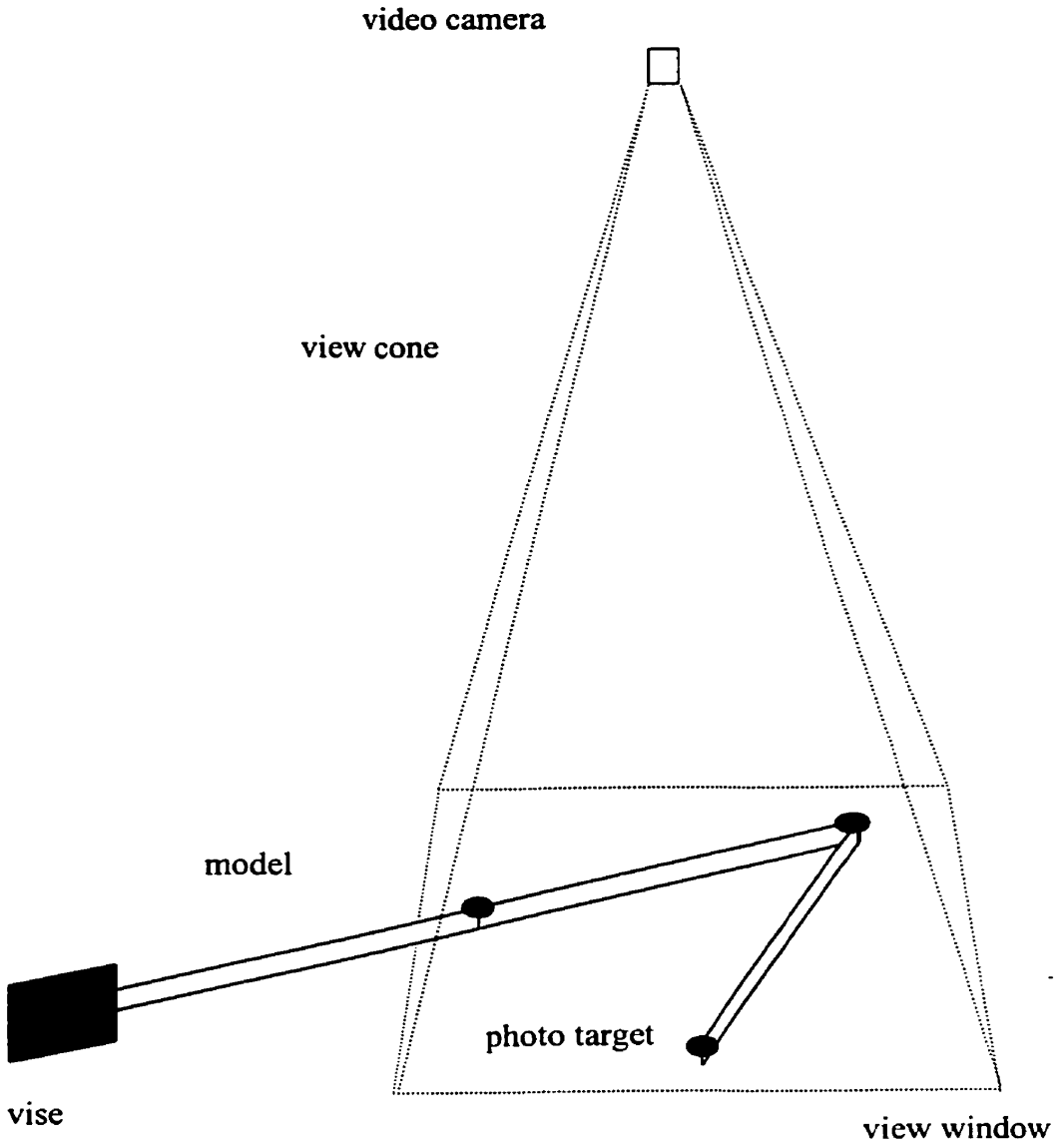

Figure 4.1: The experimental setup to capture the displacement of the link tips.

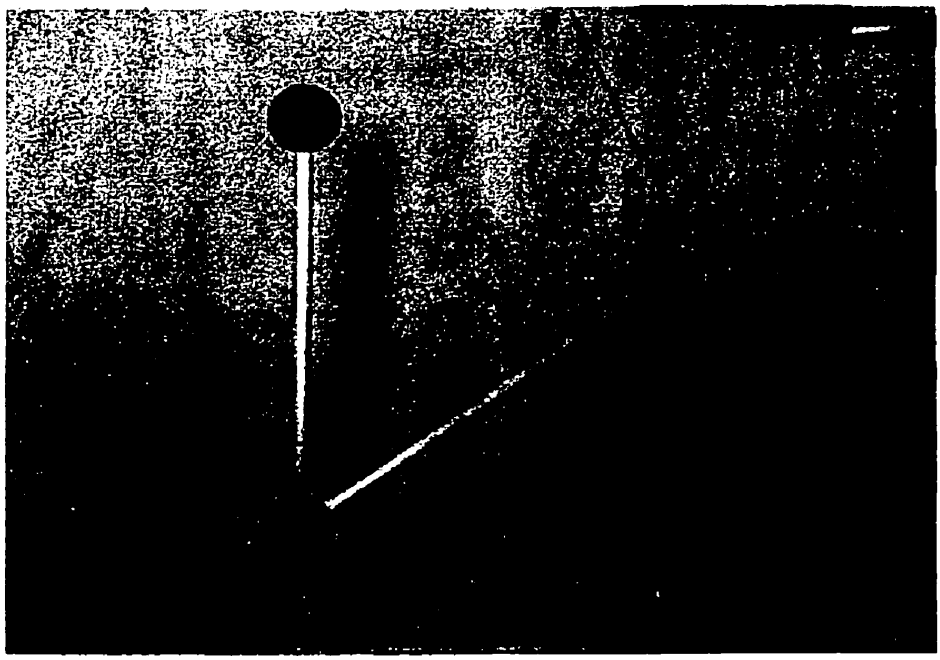

Figure 4.2: An actual captured frame. Scale 1:2.

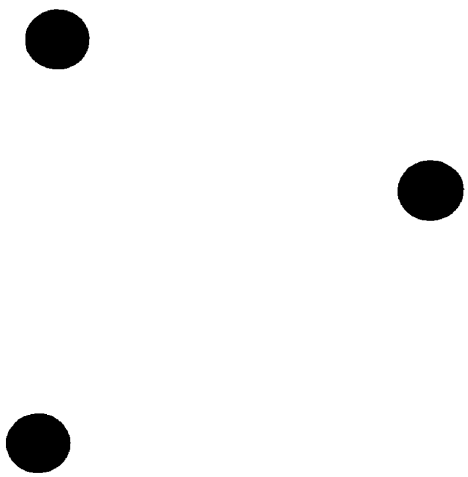

Figure 4.3: An actual captured frame for a set light intensity threshold level displaying only the black targets.

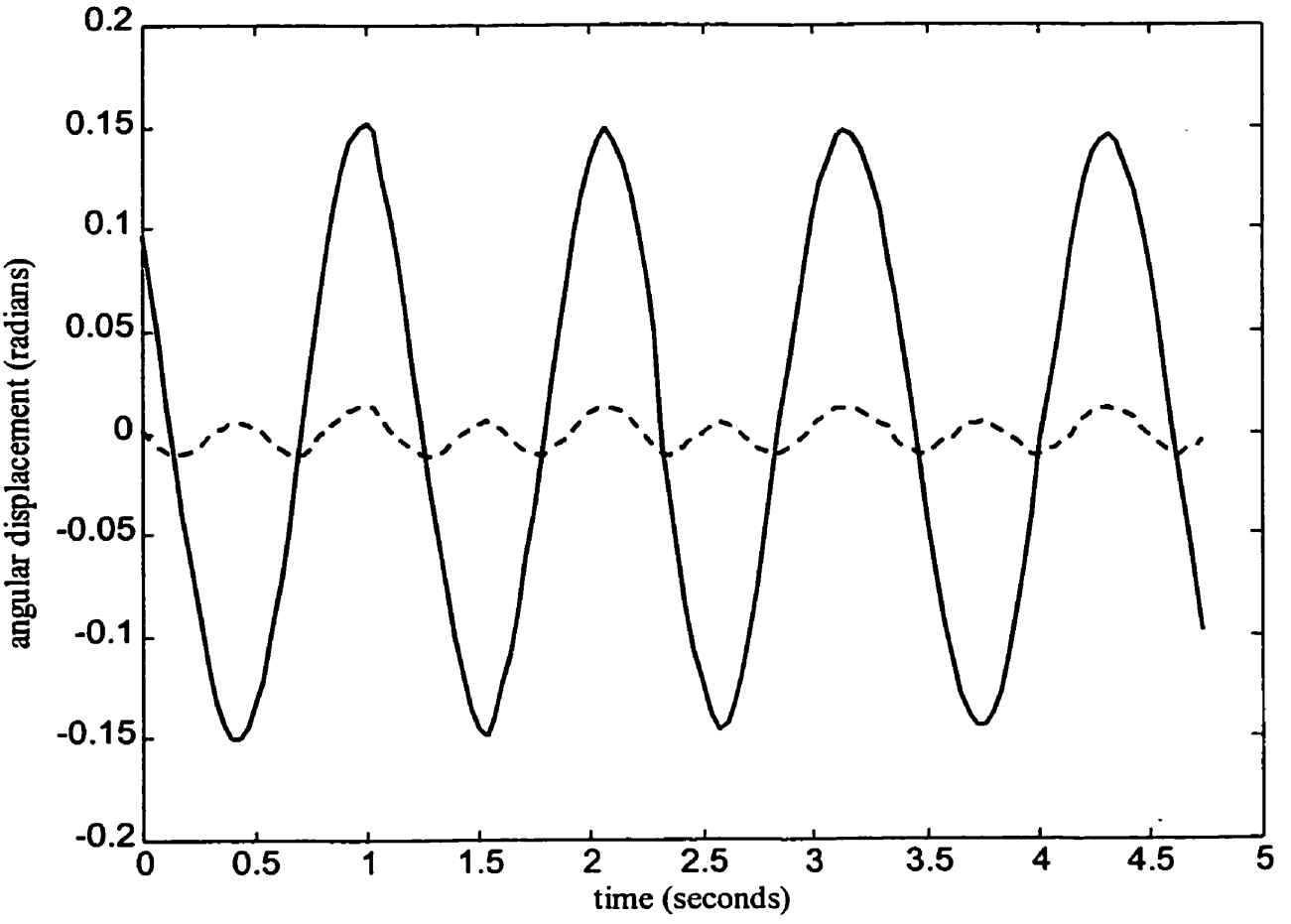

Figure 4.4: Joint angles q_2 (——) and q_3 (- - -) for the first mode plotted versus time

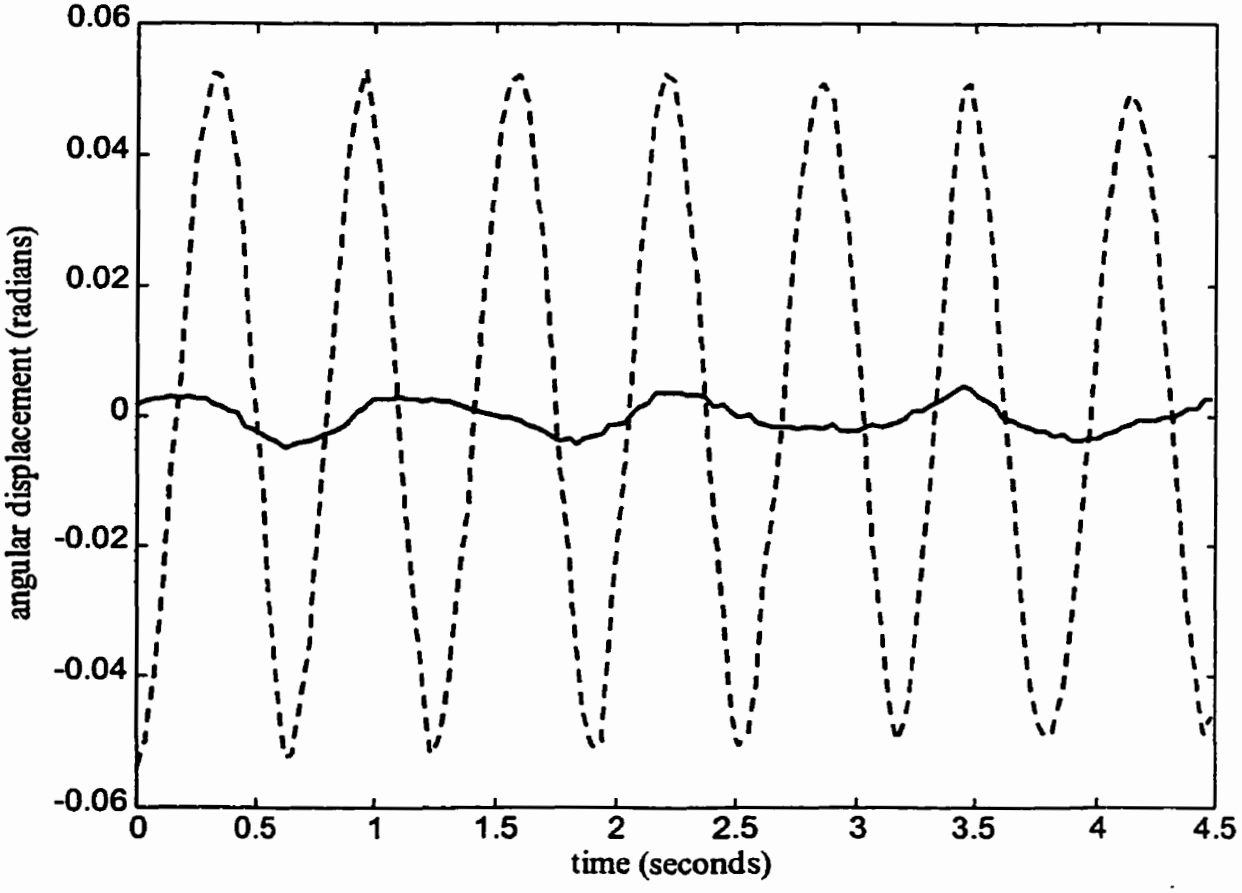

Figure 4.5: Joint angles q_2 (——) and q_3 (- - -) for the second mode plotted versus time.

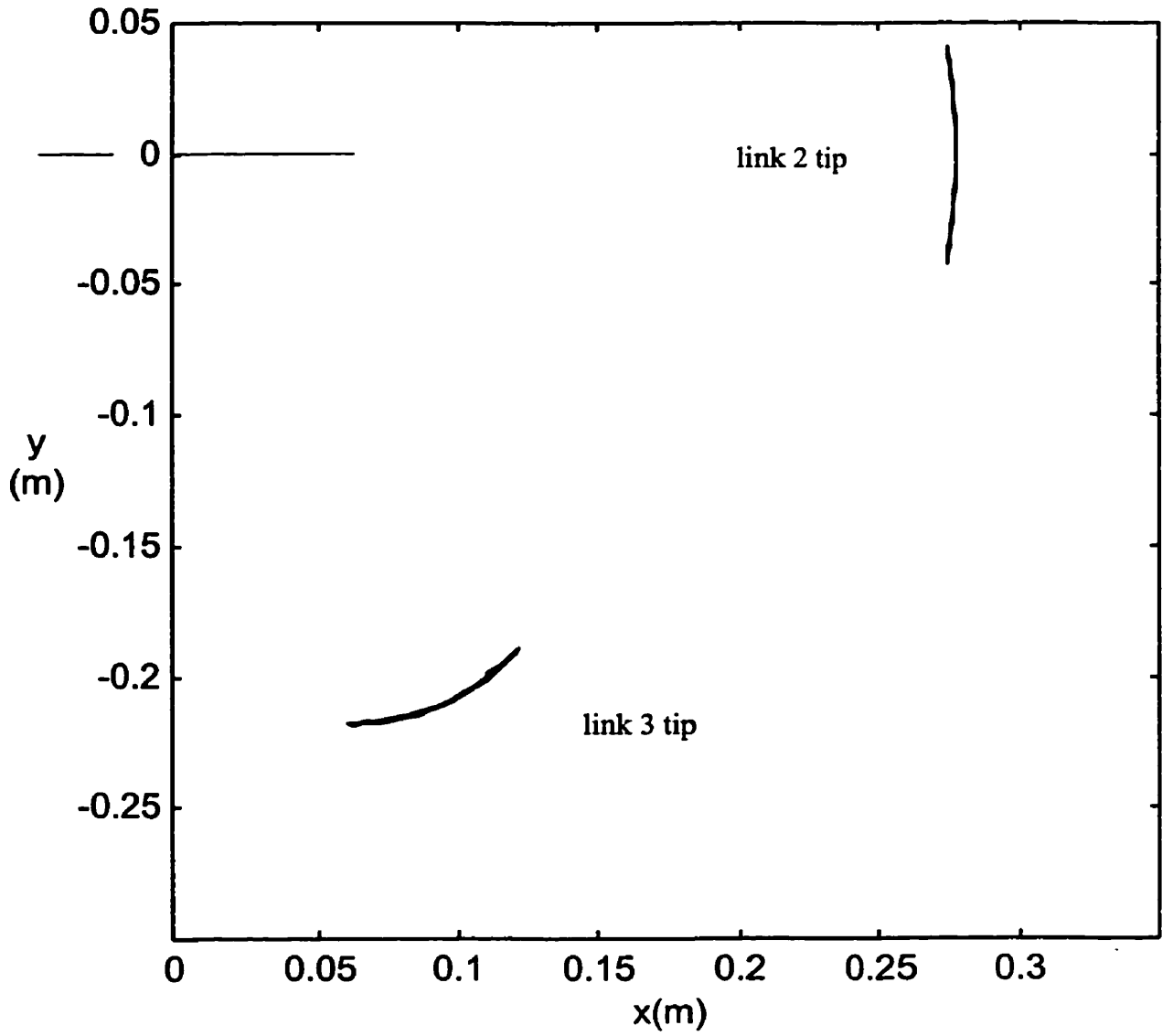

Figure 4.6: Trace of the joint motion for the first mode.

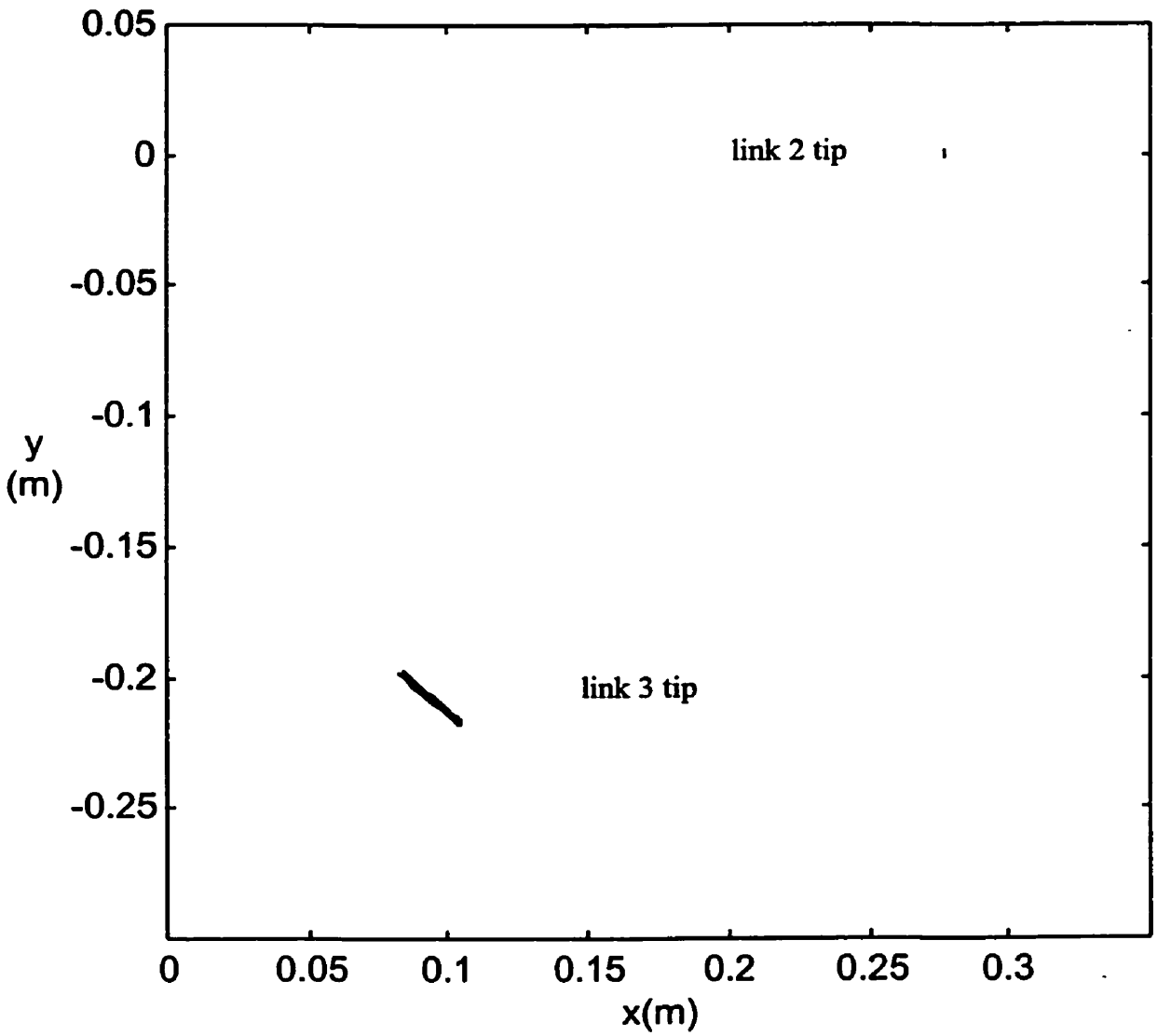

Figure 4.7Trace of joint motion for the second mode.

CHAPTER 5

NUMERICAL SIMULATION

5.1 Numerical Simulation

Numerical simulation of the system was completed using MATLab and SIMULINK. An M-file (see Appendix II) was created to compute the system parameters for each posture using Equations (2.2) – (2.28). By varying the joint angles the mass matrix was varied thus varying the natural frequencies of the system. The remaining system parameters: damping, joint stiffness and coriolis were also calculated in this file.

For example using the parameters of the physical model three equations of motion were attained for configuration of the second joint angle $Q_2 = 131.38^0$. They are

$$0.0563\ddot{q}_1 + 0.0215\ddot{q}_2 - 0.00328\ddot{q}_3 - 0.00744\dot{q}_1\dot{q}_2 - 0.0149\dot{q}_1\dot{q}_3 - 0.00372(\dot{q}_2)^2 + 0.0149\dot{q}_2\dot{q}_3 + 0.00744(\dot{q}_3)^2 + 0.326q_1 = 0 \quad (5.1)$$

$$0.0215\ddot{q}_1 + 0.00993\ddot{q}_2 - 0.00774\dot{q}_1\dot{q}_3 + 0.00774\dot{q}_2\dot{q}_3 + 0.00372(\dot{q}_1)^2 + 0.00372(\dot{q}_3)^2 + 0.326q_2 = 0 \quad (5.2)$$

$$0.00328\ddot{q}_1 + 0.00328\ddot{q}_3 + 0.00744(\dot{q}_1)^2 - 0.00372(\dot{q}_2)^2 + 0.326q_3 = 0. \quad (5.3)$$

Using software (SIMULINK) and a block diagram method, a simulated model of the physical model was created (see Figure 5.1).

5.2 Method of Numerical Simulation and Results

A numerical sinusoidal force input was used to excite the simulated system in order to calculate the response of the model. The numerical sinusoidal excitation was equivalent to the physical excitation used to excite the physical model. The base link was treated as the other links in the system instead of as cantilever beam. It was treated as a link connected with a joint that connected to the ground. The joint connected to the ground was given a stiffness equivalent to the stiffness of the cantilever beam. The excitation in the numerical model was a sinusoidal torque that was applied to the base joint. The parameters were calculated for the case where the mass matrix becomes diagonal. The variations of the first two natural frequencies with changing posture angle Q_2 were plotted (see Figure 2.4). The third natural frequency was in the range of 10 to 25 times higher than the second natural frequency. For the decoupling posture of $Q_2 = 131.38^0$ the third natural frequency was $\omega_{n3} = 212$ rads/s as compared to $\omega_{n2} = 9.97$ rad/s. The numerical model was then excited at the first natural frequency for a limited time. The input force was stopped and the system was left free to vibrate. The simulation was then repeated at the second natural frequency.

The computed joint displacements and tip displacements were saved and plotted (see Figures 5.2, 5.3, 5.4 and 5.5). The numerical results were compared with the free

vibration results of the physical model.

5.3 Comparison between the Physical and Numerical Models

The results of both the numerical simulation and the laboratory experiments were compared in three different manners. The first comparison was in terms of joint displacements (see Figures 5.6 and 5.7). The second comparison involved tip displacements (see Figures 4.6, 4.7, 5.4 and 5.5). The third comparison was done by taking the Fast Fourier Transform (FFT) of the motion results and comparing the frequency components (see Figures 5.8, 5.9, 5.10 and 5.11).

When the system was excited at the first natural frequency ω_{n1} peaks were seen in the frequency spectrum at ω_{n1} and $2\omega_{n1}$ in both the experimental and simulated results. The spectrum for the first link showed the dominant peak at ω_{n1}. The super harmonic oscillation at $2\omega_{n1}$ is due to the slight non-linearity of the system [15]. The spectrum for the experimental results for the first link also showed a slight peak at $2\omega_{n1}$, but this was not present in the simulated model. The spectrum for the second link showed a slight peak at $2\omega_{n1}$ in both the experimental and simulated results.

When the system was excited at the second natural frequency, ω_{n2}, the spectrum of the first link motion demonstrated a slight peak at ω_{n1} for both the experimental and simulated results. The second link spectrum showed the dominant frequency at ω_{n2} for both the experimental and simulated results.

Two methods were used in order to compare the experimental results with the numerical results on the same plot. This means that the displacements and phase angles were equivalent. The displacement equivalency required choosing the correct time to stop the force input to ensure equivalent amplitudes. The phase of the angular displacement for the respective links was also chosen such that the initial angular displacements of both the experimental and simulated results were the same. This allowed for a simpler comparison of one of the joint angle displacements at a time since they were in phase.

The second method to obtain equivalent initial displacements required using initial joint displacement as measured from the physical model and being imported for the numerical simulation. In this case the force input was set to zero and only the initial displacements excited the system. Both methods gave the same results (see Figure 5.6 and 5.7).

The numerical model experienced the same base excitations as the physical model. The numerical and physical model demonstrated the same results within an acceptable tolerance with a maximum of 0.52 % of natural frequencies (see Appendix III). The numerical and physical results for displacement and frequency demonstrated the accuracy of the physical model and the motion measurement method. The results also demonstrated that the simulation is an accurate representation of the physical model.

When starting and stopping the excitation force on the physical and numerical

models an impact was felt by the entire system, thus exciting all the vibration modes. In order to remove this impact the numerical model was excited by initial conditions. This meant that one of the joints was displaced by a small amount and then allowed to vibrate freely. The physical model involved much larger displacements in order to obtain accurate data with the non-contact motion measurement described in Chapter 4 section 4.2. Without the limitation of capturing the motion data using the numerical model, the initial displacements that excited the system were smaller than the displacements used in the physical model and aforementioned numerical simulations. The lack of impact and the relatively smaller initial displacement (approximately 5 – 10 times smaller) resulted in the joint motion being almost completely decoupled (see Figures 5.12 and 5.13).

5.4 Natural Frequencies for All Possible Configurations

Another numerical simulation was used to obtain a plot of the system's natural frequencies for different postures with damping included (see Appendix II). The posture angle Q_2 was varied from 0 to 180 degrees (see Figure 2.5).

To study the eigenvectors the normalized mode shapes were tabulated. The mode shapes displayed changes in sign at certain configurations (see Figures 5.14 and 5.15). The sign is determined by the position of the modal displacement with reference to the actual position (zero displacement). This also suggests that there is a point where the equations of the motion decouple as the mode component relative value goes from "plus" to "minus". Going from "plus" to "minus" suggests that zero must be crossed i.e. no

modal displacement. This is the point when the joint motion decouples (equations describing the joint motion decouples). This change in sign of the mode component relative value that corresponded to link 2 occurred at 131.4 degrees. The closer the posture angle value is to the decoupling posture angle, the smaller the magnitude of the Eigen vector. This agreed to the angle needed to diagonalize the mass matrix.

There was a correspondence between the diagonalizing posture angle and the natural frequencies at that posture angle. When the joint posture angle diagonalized the inertia matrix the second natural frequency was at an absolute minimum value (see Figure 2.4).

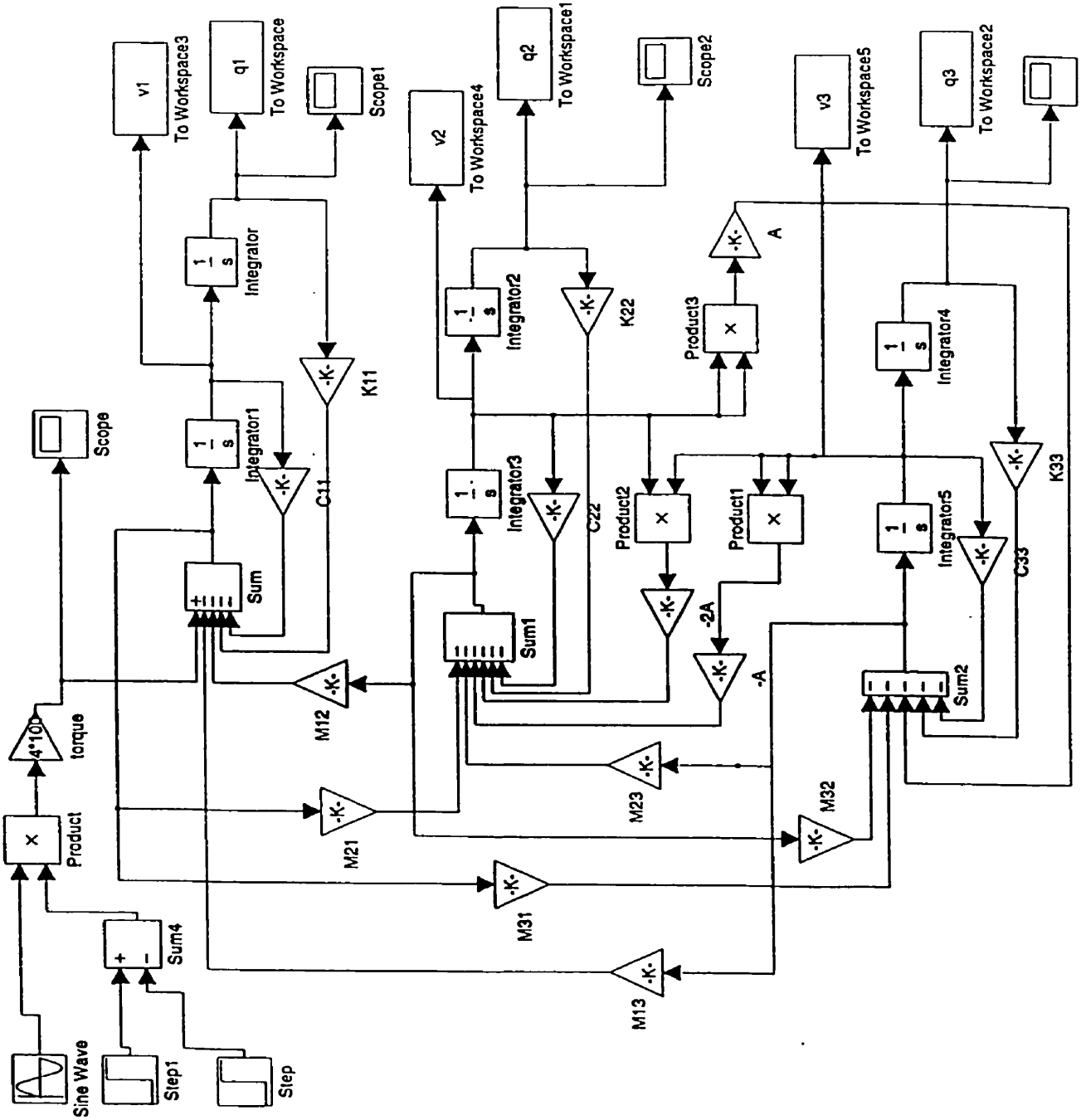

Figure 5.1: Block diagram for simulation of the equation of motion of the system that represents the physical model

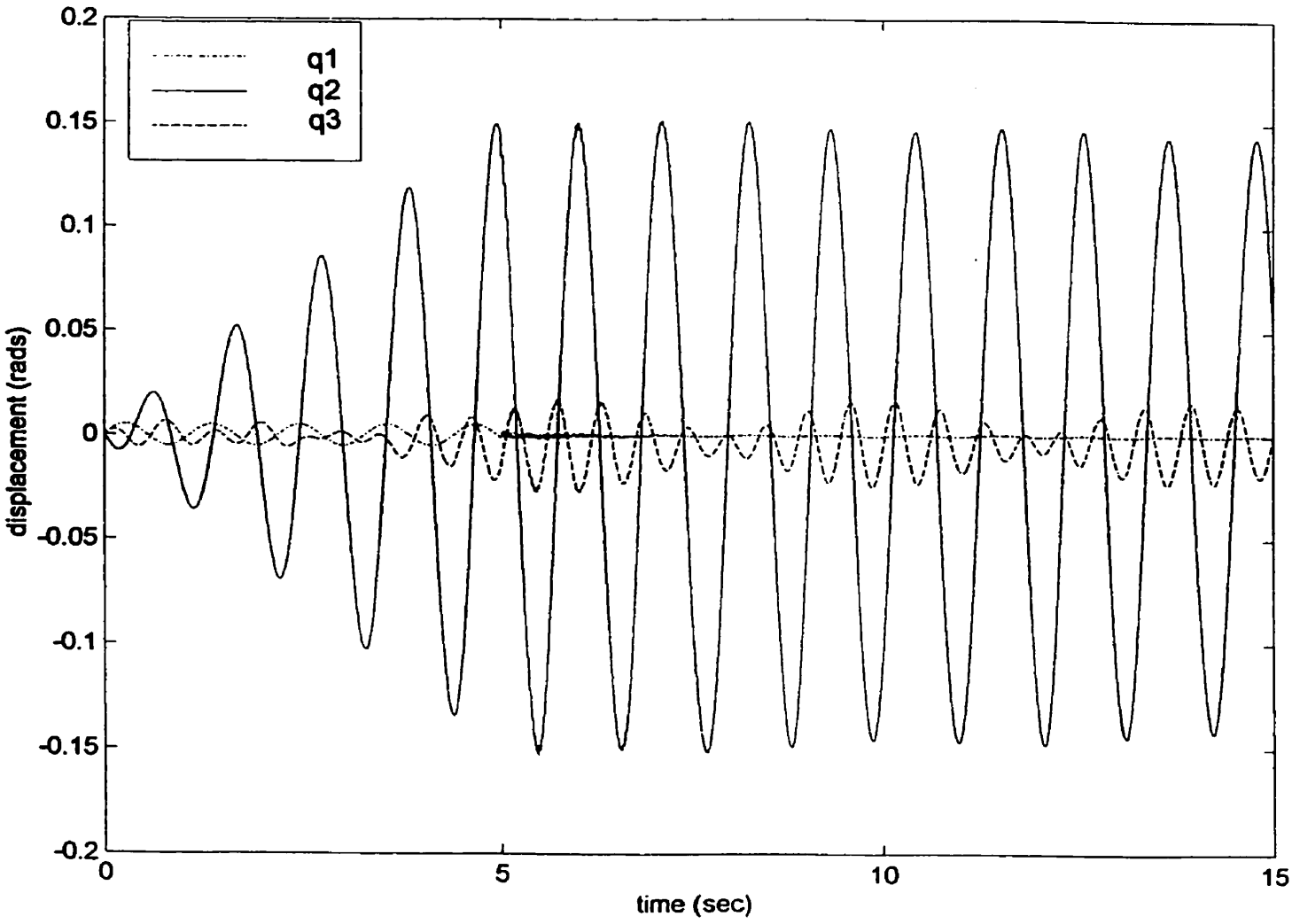

Figure 5.2: Simulated results of joint displacements for the first mode plotted versus time. The system was excited from rest.

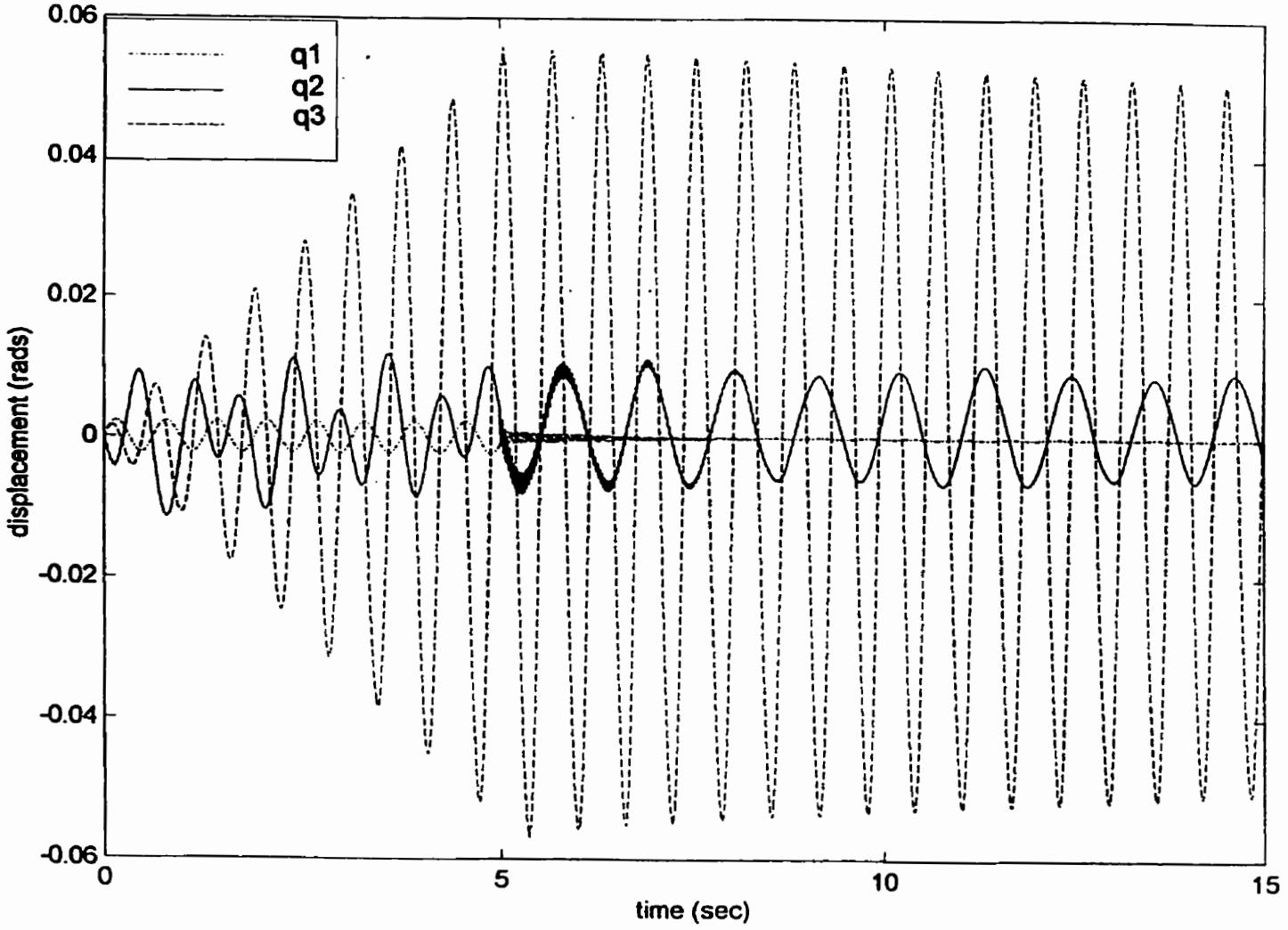

Figure 5.3: Simulated results of joint displacements for the second mode plotted versus time. The system was excited from rest.

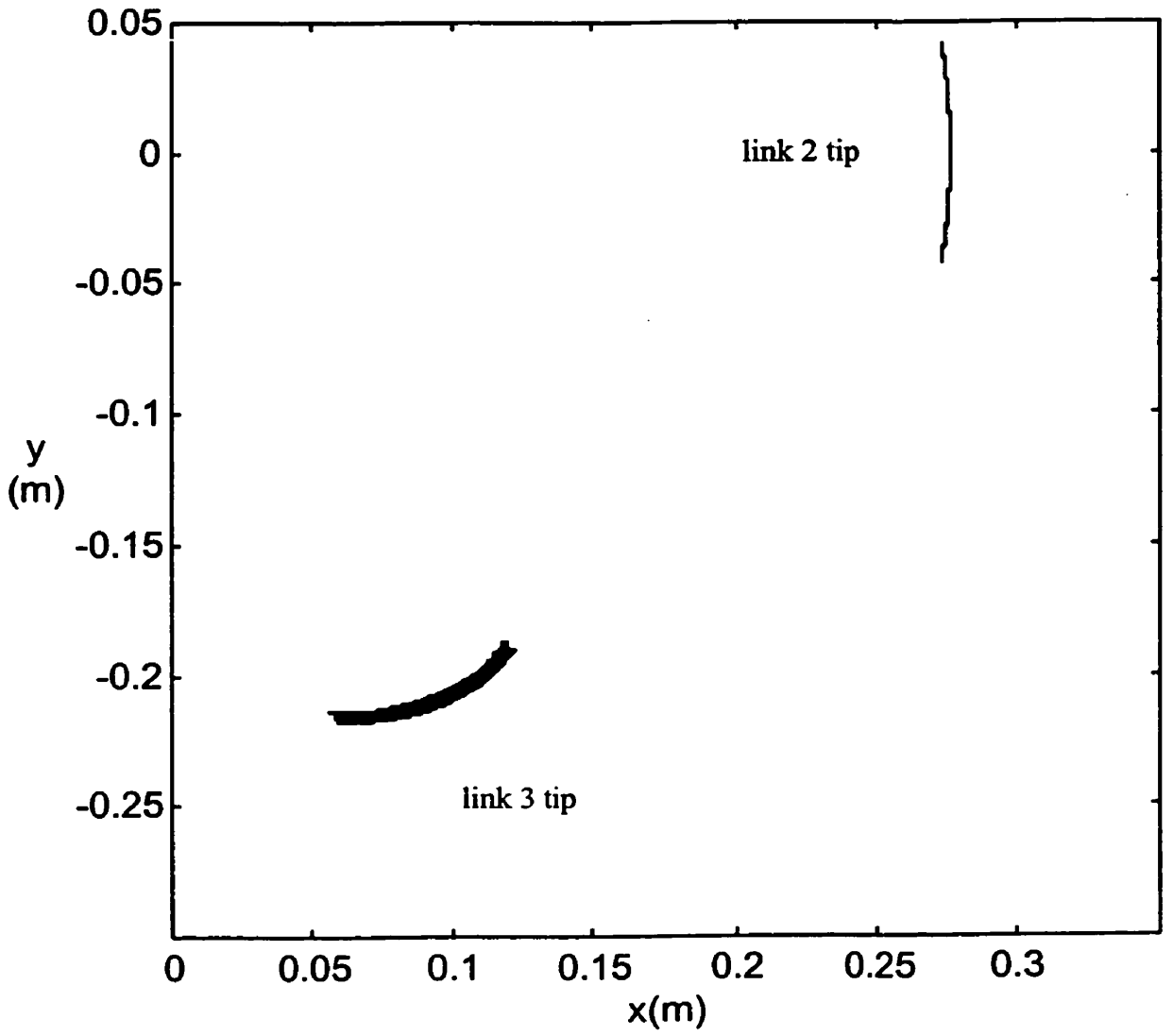

Figure 5.4: Simulated results of link tip displacements for the first mode.

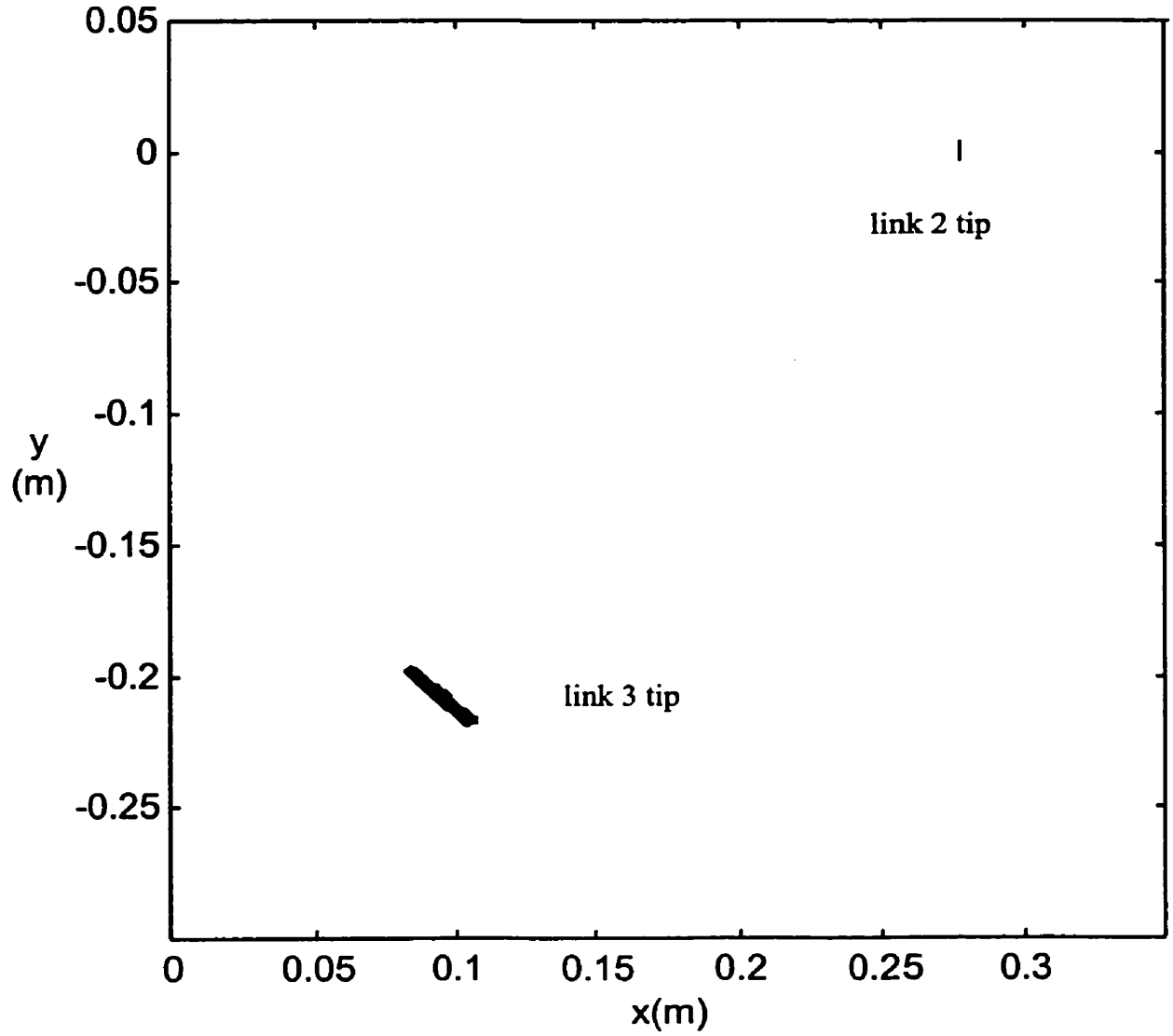

Figure 5.5: Simulated results of link tip displacements for the second mode.

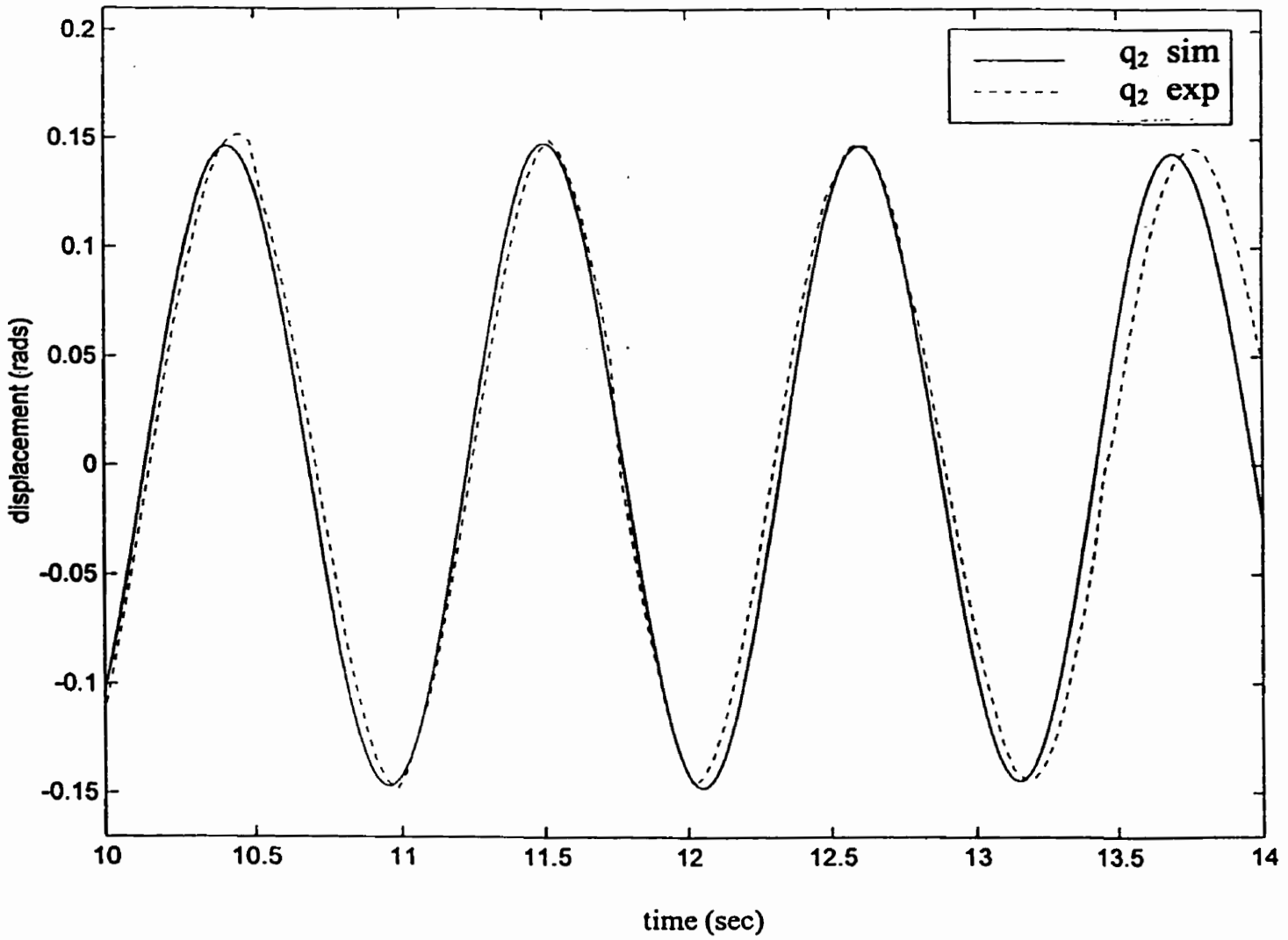

Figure 5.6: Comparison of experimental and simulated results of joint displacements for the first mode plotted versus time.

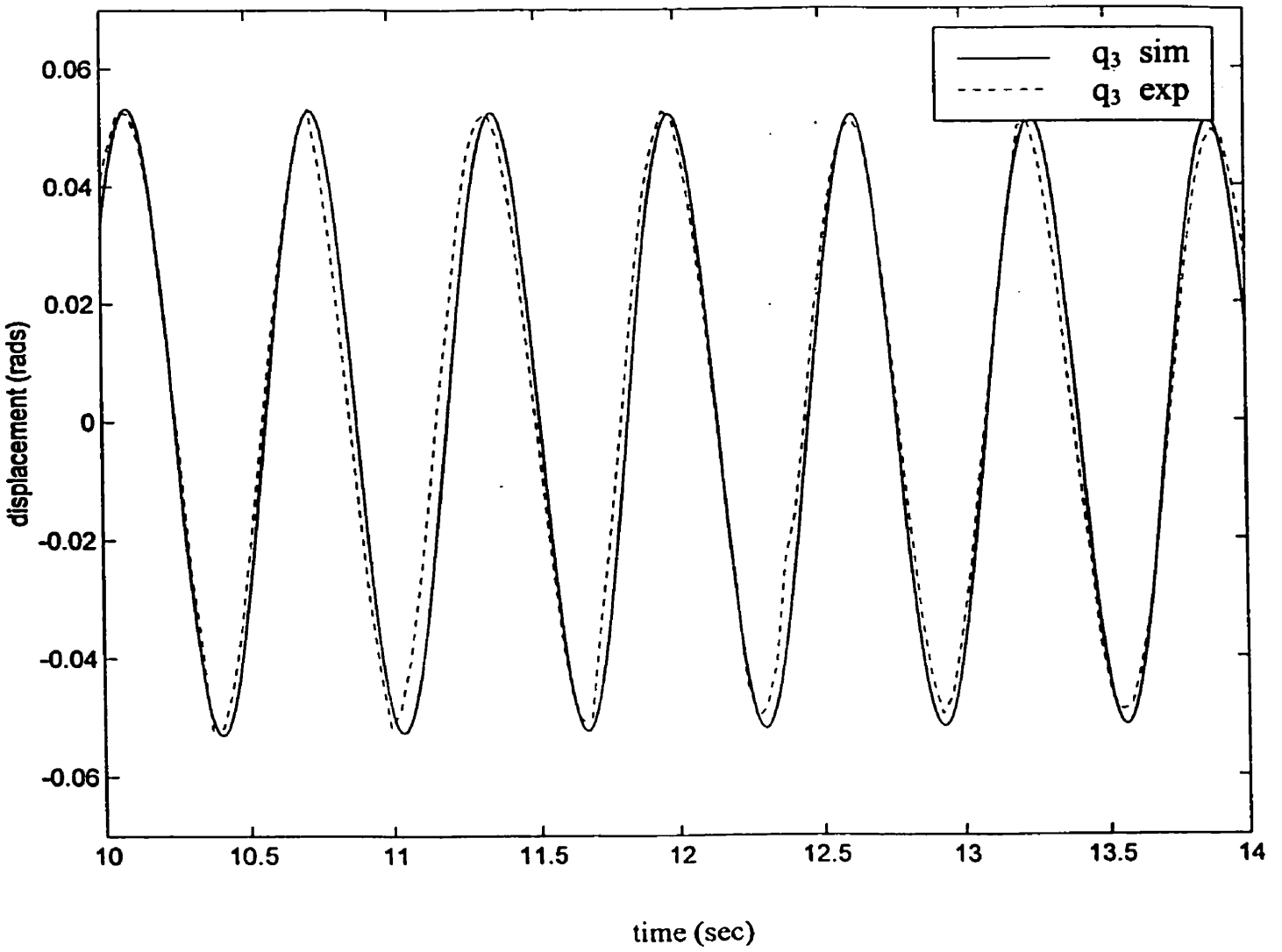

Figure 5.7: Comparison of experimental and simulated results of joint displacements for the second mode plotted versus time.

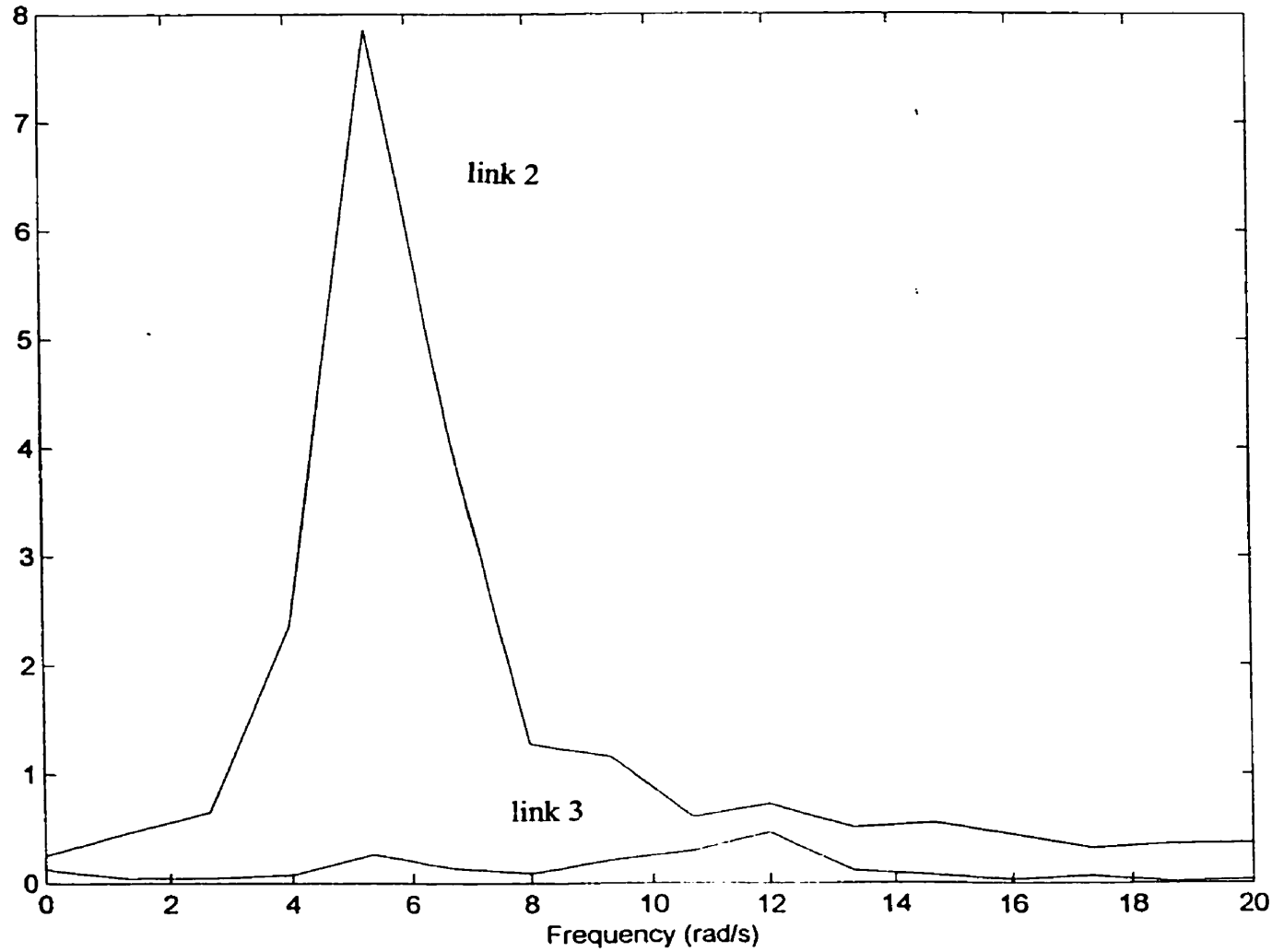

Figure 5.8: Frequency spectrum of experimental results from the first mode.

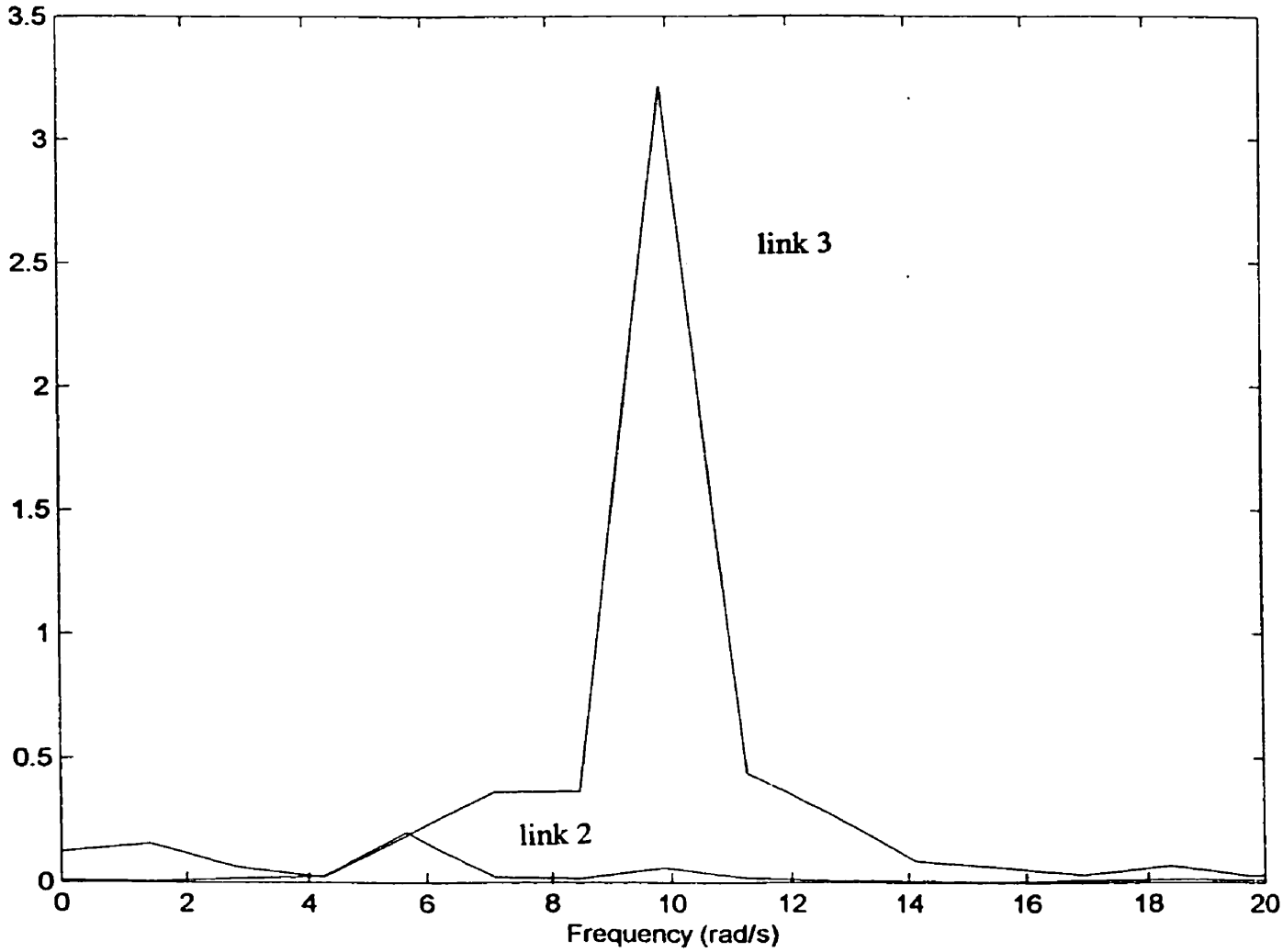

Figure 5.9: Frequency spectrum of experimental results from the second mode.

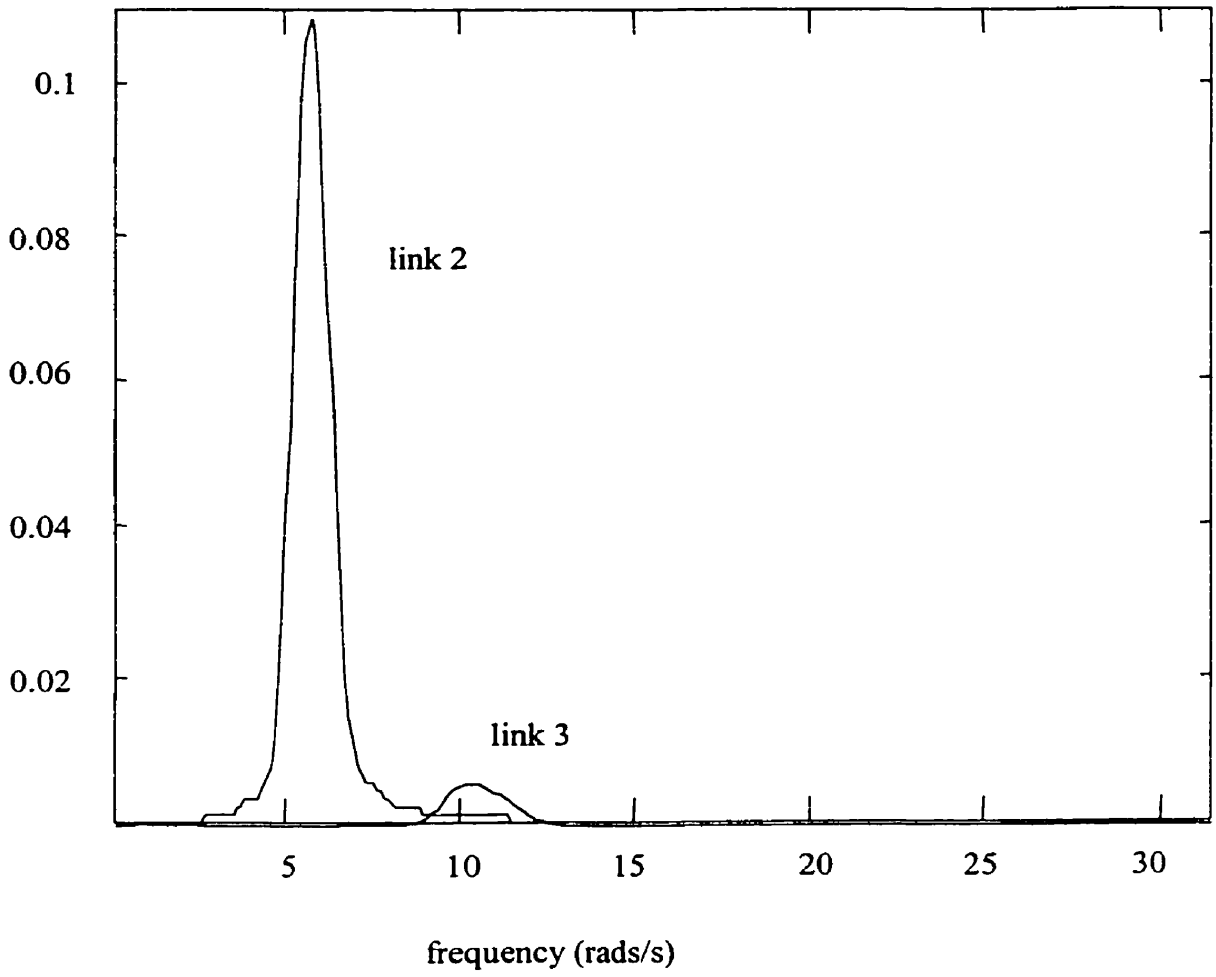

Figure 5.10: Frequency spectrum of simulated results from the first mode.

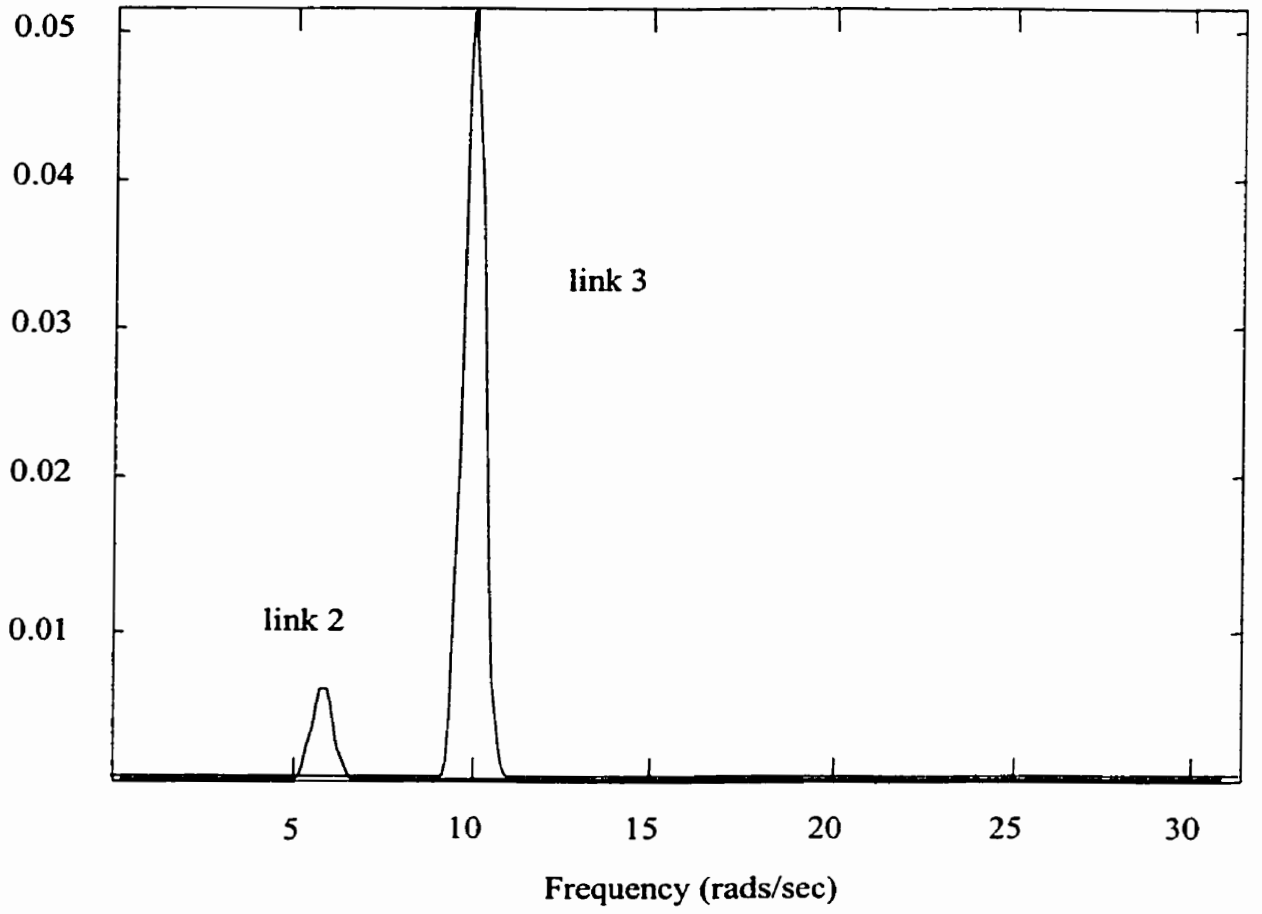

Figure 5.11: Frequency spectrum of simulated results from the second mode.

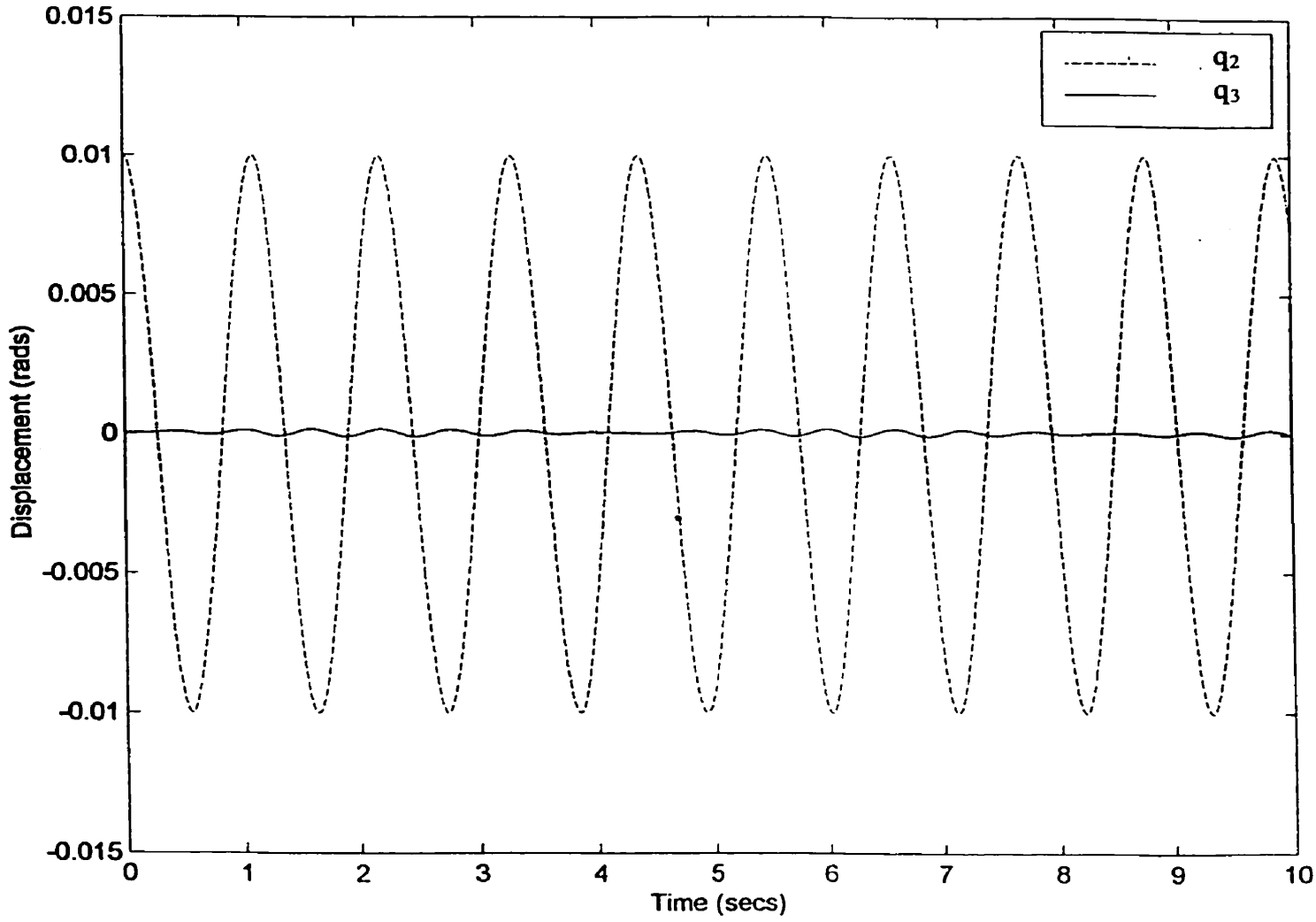

Figure 5.12: Joint displacements from initial displacement of joint 2

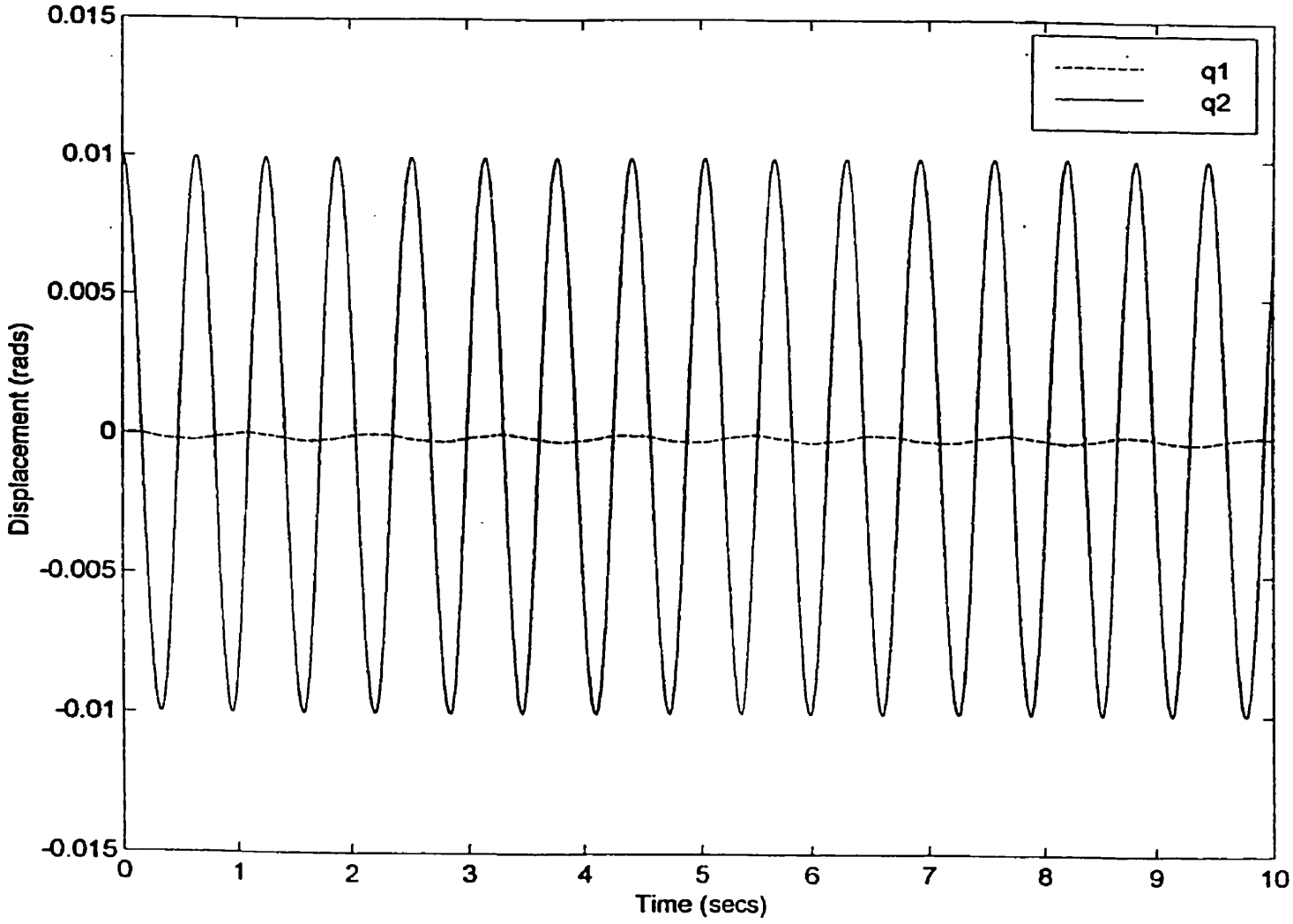

Figure 5.13: Joint displacements from initial displacement of joint 3

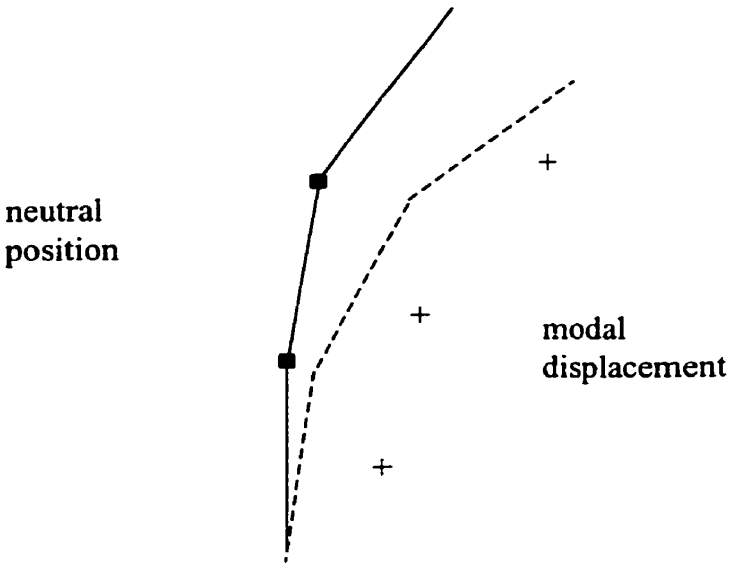

Figure 5.14: Mode Shape (+ + +).

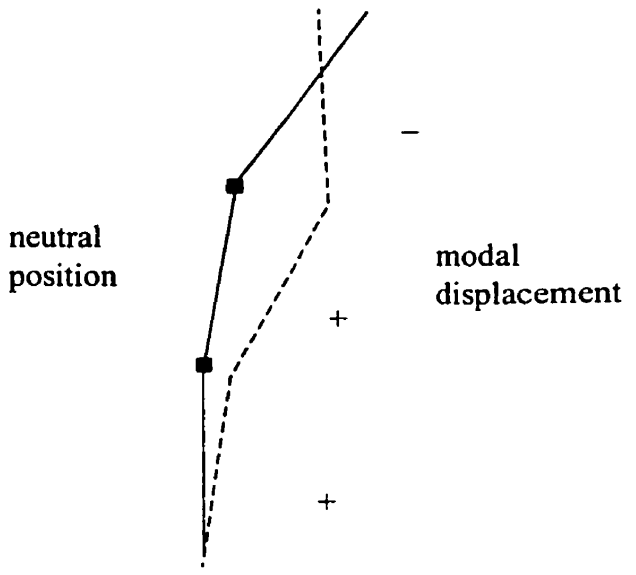

Figure 5.15: Mode Shape (++ −).

CHAPTER 6

CONCLUSION AND RECOMMENDATIONS

6.1 Conclusions

The thesis dealt with dynamics of a very flexible manipulator structure. A study of the modes of vibrations for structures that vary their geometric posture was conducted. This study lead to an investigation of mode separation by the manipulator joints. This investigation suggested that it was possible to separate the modes of vibration. To further research the possibilities of mode separation a physical model that represented planar motion of a space manipulator was successfully designed and fabricated. A low frequency harmonic exciter was also designed and fabricated. An accurate non-contact method was employed to measure motion of a delicate model. Then a laboratory setup was integrated. It included the aforementioned model, exciter and method along with sensors, computers and software.

Mathematical methods were developed to study modal motion. An investigation of experimental, numerical and analytical properties of flexible structures that vary their geometric postures was carried out. The results of this study have been published [16].

This thesis demonstrated that a linear mathematical model could accurately represent the simple 2-DOF physical model a space manipulator. The larger the off-diagonal terms of the inertia matrix become the more this linear mathematical model

degenerates.

The experimentation demonstrated that the flat spring "suspension" of the manipulator structure proved to be a practical way of simulating scaled planar motion in space where the elasticity of the joints is much greater than the elasticity of the links.

The simulation demonstrated that the angle that decouples the equations of motion occurs at the absolute minimum of the second natural frequency.

The experiments verified that at a certain posture the joint motion decouples the natural vibrational modes of the manipulator structure for a particular posture. For a planar two-DOF manipulator arm that undergoes small vibrations there exists one posture angle between the upper and lower arm that leads to uncoupling of the joint oscillations. The angle between the base and the lower arm can be arbitrary. This study demonstrated that the modes of vibration largely decoupled when the equations of motion were decoupled as predicted analytically.

6.2 **Results of the Experimentation**

The results were as predicted by the theory and numerical simulation and demonstrated that almost all the flexing motion is located in a single joint when the system is excited at a natural frequency when the manipulator is in the correct posture. As expected, there was slight motion recorded in the secondary joint that did not correspond to the natural frequency input i.e. $\mathbf{q}_2$ was comparatively small when the first mode is

excited. This motion is due to a slight cross coupling of very small Coriolis and centrifugal forces and an impact excitation felt by the system when excitation begins and ends. Another factor causing this slight motion was that the initial size of displacement needed to be relatively large as the measurement method would not allow for accurate measurement of very small displacements.

6.3 **Recommendations and Further Study**

Recommendations include further study and testing of the physical and numerical models to include higher orders of degrees of freedom. These higher orders should consist of more links and increased flexibility of the links themselves. The theory was also completed for a 3-DOF system (see Appendix V) and verification of that theory is required. The theory should be expanded to investigate the possibilities of decoupling the motion in the joints for each mode for more degrees of freedom.

Testing should be expanded to include a variety of different types of input, such as random vibrations and impact vibrations at various locations. A more in-depth study of various constant vibration inputs that are not at a natural frequency should also be done. Representation of a payload by a lump mass added to the tip of the last link should be added to all the mathematical, numerical and physical models.

6.4 Major Contributions of this Thesis

Some of the contributions of this thesis are as follow:

1. Discovery that certain manipulator postures will limit the effects of base vibration to a single joint.
2. Proving physically and numerically that decoupling of the equations of motion takes place for a certain manipulator posture.
3. Development of a joint that allows accurate physical simulation of planar vibration of a space manipulator at a fixed posture.
4. Development of a mechanism that generates low frequency harmonic forces. The force can ranges from 2 to 8 N and the frequency range from 0.6 rads/sec (0.1 Hz) to 20 rad/s (3 Hz).
5. Development of an inexpensive and non-contact method of accurately analyzing motion in the range of 0 Hz to 5 Hz.
6. A starting point for increase control of space manipulators. By placing the space manipulator in a certain posture it is necessary to only having to control motion of one joint caused by base vibrations instead of having to control the motion of two or more joints whose motions are coupled.
7. A solid base for further study in the effects of base vibrations on space manipulators.

Note that since the experimentation was conducted the ability to capture larger frames at a higher rate without dropping frames has improved dramatically. As the hardware (CPU's, hard drives and capture cards) speeds increase and the demand for free streaming

video grows for entertainment purposes this method will provide a cost effective non-contact way of measuring two dimensional motion. In the future with these improvements it will be possible to measure 3-D motion, by knowing the target size and using the aspect ratio to calculate depth and rotation by the change in size and shape of the target.

REFERENCES

[1] Amos, A., K., (1989), Microgravity Simulation Issues, Conference Proceedings for AIAA/AFOSR Workshop on Microgravity Simulation, Denver, CO., Nov. 1-2, 1989.

[2] Gronet, M., J., Brewster, R., G. and Crawley, E., F., (1989), Assembly and Suspension Issues for the DSMT Pathfinder Scale Model, Conference Proceedings for AIAA/AFOSR Workshop on Microgravity Simulation, Denver, CO., Nov. 1-2, 1989.

[3] Das, A., (1989), Air Force Programs and Facilities, Conference Proceedings for AIAA/AFOSR Workshop on Microgravity Simulation, Denver, CO., Nov. 1-2, 1989.

[4] Fay, D. and Kujath, M., R., (1999), Constant Force Mechanism, Conference Proceedings COM, Finland.

[5] Book. W., J. and Majette, M., (1983), Controller Design for Flexible, Distributed Parameters Mechanical Arm Via Combined State Space and Frequency Domain Techniques, Journal of Dynamic Systems, Measurements and Control, Vol. 105

[6] Liu, K., (1993), Vibrations of Time-Varying Mechanical Systems, Ph. D. Thesis, Technical University of Nova Scoita, Halifax, Nova Scotia.

[7] Vafa, Z., Dubousky, S., (1990), The Kinetics and Workspace of a Satellite Mounted Robot, The Journal of the Astronautical Sciences, Vol. 38, No. 4.

[8] Papadopoulos, E. and Dubousky, S., (1993) "Dynamic Singularities in Free Floating Space Manipulators (positions where the end tip can't move)", Space Robotics: Dynamics and Control, Kluwer Academic Publishers, Norwell, Mass.

[9] Longman, R., W., and Zedd, M., F., (1990), "Kinematic and Dynamic Properties of an Elbow Manipulator Mounted on a Satellite" The Journal of the Astronautical Sciences, Vol. 38, No. 4.

[10] Akpan, U., O. and Kujath, M., R., (1997), Design requirements for Minimum Vibration of Mobile Manipulators, Conference Proceedings for RAAD'97, Cassino, Italy

[11] Spong, M. W. and Vidyasagar, M., (1989), Robot Dynamics and Control, John Wiley and Sons.

[12] Inman, D. J., (1994), Engineering Vibrations, Prentice-Hall Inc., Englewood Cliff, New Jersey

[13] CDI price list for Optitrac for 1998

[14] Thomson, W. T., (1993), Theory of Vibration with Applications, Forth Edition, Prentice-Hall Inc.

[15] Rao, S., S., (1995), Mechanical Vibrations, Addison-Wesley Publishing Company, Inc., Reading Mass.

[16] Ray, M., Kujath, M. R., (1999), Space Station Manipulator Vibrations, Conference Proceedings for RAAD'99, Germany.

APPENDICES

Appendix I: Complete Derivation of Equations

Appendix II: Simulation Files

Appendix III: Calculations

Appendix IV: Transformation from Absolute Coordinates to Joint Coordinates

Appendix V: Parameters for Decoupling a 3 DOF Linkage

APPENDIX I

COMPLETE DERIVATION OF EQUATIONS

A1.1 **Equations of Motion**

Spong and Vidyasagar [11] Eq. 6.3.12 provide a rigid robotic procedure for deriving the equation of motion involving only inertia and Coriolis and centrifugal terms. In this study, damping and stiffness terms are added. The equation of motion can be written as

$$\mathbf{M}\ddot{\mathbf{p}} + \mathbf{A}\dot{\mathbf{p}} + \mathbf{C}\dot{\mathbf{p}} + \mathbf{K}\mathbf{p} = \tau \qquad \text{(A1.1)}$$

where **p** and its derivatives include both posture and motion.

The related torques have been divided into 5 categories:

- Inertia Torques $\mathbf{M}\ddot{\mathbf{p}}$
- Coriolis & centrifugal Torques $\mathbf{A}\dot{\mathbf{p}}$
- Damping Torques $\mathbf{C}\dot{\mathbf{p}}$
- Stiffness Torques $\mathbf{K}\mathbf{p}$
- Drive Torques τ

The right hand side component is the driving torque, τ.

For spatial manipulators the symmetric positive definite matrix **M** has the form ([11] Eq. 6.2.22)

$$\mathbf{M} = [J_{vGi}]^T m_i [J_{vGi}] + [J_{\omega i}]^T [R_o^i] I_i [R_o^i]^T [J_{\omega i}] \quad \text{(A1.2)}$$

and because $[\mathbf{R}_o^i][\mathbf{R}_o^i]^T$ = unit matrix

for planar manipulators I_i is a scalar and therefore

$$\mathbf{M} = [J_{vGi}]^T m_i [J_{vGi}] + [J_{\omega i}]^T I_i [J_{\omega i}], \quad \text{(A1.3)}$$

where

$\mathbf{J}_{vGi}$ - 3×n Jacobian relating linear velocity of the i-th link centroid to the base reference frame.

$\mathbf{J}_{\omega i}$ - 3×n Jacobian relating angular velocity of the i-th link to the base reference frame.

n - number of links (also number of joints)

m_i - i-th link mass

$\mathbf{I}_i$ - i-th link inertia 3×3 tensor

I_i - for planar motion: i-th link inertia scalar

$\mathbf{R}_o^i$ - rotation matrix of the i-th link with respect to the base reference frame.

The **A** matrix is composed of derivatives of the entries of the inertia matrix **M** ([11] Eq.6.3.13):

$$A_{kj} = 1/2 \sum_{i=1}^{n} (\partial M_{kj}/\partial \mathbf{p}_i + \partial M_{ki}/\partial \mathbf{p}_j - \partial M_{ij}/\partial \mathbf{p}_k)(\dot{\mathbf{p}}_i) \quad \text{(A1.4)}$$

Note: Should the inertia matrix **M** be configuration independent then **A** matrix would

disappear.

Note: The inertia tensor $\mathbf{I_i}$ is a scalar in plane motion as only one rotary DOF is possible for a single object.

To solve for the equations of motion the Jacobian matrices have to be formed.

A1.2 Jacobians for Link-1 in Planar Motion

1. The transform matrix relating the position and orientation of the centroid CG_1 of the first link to the base reference frame 0 has the following form:

$$\mathbf{T}_{G1} = \begin{bmatrix} C_1 & -S_1 & 0 & l_1C_1 \\ S_1 & C_1 & 0 & l_1 S_1 \\ 0 & 0 & 1 & 0 \\ 0 & 0 & 0 & 1 \end{bmatrix} \qquad \text{(A1.5)}$$

Note: $C_1 = \text{Cos}(\mathbf{p}_1)$, $C_2 = \text{Cos}(\mathbf{p}_2)$, $S_1 = \text{Sin}(\mathbf{p}_1)$ and $S_2 = \text{Sin}(\mathbf{p}_2)$

2. Displacement vector **d** components in (A1.5) are

$$d_X = l_1C_1 \qquad \text{(A1.6)}$$

$$d_Y = l_1S_1 \qquad \text{(A1.7)}$$

In the plane, the linear motion takes place only along two axes, the x-axis and the y-axis;

therefore for computation of $\mathbf{J}_{vG1}$ only the x and y components are considered.

3. Components of the Jacobian $\mathbf{J}_{vG1}$ relating the linear velocity v_1 of the centroid CG_1 of the first link (velocity seen in the base reference frame 0) to the joint velocities:

$$\partial d_X / \partial \mathbf{p}_1 = -l_1 S_1 \tag{A1.8}$$

$$\partial d_X / \partial \mathbf{p}_2 = 0 \tag{A1.9}$$

$$\partial d_Y / \partial \mathbf{p}_1 = l_1 C_1 \tag{A1.10}$$

$$\partial d_Y / \partial \mathbf{p}_2 = 0 \tag{A1.11}$$

The Jacobian $\mathbf{J}_{vG1}$ has the form:

$$\mathbf{J}_{vG1} = \begin{bmatrix} -l_1 S_1 & 0 \\ l_1 C_1 & 0 \end{bmatrix} \tag{A1.12}$$

4. Components of the Jacobian $\mathbf{J}_{\omega 1}$ relating the angular velocity ω_1 of the first link (velocity seen in the base reference frame 0) to the joint velocities:

$$\mathbf{J}_{\omega 1} = \begin{bmatrix} r_1 \begin{bmatrix} 0 \\ 0 \\ 1 \end{bmatrix}; & \begin{bmatrix} 0 \\ 0 \\ 0 \end{bmatrix} \end{bmatrix} \quad \text{,let } \omega_1 = 1 \text{ for ease of computation} \tag{A1.13}$$

where r_1 is the length of the link and ω_1 is the angular velocity of the link.

$$J_{\omega 1} = r_1 \begin{bmatrix} 0 & 0 \\ 0 & 0 \\ 1 & 0 \end{bmatrix} \tag{A1.14}$$

The Jacobian $\mathbf{J}_\omega$ relates the following velocity components

$$\begin{bmatrix} \omega_X \\ \omega_y \\ \omega_Z \end{bmatrix} = \begin{bmatrix} 0 & 0 \\ 0 & 0 \\ 1 & 0 \end{bmatrix} \begin{bmatrix} \dot{\mathbf{p}}_1 \\ \dot{\mathbf{p}}_2 \end{bmatrix} \tag{A1.15}$$

In plane, however, the angular motion takes place only about the z-axis therefore for derivation of $\mathbf{J}_{\omega 1}$ we consider only the z-component of $\mathbf{J}_\omega$:

$$J_{\omega 1} = [\ 1 \quad 0\ ] \tag{A1.16}$$

A1.3 **Jacobians of Link-2 in Planar Motion**

1. The transform T_{G2} relating the position and orientation of the centroid of the second link to the base reference frame 0 has the following form:

$$T_{G2} = \begin{bmatrix} C_{12} & -S_{12} & 0 & a_1 C_1 + l_2 C_{12} \\ S_{12} & C_{12} & 0 & a_1 S_1 + l_2 S_{12} \\ 0 & 0 & 1 & 0 \\ 0 & 0 & 0 & 1 \end{bmatrix} \tag{A1.17}$$

where C_{12} and S_{12} are $\mathrm{COS}(\mathbf{p}_1 + \mathbf{p}_2)$ and $\mathrm{SIN}(\mathbf{p}_1 + \mathbf{p}_2)$ respectively.

2. Displacement vector **d** components in (A1.17) are:

$$d_X = a_1C_1 + l_2C_{12} \quad \text{(A1.18)}$$

$$d_Y = a_1S_1 + l_2S_{12} \quad \text{(A1.19)}$$

3. Components of the Jacobian $\mathbf{J}_{vG2}$ relating the linear velocity v_2 of the centroid CG_2 of the second link (velocity seen in the base reference frame 0) to the joint velocities:

$$\partial d_X / \partial \mathbf{p}_1 = -a_1S_1 - l_2S_{12} \quad \text{(A1.20)}$$

$$\partial d_X / \partial \mathbf{p}_2 = -l_2S_{12} \quad \text{(A1.21)}$$

$$\partial d_Y / \partial \mathbf{p}_1 = a_1C_1 + l_2C_{12} \quad \text{(A1.22)}$$

$$\partial d_Y / \partial \mathbf{p}_2 = l_2C_{12} \quad \text{(A1.23)}$$

The Jacobian $\mathbf{J}_{vG2}$ is then:

$$\mathbf{J}_{vG2} = \begin{bmatrix} -a_1S_1 - l_2S_{12} & -l_2S_{12} \\ a_1C_1 + l_2C_{12} & l_2C_{12} \end{bmatrix} \quad \text{(A1.24)}$$

4. Components of the Jacobian $\mathbf{J}_{\omega 2}$ relating the angular velocity ω_2 of the second link (velocity seen in the base reference frame 0) to the joint velocities:

$$\mathbf{J}_{\omega 2} = \begin{bmatrix} r_1 \begin{bmatrix} 0 \\ 0 \\ 1 \end{bmatrix}; & r_2 R_0^1 \begin{bmatrix} 0 \\ 0 \\ 1 \end{bmatrix} \end{bmatrix}, \ \omega_1 = 1, \omega_2 = 1 \qquad \text{(A.25)}$$

where r_i is the length of link i and ω_i is the angular velocity of link i. By setting $\omega_i = 1$ it is easier to define the Jacobian.

In plane the angular motion takes place only about the z-axis therefore for $\mathbf{J}_{\omega 2}$ we consider only the z-component of $\mathbf{J}_{\omega}$

$$\mathbf{J}_{\omega} = [\ 1 \quad 1 \quad] \qquad \text{(A1.26)}$$

A1.4 **Matrix Components for 2 DOF**

Inertia Matrix M

$$\mathbf{M} = \begin{bmatrix} M_{11} & M_{12} \\ M_{21} & M_{22} \end{bmatrix}$$

$$\mathbf{M} = [\mathbf{J}_{vG1}]^T m_1 \mathbf{J}_{vG1} + [\mathbf{J}_{\omega 1}]^T I_1 \mathbf{J}_{\omega 1} + [\mathbf{J}_{vG2}]^T m_2 \mathbf{J}_{vG2} + [\mathbf{J}_{\omega 2}]^T I_2 \mathbf{J}_{\omega 2} \qquad \text{(A1.27)}$$

$$M_{11} = m_1 (l_1)^2 + I_1 + m_2 ((a_1)^2 + (l_2)^2 + 2a_1 l_2 C_2) + I_2 \qquad \text{(A1.28)}$$

$$M_{12} = 0 + 0 + m_2 ((l_2)^2 + a_1 l_2 C_2) + I_2 \qquad \text{(A1.29)}$$

$$M_{21} = M_{12} \qquad \text{(A1.30)}$$

$$M_{22} = 0 + 0 + m_2 (l_2)^2 + I_2 \qquad \text{(A1.31)}$$

where M_{12} and M_{21} are derived as follows:

$$M_{12} = m_2(a_1 S_1 l_2 S_{12} + (l_2 S_{12})^2 + a_1 C_1 l_2 C_{12} + (l_2 C_{12})^2) + I_2$$

$$= m_2(a_1 l_2 (S_1 S_{12} + C_1 C_{12}) + l_2^2) + I_2 \qquad \text{(A1.32)}$$

Using known trigonometric identities:

$$\mathrm{Sin}(\mathbf{p}_1+\mathbf{p}_2) = \mathrm{Sin}(\mathbf{p}_1)\mathrm{Cos}(\mathbf{p}_2) + \mathrm{Cos}(\mathbf{p}_1)\mathrm{Sin}(\mathbf{p}_2) \quad \text{(A1.33)}$$

and

$$\mathrm{Cos}(\mathbf{p}_1+\mathbf{p}_2) = \mathrm{Cos}(\mathbf{p}_1)\mathrm{Cos}(\mathbf{p}_2) - \mathrm{Sin}(\mathbf{p}_1)\mathrm{Sin}(\mathbf{p}_2) \quad \text{(A1.34)}$$

substituting them into Eq. (A1.32) the following expression is obtained

$$M_{12} = m_2(a_1 l_2(S_1^2C_2 + S_1S_2C_1 + C_1^2C_2 - S_1S_2C_1) + l_2^2) + I_2$$

$$= m_2 a_1 l_2 C_2 + m_2 l_2^2 + I_2 \quad \text{(A1.35)}$$

Coriolis and centrifugal effect matrix components

$$A_{11} = 1/2\,(\partial M_{11}/\partial \mathbf{p}_1 + \partial M_{11}/\partial \mathbf{p}_1 - \partial M_{11}/\partial \mathbf{p}_1)(\dot{\mathbf{p}}_1)$$

$$+1/2\,(\partial M_{11}/\partial \mathbf{p}_2 + \partial M_{12}/\partial \mathbf{p}_1 - \partial M_{21}/\partial \mathbf{p}_1)(\dot{\mathbf{p}}_2)$$

$$= 0\,(\dot{\mathbf{p}}_1) - m_2 a_1 l_2 S_2(\dot{\mathbf{p}}_2) \quad \text{(A1.36)}$$

$$A_{12} = 1/2\,(\partial M_{12}/\partial \mathbf{p}_1 + \partial M_{11}/\partial \mathbf{p}_2 - \partial M_{12}/\partial \mathbf{p}_1)(\dot{\mathbf{p}}_1)$$

$$+1/2\,(\partial M_{12}/\partial \mathbf{p}_2 + \partial M_{12}/\partial \mathbf{p}_2 - \partial M_{22}/\partial \mathbf{p}_1)(\dot{\mathbf{p}}_2)$$

$$= -m_2 a_1 l_2 S_2\,(\dot{\mathbf{p}}_1) - m_2 a_1 l_2 S_2(\dot{\mathbf{p}}_2) \quad \text{(A1.37)}$$

$$A_{21} = 1/2\,(\partial M_{21}/\partial \mathbf{p}_1 + \partial M_{21}/\partial \mathbf{p}_1 - \partial M_{11}/\partial \mathbf{p}_2)(\dot{\mathbf{p}}_1)$$

$$+1/2\,(\partial M_{21}/\partial \mathbf{p}_2 + \partial M_{22}/\partial \mathbf{p}_1 - \partial M_{21}/\partial \mathbf{p}_2)(\dot{\mathbf{p}}_2)$$

$$= m_2 a_1 l_2 S_2\,(\dot{\mathbf{p}}_1) \quad \text{(A1.38)}$$

$$A_{22} = 1/2\,(\partial M_{22}/\partial \mathbf{p}_1 + \partial M_{21}/\partial \mathbf{p}_2 - \partial M_{12}/\partial \mathbf{p}_2)(\dot{\mathbf{p}}_1)$$

$$+1/2\,(\partial M_{22}/\partial \mathbf{p}_2 + \partial M_{22}/\partial \mathbf{p}_2 - \partial M_{22}/\partial \mathbf{p}_2)(\dot{\mathbf{p}}_2)$$

$$= 0(\dot{\mathbf{p}}_1) + 0(\dot{\mathbf{p}}_2) \qquad \text{(A1.39)}$$

Damping components

The damping is located only in the joints therefore the C matrix is diagonal and the damping of link-1 is

$$C_{11} = c_1 \qquad \text{(A1.40)}$$

and the damping of link-2 is

$$C_{22} = c_2 \qquad \text{(A1.41)}$$

Stiffness components

The stiffness is located only in the joints therefore the **K** matrix is diagonal and the stiffness of link-1 is

$$K_{11} = k_1 \qquad \text{(A1.42)}$$

and the stiffness of link-2 is

$$K_{22} = k_2 \qquad \text{(A1.43)}$$

The total equation of motion is

$$\begin{bmatrix} M_{11} & M_{12} \\ M_{21} & M_{22} \end{bmatrix} \begin{bmatrix} \ddot{\mathbf{p}}_1 \\ \ddot{\mathbf{p}}_2 \end{bmatrix} + \begin{bmatrix} A_{11} & A_{12} \\ A_{21} & 0 \end{bmatrix} \begin{bmatrix} \dot{\mathbf{p}}_1 \\ \dot{\mathbf{p}}_2 \end{bmatrix} + \begin{bmatrix} C_{11} & 0 \\ 0 & C_{22} \end{bmatrix} \begin{bmatrix} \dot{\mathbf{p}}_1 \\ \dot{\mathbf{p}}_2 \end{bmatrix} + \begin{bmatrix} K_{11} & 0 \\ 0 & K_{22} \end{bmatrix} \begin{bmatrix} \mathbf{p}_1 \\ \mathbf{p}_2 \end{bmatrix} = \begin{bmatrix} \tau_1 \\ \tau_2 \end{bmatrix}$$

(A1.44)

A1.5 **Separation of Coordinates**

Separating the coordinate **p** into posture coordinate **Q** and local (motion) coordinate **q** the equation of motion can be written as

$$\mathbf{M}(\ddot{\mathbf{Q}} + \ddot{\mathbf{q}}) + \mathbf{A}(\dot{\mathbf{Q}} + \dot{\mathbf{q}}) + \mathbf{C}(\dot{\mathbf{Q}} + \dot{\mathbf{q}}) + \mathbf{K}(\mathbf{Q} + \mathbf{q}) = \tau \quad \text{(A1.45)}$$

Where **M** and **A** are functions of both **Q** and **q**.

$$M_{11} = m_1(l_1)^2 + m_2[(a_1)^2 + (l_2)^2 + 2a_1l_2\text{Cos}(\mathbf{Q}_2 + \mathbf{q}_2)] + I_1 + I_2 \quad \text{(A1.46)}$$

$$M_{12} = M_{21} = m_2a_1l_2\text{Cos}(\mathbf{Q}_2 + \mathbf{q}_2) + m_2l_2^2 + I_2 \quad \text{(A1.47)}$$

$$M_{22} = m_2l_2^2 + I_2 \quad \text{(A1.48)}$$

$$A_{11} = -m_2a_1l_2\text{Sin}(\mathbf{Q}_2 + \mathbf{q}_2)(\dot{\mathbf{Q}}_2 + \dot{\mathbf{q}}_2) \quad \text{(A1.49)}$$

$$A_{12} = -m_2a_1l_2\text{Sin}(\mathbf{Q}_2 + \mathbf{q}_2)(\dot{\mathbf{Q}}_1 + \dot{\mathbf{q}}_1 + \dot{\mathbf{Q}}_2 + \dot{\mathbf{q}}_2) \quad \text{(A1.50)}$$

$$A_{21} = m2\ a_1l_2\text{Sin}(\mathbf{Q}_2 + \mathbf{q}_2)(\dot{\mathbf{Q}}_1 + \dot{\mathbf{q}}_1) \quad \text{(A1.51)}$$

Using the trigonometric identities

$$\text{Cos}(\mathbf{Q}_2 + \mathbf{q}_2) = \text{Cos}(\mathbf{Q}_2)\,\text{Cos}(\mathbf{q}_2) - \text{Sin}(\mathbf{Q}_2)\text{Sin}(\mathbf{q}_2) \quad \text{(A1.52)}$$

$$\text{Sin}(\mathbf{Q}_2 + \mathbf{q}_2) = \text{Sin}(\mathbf{Q}_2)\,\text{Cos}(\mathbf{q}_2) + \text{Cos}(\mathbf{Q}_2)\text{Sin}(\mathbf{q}_2) \quad \text{(A1.53)}$$

where $\mathbf{q}_2$ is very small and the following approximations are made

$$\text{Cos}(\mathbf{q}_2) \approx 1 \quad \text{(A1.54)}$$

and

$$\text{Sin}(\mathbf{q}_2) \approx \mathbf{q}_2 \quad \text{(A1.55)}$$

we obtain:

$$\text{Cos}(\mathbf{Q}_2 + \mathbf{q}_2) = \text{Cos}(\mathbf{Q}_2) - \mathbf{q}_2\text{Sin}(\mathbf{Q}_2) \text{ and} \quad \text{(A1.56)}$$

$$\text{Sin}(\mathbf{Q}_2 + \mathbf{q}_2) = \text{Sin}(\mathbf{Q}_2) + \mathbf{q}_2\text{Cos}(\mathbf{Q}_2) \quad \text{(A1.57)}$$

We can linearize the components of **M** by substituting Eq. (A1.56) into Equations (A1.46) to (A1.48) and neglecting the higher order terms, i.e., $\mathbf{q}_2 \ddot{\mathbf{q}}_1 \text{ Sin}(\mathbf{Q}_2) \approx 0$ and $\mathbf{q}_2 \ddot{\mathbf{q}}_2 \text{ Sin}(\mathbf{Q}_2) \approx 0$, giving **M** as a function of **Q** only.

$$M_{11} = m_1(l_1)^2 + m_2[(a_1)^2 + (l_2)^2 + 2a_1l_2\text{Cos}(\mathbf{Q}_2)] + I_1 + I_2 \quad \text{(A1.58)}$$

$$M_{12} = M_{21} = m_2a_1l_2\text{Cos}(\mathbf{Q}_2) + m_2l_2^2 + I_2 \quad \text{(A1.59)}$$

$$M_{22} = m_2l_2^2 + I_2 \quad \text{(A1.60)}$$

We can linearize the components of **A** by substituting Eq. (A1.57) into Equations (A1.49) to (A1.51) and neglecting the higher order terms, i.e., $\mathbf{q}_2 \dot{\mathbf{q}}_2 \approx 0$, $\mathbf{q}_2(\dot{\mathbf{q}}_1 + \dot{\mathbf{q}}_2) \approx 0$ and $\mathbf{q}_2\dot{\mathbf{q}}_1 \approx 0$.

$$A_{11} = -m_2a_1l_2\text{Sin}(\mathbf{Q}_2)(\dot{\mathbf{Q}}_2 + \dot{\mathbf{q}}_2) \quad \text{(A1.61)}$$

$$A_{12} = -m_2a_1l_2\text{Sin}(\mathbf{Q}_2)(\dot{\mathbf{Q}}_1 + \dot{\mathbf{q}}_1 + \dot{\mathbf{Q}}_2 + \dot{\mathbf{q}}_2) \quad \text{(A1.62)}$$

$$A_{21} = m2\ a_1l_2\text{Sin}(\mathbf{Q}_2)(\dot{\mathbf{Q}}_1 + \dot{\mathbf{q}}_1) \quad \text{(A1.63)}$$

Because in the reported study the vibration **q** takes place when the posture **Q** is constant, the derivatives $\ddot{\mathbf{Q}}$ and $\dot{\mathbf{Q}}$ vanish. Secondly because the elasticity and damping are located

only in the joints the elastic forces depend only on $\mathbf{q}$ and $\mathbf{K(Q+q) = K\,q}$.

Since the angular motion is relatively small the effects of changing posture due to motion have been neglected. This indicates that the influence of $\mathbf{q}$, $\dot{\mathbf{q}}$ in the terms of **M** and **A** are neglected. The equation of motion can now be written as

$$\mathbf{M}\ddot{\mathbf{q}} + \mathbf{A}\dot{\mathbf{q}} + \mathbf{C}\dot{\mathbf{q}} + \mathbf{K}\mathbf{q} = \tau \tag{A1.64}$$

The inertia matrix **M**, and the Coriolis & centrifugal matrix **A** are posture dependent, i.e. they are functions of the posture coordinates **Q**.

When $\mathbf{Q_2}$ is chosen such that the mass matrix decouples and the following equation is the result:

$$\begin{bmatrix} M_{11} & 0 \\ 0 & M_{22} \end{bmatrix} \begin{bmatrix} \ddot{\mathbf{q}}_1 \\ \ddot{\mathbf{q}}_2 \end{bmatrix} + \begin{bmatrix} A_{11} & A_{12} \\ A_{21} & 0 \end{bmatrix} \begin{bmatrix} \dot{\mathbf{q}}_1 \\ \dot{\mathbf{q}}_2 \end{bmatrix} + \begin{bmatrix} C_{11} & 0 \\ 0 & C_{22} \end{bmatrix} \begin{bmatrix} \dot{\mathbf{q}}_1 \\ \dot{\mathbf{q}}_2 \end{bmatrix} + \begin{bmatrix} K_{11} & 0 \\ 0 & K_{22} \end{bmatrix} \begin{bmatrix} \mathbf{q}_1 \\ \mathbf{q}_2 \end{bmatrix} = \tau \tag{A1.65}$$

giving the following two equations:

$$M_{11}\ddot{\mathbf{q}}_1 + A_{11}\dot{\mathbf{q}}_1 + A_{12}\dot{\mathbf{q}}_2 + C_{11}\dot{\mathbf{q}}_1 + K_{11}\mathbf{q}_1 = \tau_1 \tag{A1.66}$$

and

$$M_{22}\ddot{\mathbf{q}}_2 + A_{21}\dot{\mathbf{q}}_1 + C_{22}\dot{\mathbf{q}}_2 + K_{22}\mathbf{q}_2 = \tau_2 \tag{A1.67}$$

A1.6 **Parameters of the Experimental Model**

The parameters of the physical model are listed in the following table.

Table A1 – Parameters of the physical model and necessary values for $\mathbf{Q}_1$ and $\mathbf{Q}_2$ for diagonalizing the mass matrix.

a of bar 1&2	0.277 m
l of bar 1&2	0.1385 m
$\mathbf{Q}_1$	any value
$\mathbf{Q}_2$ (calculated)	131.38 degrees
I of bar 1&2	0.000799776 m^4
m of bar 1&2	0.129399 kg
k (experimentally)	0.326 N-m/rad
ξ	0.0001
link material	aluminum

These parameters give the following two equations

$$0.009929\,\ddot{\mathbf{q}}_1 + .000745\dot{\mathbf{q}}_2^{\,2} + .0003725\dot{\mathbf{q}}_1\,\dot{\mathbf{q}}_2 + 0.326\mathbf{q}_1 = \tau_1 \qquad \text{A1.68a}$$

solving for $\ddot{\mathbf{q}}_1$

$$\ddot{\mathbf{q}}_1 = -\,0.0750327\dot{\mathbf{q}}_2^{\,2} - \,0.37516\dot{\mathbf{q}}_1\,\dot{\mathbf{q}}_2 - 32.83311\mathbf{q}_1 + \tau_1/0.009929 \qquad \text{A1.68b}$$

and

$$0.003282\,\ddot{q}_2 - .0003725\dot{q}_1^{\,2} + 0.326q_2 = \tau_2 \qquad \text{A1.69a}$$

solving for $\ddot{q}_2$

$$\ddot{q}_2 = 1.13497\dot{q}_1^{\,2} - 99.3297q_2 + \tau_2/0.003282 \qquad \text{A1.69b}$$

A1.6 Equations of Motion for Three-Link Manipulator

To represent the physical model the equations of motion need to be expanded to a three-link manipulator.

In this case the parameters are as follows:

$$M_{11} = m_1 l_1^2 + m_2(a_1^2 + l_2^2 + 2a_1 l_2 C_2) + m_3(l_3(l_3 + a_2 C_3 + a_1 C_{23}) + a_2(l_3 C_3 + a_2 + a_1 C_2)) + a_1(l_3 C_{23} + a_2 C_2 + a_1)) + I_1 + I_2 + I_3 \qquad \text{A1.70}$$

$$M_{12} = m_2(l_2^2 + a_1 l_2 C_2) + m_3(l_3(l_3 + a_2 C_3 + a_1 C_{23}) + a_2(l_3 C_3 + a_2 + a_1 C_2)) + I_2 + I_3 \qquad \text{A1.71}$$

$$M_{13} = m_3(l_3(l_3 + a_2 C_3 + a_1 C_{23})) + I_3 \qquad \text{A1.72}$$

$$M_{21} = m_2(l_2^2 + a_1 l_2 C_2) + m_3(l_3(l_3 + a_2 C_3 + a_1 C_{23}) + a_2(l_3 C_3 + a_2 + a_1 C_2)) + I_2 + I_3 \qquad \text{A1.73}$$

$$M_{31} = m_3(l_3(l_3 + a_2 C_3 + a_1 C_{23})) + I_3 \qquad \text{A1.74}$$

$$M_{22} = m_2 l_2^2 + m_3(l_3(l_3 + a_2 C_3) + a_2(l_3 C_3 + a_2)) + I_2 + I_3 \qquad \text{A1.75}$$

$$M_{23} = m_3(l_3(l_3 + a_2 C_3)) + I_3 \qquad \text{A1.76}$$

$$M_{32} = m_3(l_3(l_3 + a_2 C_3)) + I_3 \qquad \text{A1.77}$$

$$M_{33} = m_3 l_3^2 + I_3 \qquad \text{A1.78}$$

$$A_{11} = (-m_2a_1l_2S_2 - m_3a_1l_3S_{23} - m_3a_1a_2S_2)\dot{q}_2 + (-m_3a_2l_3S_3 - m_3a_1l_3S_{23})\dot{q}_3 \quad \text{A1.79}$$

$$A_{12} = (-m_2a_1l_2S_2 - m_3a_1a_2S_2 - m_3a_1l_3S_{23})\dot{q}_1 + (-m_2a_1l_2S_2 - m_3a_1a_2S_2 - m_3a_1l_3S_{23})\dot{q}_2 + (-m_3a_2l_3S_3 - m_3a_1l_3S_{23})\dot{q}_3 \quad \text{A1.80}$$

$$A_{13} = (-m_3a_2l_3S_3 - m_3a_1l_3S_{23})\dot{q}_1 + (-m_3a_2l_3S_3)\dot{q}_3 \quad \text{A1.81}$$

$$A_{21} = (-m_2a_1l_2S_2 - m_3a_1a_2S_2 - m_3a_1l_3S_{23})\dot{q}_1 + l_2(-m_3a_1l_3S_2 - m_3a_1a_2S_2)\dot{q}_2 + (- m_3a_2l_3S_3)\dot{q}_3 \quad \text{A1.82}$$

$$A_{22} = (-m_3a_2l_3S_3)\dot{q}_3 \quad \text{A1.83}$$

$$A_{23} = (-m_3a_2l_3S_3)\dot{q}_1 + (-m_3a_2l_3S_3)\dot{q}_2 + (-m_3a_2l_3S_3)\dot{q}_3 \quad \text{A1.84}$$

$$A_{31} = (-m_3a_2l_3S_3 - m_3a_1l_3S_{23})\dot{q}_1 + (-m_3a_2l_3S_3)\dot{q}_2 \quad \text{A1.85}$$

$$A_{32} = (-m_3a_2l_3S_3)\dot{q}_1 + (-m_3a_2l_3S_3)\dot{q}_2 \quad \text{A1.86}$$

$$A_{33} = 0 \quad \text{A1.87}$$

$$C_{11} = \xi(2)\sqrt{K_{11}M_{11}} \quad \text{A1.88}$$

$$C_{22} = \xi(2)\sqrt{K_{22}M_{22}} \quad \text{A1.89}$$

$$C_{33} = \xi(2)\sqrt{K_{33}M_{33}} \quad \text{A1.90}$$

$$C_{12} = C_{13} = C_{21} = C_{23} = C_{31} = C_{32} = 0 \quad \text{A1.91}$$

$$K_{11} = K_{22} = K_{33} = k \quad \text{A1.92}$$

$$K_{12} = K_{13} = K_{21} = K_{23} = K_{31} = K_{32} = 0 \quad \text{A1.93}$$

APPENDIX II

SIMULATION FILES

A2.1 **Block Diagrams**

First the equations of motion (Eq. 2.34) were reorganized for $\ddot{q}_1$ and $\ddot{q}_2$. With these equations block diagrams were created using software called SIMULINK, which is part of MATLab. These block diagrams are found in figure 5.1. The system parameters for various postures were calculated using a MATLab file named *massmatrix*.

A2.2 **MATLab Files**

A2.2.1 **System Parameters**

This routine file was used to calculate the parameters of the three-link system for a chosen posture. Typing *massmatrix* in the MATLab command window ran this file. The input parameters here are listed in the file. The posture varying parameters are Q1deg, Q2deg and Q3deg. The mass parameters for each link are m1, m2 and m3 with m1 referring to the base link. The length parameters for each link are a1, a2 and a3.

```
m1=0.129399;
m2=0.129399;
m3=0.129399;
a1=0.277;
a2=0.277;
a3=0.277;
l1=a1/2;
l2=a2/2;
```

```
l3=a3/2;
Q1deg=0;
Q2deg=0;
Q3deg=360-228.61583
Q1=Q1deg*pi/180;
Q2=Q2deg*pi/180;
Q3=Q3deg*pi/180;
C1=cos(Q1);
C2=cos(Q2);
C3=cos(Q3);
C12=cos(Q1+Q2);
C23=cos(Q2+Q3);
C123=cos(Q1+Q2+Q3);
S12=sin(Q1+Q2);
S23=sin(Q2+Q3);
S123=sin(Q1+Q2+Q3);
S1=sin(Q1);
S2=sin(Q2);
S3=sin(Q3);
I1=0.000799776;
I2=0.000799776;
I3=0.000799776;
M11=m1*l1^2+m2*(a1^2+l2^2+2*a1*l2*C2)+m3*(l3*(l3+a2*C3+a1*C2
3)+a2*(l3*C3+a2+a1*C2)+a1*(l3*C23+a2*C2+a1))+I1+I2+I3;
M12=m2*(l2^2+a1*l2*C2)+m3*(l3*(l3+a2*C3+a1*C23)+a2*(l3*C3+a2
+a1*C2))+I2+I3;
M13=m3*(l3*(l3+a2*C3+a1*C23))+I3;
M21=m2*(l2^2+a1*l2*C2)+m3*(l3*(l3+a2*C3+a1*C23)+a2*(l3*C3+a2
+a1*C2))+I2+I3;
M31=m3*(l3*(l3+a2*C3+a1*C23))+I3;
M22=m2*l2^2+m3*(l3*(l3+a2*C3)+a2*(l3*C3+a2))+I2+I3;
M23=m3*(l3*(l3+a2*C3))+I3;
M32=m3*(l3*(l3+a2*C3))+I3;
M33=m3*l3^2+I3;
M=[M11 M12 M13;
   M21 M22 M23;
   M31 M23 M33];
K=[.326*860 0 0;
   0 .326 0;
   0 0 .326];
K11=K(1,1);
K22=K(2,2);
K33=K(3,3);
A=m3*a2*l2*S3;
A11a=0;
A11b=(-a1*l2*m2*S2-m3*a1*l3*S23-m3*a1*a2*S2);
A11c=(-m3*a2*l3*S3-m3*a1*l3*S23);
```

```
A12a=(-m2*a1*l2*S2-m3*a1*a2*S2-m3*a1*l3*S23);
A12b=-m2*a1*l2*S2-m3*l3*a1*S23-m3*a1*a2*S2;
A12c=-m3*a2*l3*S3-m3*a1*l3*S23;
A13a=(-m3*a2*l3*S3-m3*a1*l3*S23);
A13b=0;
A13c=-m3*a2*l3*S3;
A21a=(m2*a1*l2*S2+m3*a1*l3*S23+m3*a1*a2*S2);
A21b=.5*(m3*l3*a1*S2-m3*a1*a2*S2);
A21c=-m3*a2*l3*S3;
A31a=m3*a2*l3*S3+m3*a1*l3*S23;
A31b=m3*a2*l3*S3;
A31c=0;
A22a=0;
A22b=0;
A22c=-m3*a2*l3*S3;
A23a=-m3*a2*l3*S3;
A23b=-m3*a2*l3*S3;
A23c=-m3*a2*l3*S3;
A32a=-m3*a2*l3*S3;
A32b=-m3*a2*l3*S3;
A32c=0;
A33=0;
C(1,1)=.001*2*sqrt(K(1,1)*M(1,1));
C(2,2)=.001*2*sqrt(K(2,2)*M(2,2));
C(3,3)=.001*2*sqrt(K(3,3)*M(3,3));
D=eig(inv(M)*K);
[V,D]=eig(inv(M)*K);
Lamda=[D(1,1)
    D(2,2)
    D(3,3)]
Lamda1=sort(Lamda)
natfreq=sqrt(Lamda1)
```

A2.2.2 **Natural Frequencies for All Postures and Eigen vectors**

This file was used to calculate the parameters of the three-link system for a range of values of the posture angle between 0 and 180^0. Application of this file also plotted the magnitudes of the first two natural frequencies versus the angle of the second joint. The eigen vectors were calculated and sorted when running this file. Typing *allconfig* in the

MATLab command window ran this file. The input data for the application of this file were the same physical parameters of the physical model namely, each link had a mass of 0.129339 Kg, a length of 0.277 m, a moment of inertia of 0.000799776 kg-m^2 and a stiffness of 280. 36 N-m/rad. Each flat spring joint had a stiffness of 0.326 N-m/rad.

```
natfreq1=0;
natfreq2=0;
natfreq3=0;
D11=0;
D22=0;
D33=0;
m1=0.129399;
m2=0.129399;
m3=0.129399;
a1=0.277;
a2=0.277;
a3=0.277;
l1=a1/2;
l2=a2/2;
l3=a3/2;
Q1deg=0;
Q2deg=0;
for n=1:181;
Q3deg=(n-1)
Q1=Q1deg*pi/180;
Q2=Q2deg*pi/180;
Q3=Q3deg*pi/180;
C1=cos(Q1);
C2=cos(Q2);
C3=cos(Q3);
C12=cos(Q1+Q2);
C23=cos(Q2+Q3);
C123=cos(Q1+Q2+Q3);
S12=sin(Q1+Q2);
S23=sin(Q2+Q3);
S123=sin(Q1+Q2+Q3);
S1=sin(Q1);
S2=sin(Q2);
S3=sin(Q3);
I1=0.000799776;
I2=0.000799776;
I3=0.000799776;
```

```
M11=m1*l1^2+m2*(a1^2+l2^2+2*a1*l2*C2)+m3*(l3*(l3+a2*C3+a1*C2
3)+a2*(l3*C3+a2+a1*C2)+a1*(l3*C23+a2*C2+a1))+I1+I2+I3;
M12=m2*(l2^2+a1*l2*C2)+m3*(l3*(l3+a2*C3+a1*C23)+a2*(l3*C3+a2
+a1*C2))+I2+I3;
M13=m3*(l3*(l3+a2*C3+a1*C23))+I3;
M21=m2*(l2^2+a1*l2*C2)+m3*(l3*(l3+a2*C3+a1*C23)+a2*(l3*C3+a2
+a1*C2))+I2+I3;
M31=m3*(l3*(l3+a2*C3+a1*C23))+I3;
M22=m2*l2^2+m3*(l3*(l3+a2*C3)+a2*(l3*C3+a2))+I2+I3;
M23=m3*(l3*(l3+a2*C3))+I3;
M32=m3*(l3*(l3+a2*C3))+I3;
M33=m3*l3^2+I3;
M=[M11 M12 M13;
   M21 M22 M23;
   M31 M23 M33];
K=[.326*860 0 0;
   0 .326 0;
   0 0 .326];
K11=K(1,1);
K22=K(2,2);
K33=K(3,3);
A=m3*a2*l2*S3;
C(1,1)=.001*2*sqrt(K(1,1)*M(1,1));
C(2,2)=.001*2*sqrt(K(2,2)*M(2,2));
C(3,3)=.001*2*sqrt(K(3,3)*M(3,3));
D=eig(inv(M)*K);
[V,D]=eig(inv(M)*K);
i=1;
for j=1:3
   DD(j)=D(i,i);
   i=i+1;
end
[SDD, SI]=sort(DD);
i=1;
for j=1:3;
   TEMP(:,j)=V(1:3,i);
   TD1(j)=D(i,i);
   i=i+1;
end
PSI=TEMP(:,SI);
TD2=TD1(SI);
for i=1:3;
      Lambda(i,i)=TD2(i); % sorted eigenvalue matrix
   end
Lamda1=[Lambda(1,1);
   Lambda(2,2);
   Lambda(3,3)];
```

```
natfreq=sqrt(Lamda1);
V11(n)=PSI(1,1);
V12(n)=PSI(1,2);
V13(n)=PSI(1,3);
V21(n)=PSI(2,1);
V22(n)=PSI(2,2);
V23(n)=PSI(2,3);
V31(n)=PSI(3,1);
V32(n)=PSI(3,2);
V33(n)=PSI(3,3);
natfreq1(n)=natfreq(1,1);
natfreq2(n)=natfreq(2,1);
natfreq3(n)=natfreq(3,1);
end
z=0:n-1;
plot(z,natfreq1,:,z,natfreq2)
ylabel('Frequency (rads/s)')
xlabel('Angle of Joint 2 (degrees)')
title('The First Two Natural Frequencies Versus Joint
Configuration')
%eigenvectors
a1=V11';
b1=V21';
c1=V31';
d1=natfreq1';
a2=V12';
b2=V22';
c2=V32';
d2=natfreq2';
a3=V13';
b3=V23';
c3=V33';
d3=natfreq3';
XX=[a1 b1 c1 d1 z'];
YY=[a2 b2 c2 d2 z'];
ZZ=[a3 b3 c3 d3 z'];
Y=cat(3,XX,YY,ZZ)
damped1=(natfreq1')*sqrt(1-(0.001)^2);
damped2=(natfreq2')*sqrt(1-(0.001)^2);
damped3=(natfreq3')*sqrt(1-(0.001)^2);
```

A2.2.3 **Frequency Spectrums of Experimental Results**

Application of this file calculated and plotted the frequency spectrum of the experimental results. Taking the Fast Fourier Transform (FFT) of the results and plotting them versus frequency did this. After loading the experimental results into MATLab and typing *fftest* in the MATLab command window ran this file. The input data used is the angular position and corresponding time obtained from the experimental results.

```
t=t1;
x1=q1x;
x2=q2x;
X1=fft(x1);
X2=fft(x2);
Ts=t(2)-t(1);
Ws=2*pi/Ts;
Wn=Ws/2;
w=linspace(0,Wn,length(t)/2);
Xp1=abs(X1(1:length(t)/2));
Xp2=abs(X2(1:length(t)/2));
plot(w,Xp1,w,Xp2)
```

A2.2.4 **Conversion of Angular Coordinates to Cartesian Coordinates**

This file converted joint angles to tip displacement in Cartesian coordinates. This file also plotted the tips of links 2 and 3. After loading the joint angle coordinates (experimental or simulated) into MATLab and typing tip in the MATLab command window ran this file.

```
X2=a2*cos(q2);
Y2=a2*sin(q2);
F=(180-131.38)*pi/180+q3;
```

```
f=sqrt(a2^2+a3^2-2*a2*a3*cos(F));
A3=asin(a3*sin(F)./f);
o=-(A3+q2);
X3=f.*cos(o);
Y3=f.*sin(o);
plot(X2,Y2,'k',X3,Y3,'k')
axis square
axis ([0 0.35 -.3 .05])
xlabel('x(m)')
ylabel('y(m)')
```

APPENFDIX III

CALCULATIONS

A3.1 Moment of Inertia

Calculations for the moment of inertia I for the links, where a and b are length and height respectively of the corresponding part, are as follows:

$$I_{ext} = \frac{1}{12} m_{bar} (a_{ext}^2 + b_{ext}^2) \quad \text{A3.1}$$

$$I_{hinge} = \frac{1}{12} m_{1/2\ hinge} (a_{hinge}^2 + b_{1/2\ hinge}^2) \quad \text{A3.2}$$

$$I_0 = \frac{1}{12} m_{bar} (a_{bar}^2 + b_{bar}^2) + 2 (I_{ext} + m_{ext} r_1^2) + 2 I_{1/2\ hinge} + m_{hinge} r_2^2 \quad \text{A3.3}$$

I_{ext} represents the moment of inertia of the extension.

I_{hinge} represents the moment of inertia of half of the hinge.

I_0 represents the moment of inertia of the link, the extension and half of the hinge.

The mass and moment of inertia of the shim (flat spring) was considered negligible.

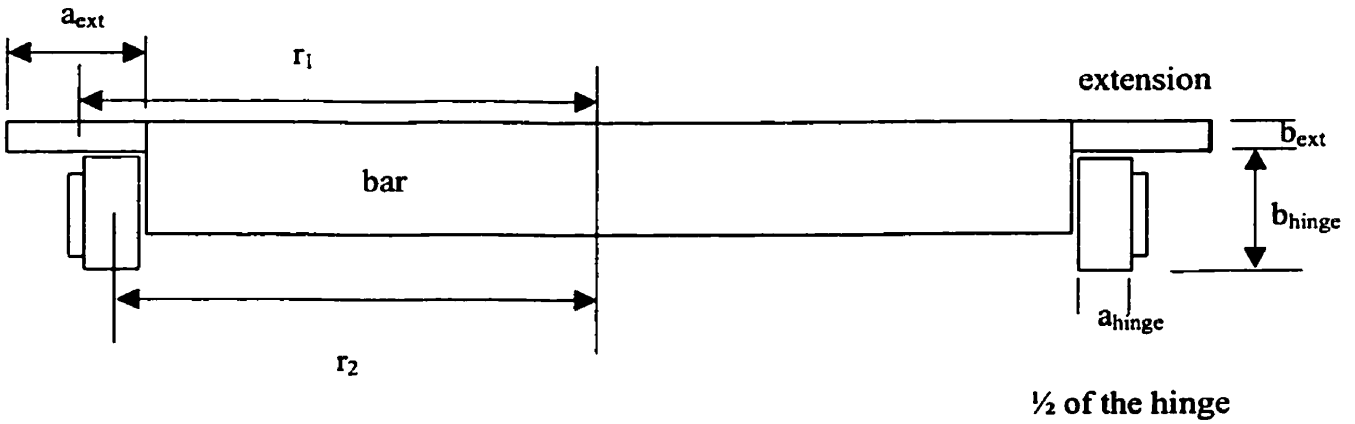

Figure A3.1: Link components for moment of inertia calculations

A3.2 **Angle of Joints to Prevent Torsion**

Since the center of gravity of each link was at its geometrical center by design it was possible to use simple geometry and trigonometry to solve for the position of the center of gravity of the chain of links. The angle γ is the angle which the flat spring must be in-line with to avoid torsion in the first joint.

Angle A is known since $A = q - 180^0$ A3.4

$c = b = \text{length}/2$ A3.5

therefore, $a^2 = b^2 + c^2 - 2bc\text{Cos}A$. A3.6

solve for $B = \sin^{-1}\left(\frac{\sin(A)}{ab}\right)$ A3.7

$\beta = 180^0 - B$ A3.8

$d^2 = (a/2)^2 + c^2 - ac\text{Cos}\beta$ A3.9

$\gamma = \sin^{-1}\left(2\frac{\sin(\beta)}{ac}\right)$ A3.10

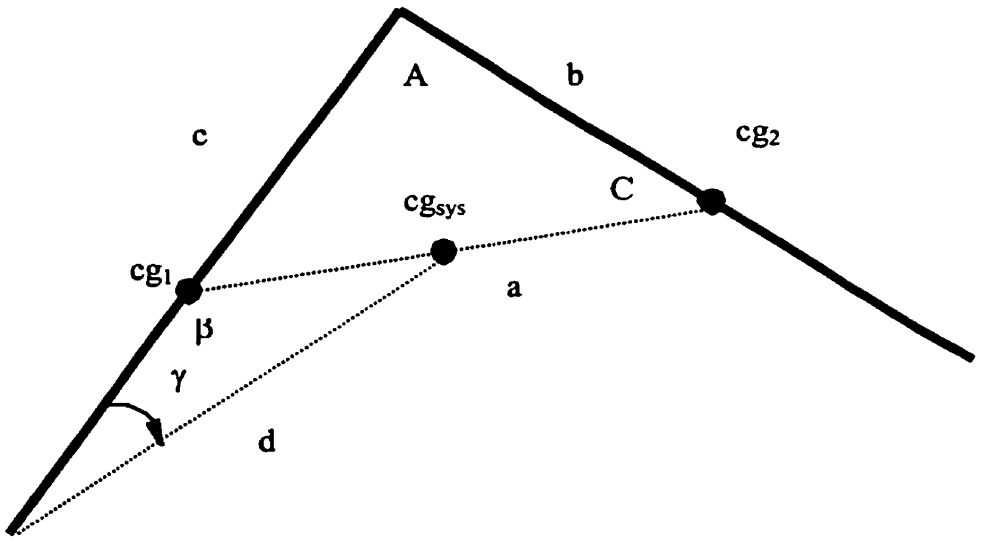

Figure A3.2: Location of center of gravity

A3.3 Natural Frequency

$$\omega_{n1} = \sqrt{\frac{K_{11}}{M_{11}}} = \sqrt{\frac{.326}{.00993}} = 5.73 \text{ rads/s} \qquad \text{A3.11}$$

$$\omega_{n1} = \sqrt{\frac{K_{22}}{M_{22}}} = \sqrt{\frac{.326}{.00328}} = 9.97 \text{ rads/s} \qquad \text{A3.12}$$

Conversion from rads/s to hertz

$$\omega_{n1} = \frac{5.73 \text{ rads/s}}{2\pi \text{ rads/cyc}} = 0.911 \text{ Hz} \qquad \text{A3.13}$$

$$\omega_{n1} = \frac{9.97 \text{ rads/s}}{2\pi \text{ rads/cyc}} = 1.59 \text{ Hz}$$

3.4 Error Calculations

$$\text{error} = \frac{\omega_{n(theo)} - \omega_{n(exp)}}{\omega_{n(theo)}} \times 100\% \qquad \text{A3.14}$$

$$= \frac{5.73 - 5.70}{5.73} \times 100\%$$

$$= 0.52\ \%$$

$$\text{error} = \frac{\omega_{n(theo)} - \omega_{n(exp)}}{\omega_{n(theo)}} \times 100\%$$

$$= \frac{9.97 - 9.95}{9.97} \times 100\%$$

$$= 0.20\ \%$$

A3.5 Conversion of Cartesian Coordinates to Angular Coordinates

When given the x and y coordinates of positions 1, 2 and 3 it is possible to find the angle of the triangle using trigonometry.

$$a = \sqrt{(x_1 - x_2)^2 + (y_1 - y_2)^2} \quad \text{A3.15}$$

$$b = \sqrt{(x_1 - x_3)^2 + (y_1 - y_3)^2} \quad \text{A3.16}$$

$$c = \sqrt{(x_2 - x_3)^2 + (y_2 - y_3)^2} \quad \text{A3.17}$$

$$A = \cos^{-1}\left(\frac{b^2 + c^2 - a^2}{2bc}\right) \quad \text{A3.18}$$

$$B = \sin^{-1}\left(\frac{\sin(A)}{ab}\right) \quad \text{A3.19}$$

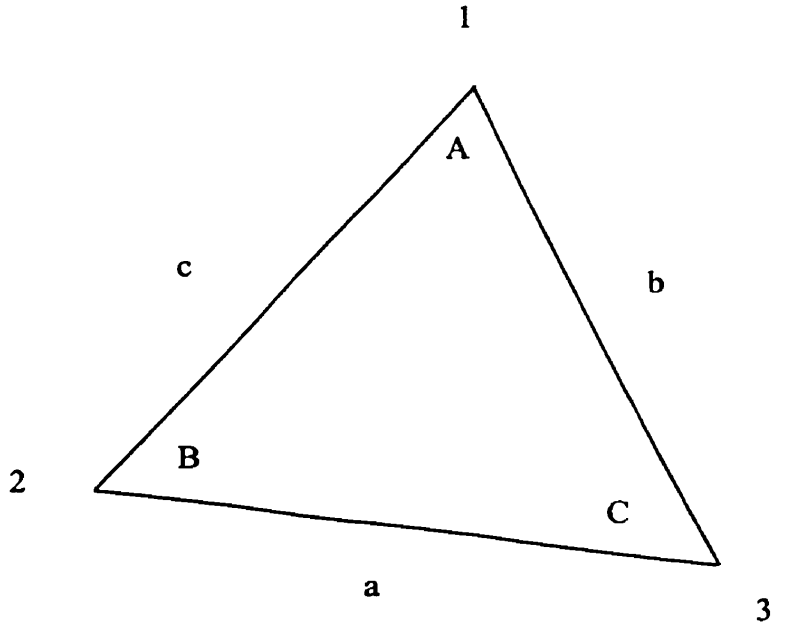

Figure A3.3: Conversion of Cartesian coordinates to angular coordinates

A3.6 **Damping**

$$\delta_n = \frac{1}{n} \ln \frac{X_1}{X_n} \tag{A3.20}$$

where n is the number of cycles since the original measurement and X is the displacement of the amplitude.

$$\xi_n = 2\pi\delta_n \tag{A3.21}$$

$$c_i = 2\xi_n \sqrt{M_{ii} K_{ii}}\text{ , for } i = 1, 2 \tag{A3.22}$$

A3.7 **Angle for Decoupling the Inertia Matrix**

$$Q_2 = \cos^1 \left(\frac{(-I_2 - m_2^2 l_2^2)}{m_2 a_1 l_2} \right) \tag{A3.23}$$

APPENDIX IV

TRANSFORMATION FROM ABSOLUTE COORDINATES TO JOINT COORDINATES AND VISE VERSA

A4.1 Developing the Equations of Motion for Absolute Coordinates

Energy methods are used in this procedure. The absolute coordinates are shown in Figure A4.1.

First the velocities must be solved for the center of masses of links 1 and 2 [14].

$$v_1^2 = (l_1\dot{\theta}_1)^2 \qquad \text{A4.1}$$

$$v_2^2 = [\, a_1\dot{\theta}_1 + l_2\dot{\theta}_2 \cos(\theta_2 - \theta_1)]^2 + [\, l_2\dot{\theta}_2 \sin(\theta_2 - \theta_1)]^2$$

$$= a_1^2\,\dot{\theta}_1^2 + 2a_1l_2\cos(\theta_2-\theta_1)\dot{\theta}_1\,\dot{\theta}_2 + l_2^2\cos^2(\theta_2 - \theta_1)\dot{\theta}_2^2 + l_2^2\sin^2(\theta_2 - \theta_1)\dot{\theta}_2^2$$

$$= (a_1^2\dot{\theta}_1^2 + 2a_1l_2\cos(\theta_2-\theta_1)\dot{\theta}_1\dot{\theta}_2 + l_2^2\,\dot{\theta}_2^2) \qquad \text{A4.2}$$

Solving for kinetic energy of links 1 and 2

$$T_1 = \frac{1}{2} I_{1o}\dot{\theta}_1^2 = \frac{1}{2}\left(\frac{1}{3}m_1a_1^2\dot{\theta}_1^2\right) \qquad \text{A4.3}$$

$$T_2 = \frac{1}{2} I_2\,\dot{\theta}_2^2 + \frac{1}{2} m_2\,(a_1^2\dot{\theta}_1^2 + 2a_1l_2\cos(\theta_2-\theta_1)\dot{\theta}_1\dot{\theta}_2 + l_2^2\,\dot{\theta}_2^2) \qquad \text{A4.4}$$

$$T = \frac{1}{2}\left(\frac{1}{3}m_1a_1^2\dot{\theta}_1^2\right) + \frac{1}{2} I_2\,\dot{\theta}_2^2 + \frac{1}{2} m_2\,(a_1^2\dot{\theta}_1^2 + 2a_1l_2\cos(\theta_2-\theta_1)\dot{\theta}_1\dot{\theta}_2 + l_2^2\,\dot{\theta}_2^2) \qquad \text{A4.5}$$

$$\partial T/\partial\dot{\theta}_1 = \frac{1}{3}\, m_1a_1^2\dot{\theta}_1 + m_2a_1^2\dot{\theta}_1 + m_2a_1l_2\cos(\theta_2 - \theta_1)\dot{\theta}_2 \qquad \text{A4.6}$$

$$\frac{d}{dt}(\partial T/\partial\dot{\theta}_1) = \frac{1}{3}\, m_1a_1^2\ddot{\theta}_1 + m_2a_1^2\ddot{\theta}_1 + m_2a_1l_2\cos(\theta_2 - \theta_1)\ddot{\theta}_2$$

$$- m_2a_1l_2(\sin(\theta_2 - \theta_1))\,(\dot{\theta}_2 - \dot{\theta}_1)(\dot{\theta}_2) \qquad \text{A4.7}$$

$$\partial T/\partial \dot{\theta}_2 = I_2 \dot{\theta}_2 + m_2 a_1 l_2 \cos(\theta_2 - \theta_1)\dot{\theta}_1 + m_2 l_2^2 \dot{\theta}_2 \quad \text{A4.8}$$

$$\frac{d}{dt}(\partial T/\partial \dot{\theta}_2) = I_2 \ddot{\theta}_2 + m_2 l_2^2 \ddot{\theta}_2 + m_2 a_1 l_2 \cos(\theta_2 - \theta_1)\ddot{\theta}_1 - m_2 a_1 l_2 (\sin(\theta_2 - \theta_1))(\dot{\theta}_2 - \dot{\theta}_1)\dot{\theta}_1 \quad \text{A4.9}$$

Solving for potential energy of links 1 and 2.

$$U_1 = \frac{1}{2} k_1 \theta_1^2 \quad \text{A4.10}$$

$$U_2 = \frac{1}{2} k_2 (\theta_2 - \theta_1)^2 \quad \text{A4.11}$$

$$U_{total} = \frac{1}{2} [k_1 \theta_1^2 + k_2 (\theta_2^2 - 2\theta_1\theta_2 + \theta_1^2)] \quad \text{A4.12}$$

$$\partial U/\partial \theta_1 = [k_1\theta_1 - k_2\theta_2 + k_2\theta_1] \quad \text{A4.13}$$

$$\partial U/\partial \theta_2 = [k_2\theta_2 - k_2\theta_1] \quad \text{A4.14}$$

Forming the inertia matrix

$$\begin{bmatrix} M_{11} & M_{12} \\ M_{21} & M_{22} \end{bmatrix} \begin{bmatrix} \ddot{\theta}_1 \\ \ddot{\theta}_2 \end{bmatrix} \quad \text{A4.15}$$

$$M_{11} = \frac{1}{3} m_1 a_1^2 + m_2 a_1^2 = I_1 + m_1 l_1^2 + m_2 a_1^2 \quad \text{A4.16}$$

$$M_{12} = m_2 a_1 l_2 \cos(\theta_2 - \theta_1) \quad \text{A4.17}$$

$$M_{21} = M_{21} \quad \text{A4.18}$$

$$M_{22} = I_2 + m_2 l_2^2 \quad \text{A4.19}$$

Forming the Coriolis and centrifugal forces matrix.

$$\begin{bmatrix} A_{11} & A_{12} \\ A_{21} & A_{22} \end{bmatrix} \begin{bmatrix} \dot{\theta}_1 \\ \dot{\theta}_2 \end{bmatrix} \quad \text{A4.20}$$

$$A_{11} = 0 \qquad \text{A4.21}$$

$$A_{12} = - m_2 a_1 l_2 (\sin(\theta_2 - \theta_1)) (\dot{\theta}_2 - \dot{\theta}_1) \qquad \text{A4.22}$$

$$A_{21} = -m_2 a_1 l_2 (\sin(\theta_2 - \theta_1)) (\dot{\theta}_2 - \dot{\theta}_1) \qquad \text{A4.23}$$

$$A_{22} = 0 \qquad \text{A4.24}$$

or

$$A_{11} = m_2 a_1 l_2 (\sin(\theta_2 - \theta_1)) (\dot{\theta}_2) \qquad \text{A4.25}$$

$$A_{12} = - m_2 a_1 l_2 (\sin(\theta_2 - \theta_1)) (\dot{\theta}_2) \qquad \text{A4.25}$$

$$A_{21} = m_2 a_1 l_2 (\sin(\theta_2 - \theta_1)) (\dot{\theta}_1) \qquad \text{A4.26}$$

$$A_{22} = - m_2 a_1 l_2 (\sin(\theta_2 - \theta_1)) (\dot{\theta}_1) \qquad \text{A4.27}$$

Forming the stiffness matrix.

$$\begin{bmatrix} K_{11} & K_{12} \\ K_{21} & K_{22} \end{bmatrix} \begin{bmatrix} \theta_1 \\ \theta_2 \end{bmatrix} \qquad \text{A4.28}$$

$$K_{11} = k_1 + k_2 \qquad \text{A4.29}$$

$$K_{12} = K_{21} = -k_2 \qquad \text{A4.30}$$

$$K_{22} = k_2 \qquad \text{A4.31}$$

For a manipulator that is in a constant posture it is necessary to define the coordinates that will allow for small motions. This is done by defining

$$\theta = \psi - \gamma, \qquad \text{A4.32}$$

where ψ is the configuration coordinate and γ is the small motion coordinate.

Since γ is small,

$$\theta \approx \psi \,. \qquad \text{A4.33}$$

Since ψ is constant,

$$\dot{\theta} = \dot{\gamma} \text{ and} \qquad \text{A4.34}$$

$$\ddot{\theta} = \ddot{\gamma} \,. \qquad \text{A4.35}$$

A4.2 **Jacobian Transformations**

The next step is to solve for the Jacobian matrix that will allow a transfer from absolute coordinates, ψ (posture coordinate) and γ (small motion coordinate), to joint coordinates, **Q** (posture coordinate) and **q** (small motion coordinate).

This is done by writing θ_1 and θ_2 in terms of $\mathbf{q}_1$ and $\mathbf{q}_2$ and forming a matrix

$$\psi_1 = \mathbf{q}_1 \qquad \text{A4.36}$$

$$\psi_2 = \mathbf{q}_2 + \mathbf{q}_1 \qquad \text{A4.37}$$

writing the Jacobian Matrix gives

$$\begin{bmatrix} \psi_1 \\ \psi_2 \end{bmatrix} = \begin{bmatrix} 1 & 0 \\ 1 & 1 \end{bmatrix} \begin{bmatrix} \mathbf{q}_1 \\ \mathbf{q}_2 \end{bmatrix} \qquad \text{A4.38}$$

To transfer the Inertia and stiffness matrices they are pre-multiplied by the transpose of the Jacobian Matrix and post multiplied by the Jacobian Matrix.

$$[Y] = \begin{bmatrix} 1 & 1 \\ 0 & 1 \end{bmatrix} \begin{bmatrix} X_{11} & X_{12} \\ X_{21} & X_{22} \end{bmatrix} \begin{bmatrix} 1 & 0 \\ 1 & 1 \end{bmatrix} = \begin{bmatrix} X_{11} + X_{12} + X_{21} + X_{22} & X_{12} + X_{22} \\ X_{21} + X_{22} & X_{22} \end{bmatrix} \qquad \text{A4.39}$$

For the inertia matrix:

$$Y_{M11} = I_1 + m_1 l_1^2 + m_2 a_1^2 + 2m_2 a_1 l_2 \cos(\psi_2 - \psi_1) + I_2 + m_2 l_2^2 \quad \text{A4.40}$$

$$Y_{M12} = m_2 a_1 l_2 \cos(\psi_2 - \psi_1) + I_2 + m_2 l_2^2 \quad \text{A4.41}$$

$$Y_{M21} = m_2 a_1 l_2 \cos(\psi_2 - \psi_1) + I_2 + m_2 l_2^2 \quad \text{A4.42}$$

$$Y_{M22} = I_2 + m_2 l_2^2 \quad \text{A4.42}$$

For the Coriolis and centrifugal matrix:

This is not possible since a Jacobian transfer is a linear function and the Coriolis and centrifugal parameters are not linear.

For the stiffness matrix

$$Y_{K11} = k_1 \quad \text{A4.43}$$

$$Y_{K12} = Y_{K21} = 0 \quad \text{A4.44}$$

$$Y_{K22} = k_2 \quad \text{A4.45}$$

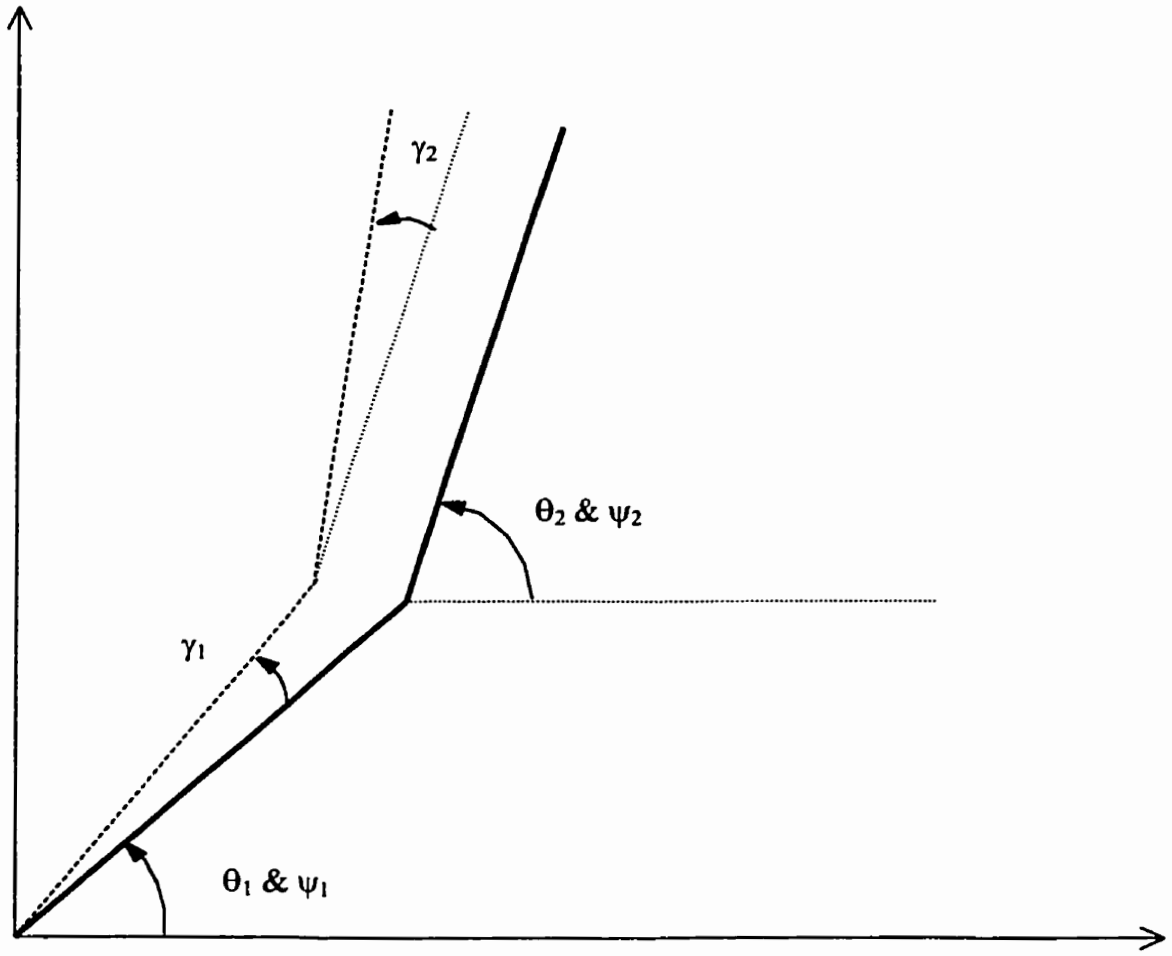

Figure A4.1: Definition of Absolute Coordinates

APPENDIX V

PARAMETERS FOR DECOUPLING A 3 DOF LINKAGE

Using Jacobian velocity kinematics and derived Euler-Lagrange equations [11] the equation of motion for a 2 DOF linkage was found. This method was expanded to a 3 DOF linkage system.

Mathematically speaking, the separating of modal motion occurs because at the appropriate angles, all the terms that are not along the diagonal in the inertia matrix become zero.

Using this information and the fact the M_{22}, M_{23}, M_{32} and M_{33} for the inertia matrix of the 3-DOF system correspond respectively to M_{11}, M_{12}, M_{21} and M_{22} for the inertia matrix of the 2-DOF system we are left only having to solve for two equations.

For a 3-DOF

$M_{23} = M_{32} = m_3((l_3)^2 + a_2 l_3 \mathrm{Cos}(\mathbf{Q}_3)) + I_3 = 0$

when $\mathbf{Q}_3 = 228.65$ degrees

$M_{13} = M_{31} = m_3((l_3)^2 + a_2 l_3 \mathrm{Cos}(\mathbf{Q}_3)) + I_3 + m_3 a_1 l_3 \mathrm{Cos}(\mathbf{Q}_2 + \mathbf{Q}_3)$

$0 = 0 + m_3 a_1 l_3 \mathrm{Cos}(\mathbf{Q}_2 + \mathbf{Q}_3)$

Therefore $\mathbf{Q}_2 = -138.35$

$M_{12} = M_{21} = M_{13} + m3(a_2 l_3 \mathrm{Cos}(\mathbf{Q}_3) + (a_2)^2 + a_1 a_2 \mathrm{Cos}(\mathbf{Q}_3)) + I_2$

$0 = 0 + m3(a_2 l_3 \mathrm{Cos}(\mathbf{Q}_3) + (a_2)^2 + a_1 a_2 \mathrm{Cos}(\mathbf{Q}_3)) + I_2$

Therefore $a_1 = 277$ mm

The top view of necessary configuration for limiting modal response to a single corresponding joint is found in figure A6.1.

Table A6.1 – Parameters of physical model and necessary values for Q_2, Q_3 and a_1 for diagonalizing the inertia matrix.

a of bar 2&3	0.277 m
l of bar 2&3	0.1385 m
Q_1	any value
Q_2	-138.35 degrees
Q_3	228.65 degrees
I of bar 1, 2 & 3	0.000799776 m^4
a of bar 3	0.277 m
l of bar 3	0.1385 m
I of bar 3	0.000799776 m^4
m of bar 2&3	0.129399 kg
m of bar 1	0.129399 kg
a of bar 1	0.277 m
l of bar 1	0.1385 m

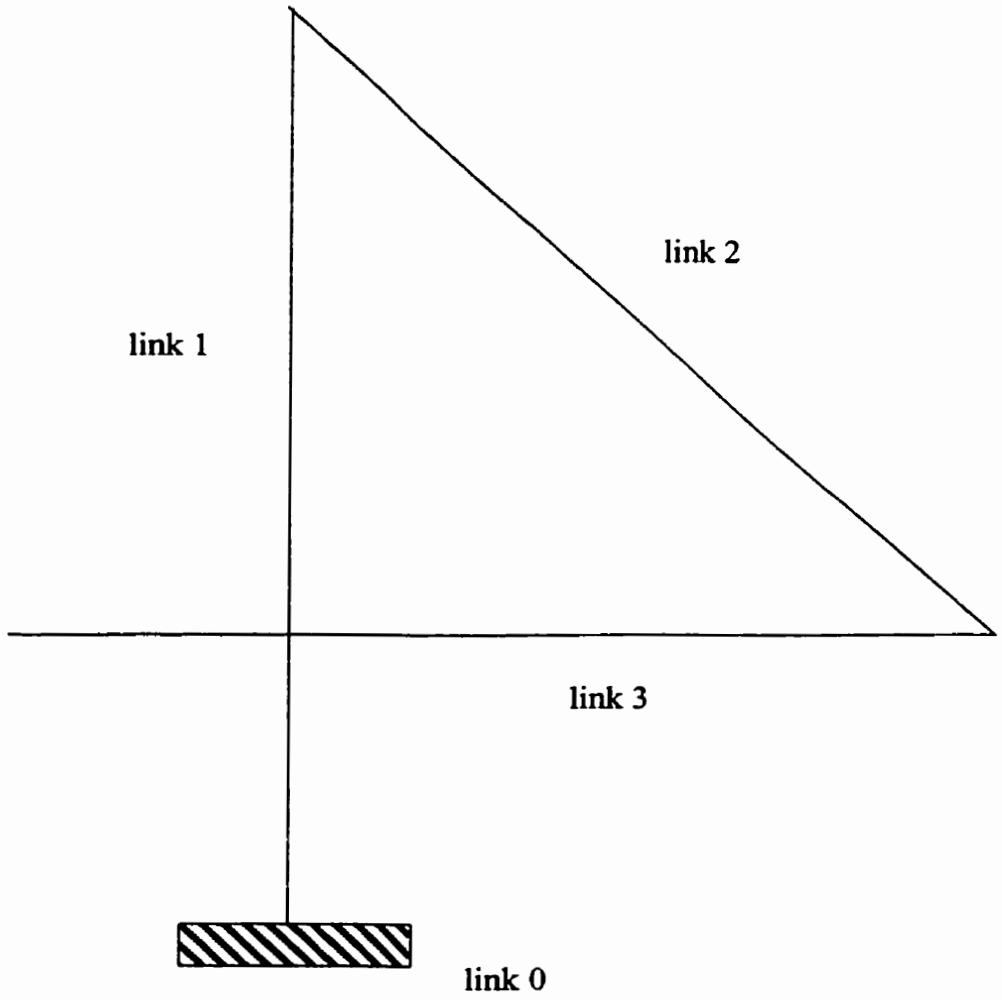

Figure A6.1: Configuration for decoupling of a 3-DOF-linkage